DTU Wind and Energy Systems

Dynamic analysis of a floating wind turbine with a tension leg platform in deep water

Stephen Mark Phillips

DTU Wind and Energy Systems-M-0567

July 2022

Author: Stephen Mark Phillips

DTU Wind and Energy Systems M-0567
July 2022

Title:
Dynamic analysis of a floating wind turbine with a tension leg platform in deep water

Project period:
February - July 2022

ECTS: 30

Education: Master of Science

Supervisor(s):

Fabio Pierella
Taeseong Kim
DTU Wind and Energy Systems

Remarks:
This report is submitted as partial fulfillment of the requirements for graduation in the above education at the Technical University of Denmark.

DTU Wind and Energy Systems is a department of the Technical University of Denmark with a unique integration of research, education, innovation and public/private sector consulting in the field of wind and energy. Our activities develop new opportunities and technology for the global and Danish exploitation of wind and energy. Research focuses on key technical-scientific fields, which are central for the development, innovation and use of wind energy and provides the basis for advanced education.

Technical University of Denmark
Department of Wind and Energy Systems
Frederiksborgvej 399
DK-4000 Roskilde
www.vindenergi.dtu.dk

Abstract

This master's thesis presents the results from numerical modelling of a 15MW floating wind turbine supported by a Tension Leg Platform at varying water depths of 120m, 250m, and 1000m. The goal is to study the influence of mooring depth on the system dynamics, and to investigate advantages, challenges, and relevant design considerations for adapting the TLP model to deep water.

The wind turbine is the IEA 15MW reference wind turbine [1], and the TLP support structure consists of a concrete floater with eight steel rod tendons anchored to the sea bed with suction buckets (developed as collaboration between BlueNewables, DTU, Tubacex, and GMC deepwater). Hydrodynamic loads are calculated in WAMIT using first order potential flow theory. HAWC2, an Aeroelastic modelling tool developed by DTU, is then used to solve the equations of motion for the entire coupled system in the time domain. To provide a clear comparison of system dynamics for the different mooring depths, the same platform/turbine model and external conditions are used for all depths, followed up with suggested design changes for the deep water models.

Decay tests are first run in heave, surge, pitch and yaw to investigate the system natural frequencies including the effect of mooring depth and tower stiffness. This is followed by a number of steady state simulations and dynamic simulations of selected DLCs (1.1, 1.6, and 6.1) [2], which are based on metocean conditions at Buchan Deep [3].

Increasing the mooring depth had only a minor and often insignificant impact on the turbine and structural loads while the turbine was operating. Furthermore, the aerodynamic performance of the turbine is not sensitive to mooring depth.

The most significant challenges faced by a deep water TLP design include resonance in pitch during extreme conditions where the rotor is shut down, limiting aerodynamic damping effects. For the 250m and 1000m platform, the pitch natural frequency is excited by high frequency wave loads leading to an increase extreme tower bottom bending moment. Additionally, the deep water TLP platforms with low yaw stiffness are susceptible to a large low frequency yaw motion. Finally, deep water TLP platforms with heavy moorings that are exposed to extreme sea conditions of low tide, negative storm surge, and large waves are at higher risk for loss of pretension in the tendons which can lead to instability of the system.

Acknowledgements

This Master's thesis was written from Feburary to July 2022 in the Wind Energy Department at DTU.

First and foremost I would like to thank my project supervisors, Fabio Pierella and Taeseong Kim, who have guided me throughout this thesis project. Their many hours of support have been invaluable in the process of modelling, troubleshooting, and interpreting results. They have also contributed significantly to my understanding the theoretical background and to preparing this report, making it a meaningful learning experience. A special thanks to Fabio for providing the baseline HAWC2 model and the WAMIT modelling.

I would also like to thank all of my other professors, lecturers, and teaching assistants at DTU who have given me the background over the last 2 years to be able to tackle this topic. A special thank you to Jenni Rinker, whose enthousiastic teaching and engagement with her students has helped to make learning the fundamentals of aeroelasticity and HAWC2 a good experience. And a thank you to my classmates, especially to Matthieu and Nicolas, who have made my time at DTU even more enjoyable.

I would like to thank my fellow MSc student Stefanos Masalas who provided a partner to collaborate with and share ideas, leanings, and frustrations. And a thank you the team at BlueNewables for allowing us to use their TLP platform design in this MSc project, and also for providing support and guidance in the process.

Finally, I would like to thank my friends and family who have always supported me unconditionally throughout my educational journey.

Contents

Abstract . . . iii
Acknowledgements . . . iv
Terms and Abbreviations . . . vii

1 Introduction **1**
1.1 Background and Motivation . . . 1
1.2 Project Scope . . . 1

2 Presenting the TLP Model **3**
2.1 Wind Turbine and Support Structure . . . 3
2.2 Numerical Modelling . . . 4
2.3 Coordinate Systems . . . 7
2.4 Equation of Motion . . . 8
2.5 Design Considerations . . . 12
2.6 Model Limitations and Improvements . . . 12

3 System Natural Frequencies **14**
3.1 Theoretical Values . . . 14
3.2 HAWC2 Simulation and Results . . . 15

4 Mooring and Platform Stability **18**
4.1 Buoyancy and Pretension . . . 18
4.2 Pitch Stability . . . 19

5 Wind and Wave Loads **20**
5.1 Steady Wind . . . 20
5.2 Step Wind . . . 22
5.3 Regular Waves . . . 23
5.4 Regular Waves and Steady Wind . . . 27

6 Dynamic Response to Environmental Conditions: DLCs 1.1, 1.6, 6.1 **29**
6.1 Simulation Design . . . 29
6.2 Analysis of Results . . . 32

7 Advantages and Challenges of TLP in Deep Water **51**
7.1 Advantages . . . 51
7.2 Challenges . . . 53

8 Conclusion **58**

Bibliography **60**

A Model Characteristics **62**
A.1 IEA 15MW Turbine [1] . . . 62
A.2 System Mass and Inertia . . . 63
A.3 CTBos Floater and Mooring . . . 64

B Extreme Loads and Platform Motion **65**

C Buchan Deep **66**

D Linear Wave Theory **67**

E Linear Potential Flow Theory **69**

F BEM Theory **71**

G DeepRope® Dyneema® Properties **73**

Terms and Abbreviations

Important and commonly used terms and abbreviations in this report are presented in table 1.

Term	Definition
AoA	Angle of Attack
BEM	Blade Element Momentum
COG	Center of Gravity
DLC	Design Load Case, from [2]
DOF	Degree of freedom
HAWC2	Horizontal Axis Wind turbine simulation Code 2nd generation
IP-BRM	In Plane Blade Root Moment
OoP-BRM	Out of Plane Blade Root Moment
MSL	Mean Sea Level
PSD	Power Spectral Density (plot)
RNA	Rotor Nacelle Assembly
SWL	Still Water Level
TB-FA	Tower base fore-aft
TT-FA	Tower Top fore-aft
TB-SS	Tower base side-side
TT-SS	Tower Top side-side
TLP	Tension Leg Platform
WAMIT	Wave Analysis MIT software
YBP	Yaw Bearing Pitch
YBR	Yaw Bearing Roll
1P, 3P, 6P	1, 3, or 6 (times) per rotor revolution

Table 1: Terms and Abbreviations.

1 Introduction

1.1 Background and Motivation

Offshore platforms and in particular floating offshore platforms have a long history of use in the oil & gas industry. The first tension leg platform was installed in the early 1980's in the north sea, at a depth of 147m. Since then the application of TLPs has grown significantly, with 30 platforms installed or decommissioned globally as of 2020 at depths of up to 1615 m [4]. As shown in figure 1.1, TLPs are among the oil & gas platforms used for the deepest water applications.

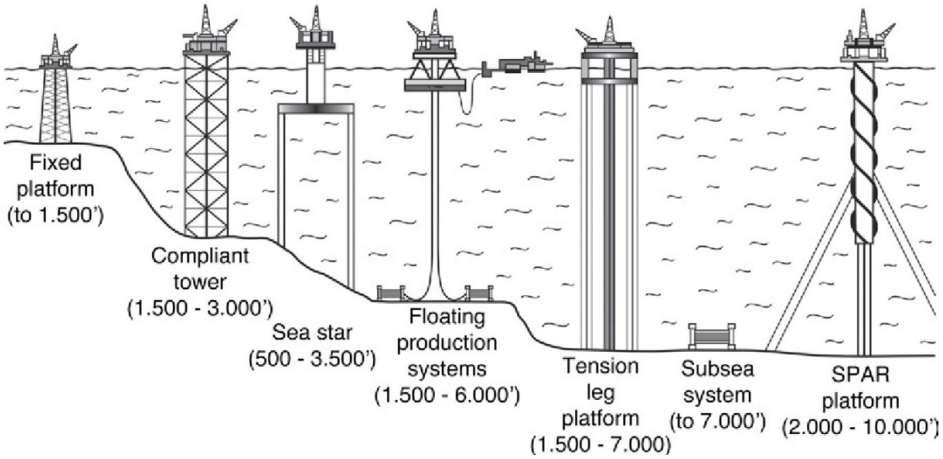

Figure 1.1: Common offshore production systems and the depth range of their application (in feet) [5].

While the fundamentals of the TLP remain the same when applied to wind energy, the dynamics of the system are quite different. The floating wind turbine becomes a complex problem coupling the system motion, hydrodynamics, wind turbine aerodynamics, aeroelasticity, controller operation, and mooring reactions.

Although (as of July 2022) there are no commercially operating wind turbines with a TLP support structure, it is a promising area of development and an active area of research. According to [6], the technical (resource) potential of offshore wind globally is 36,000 TWh per year in waters less than 60m, and in deeper water it is more than 330,000 TWh per year (current global electricity consumption is $\sim$ 23,000 TWh). A 60m depth represents the upper limit of what is suitable for bottom fixed foundations based on current technology. By developing commercially viable floating turbines, it will be possible to tap into the vast available wind resource in deeper waters which will be key for meeting energy transition targets.

1.2 Project Scope

The use of TLPs for supporting floating wind turbines is a fairly recent but active area of research. The goal of this report is to perform a detailed dynamic investigation of a TLP model, while exploring the benefits and challenges of using TLP supported wind turbines for deep water applications. The TLP in scope of this project is the CT-bos floating platform developed in collaboration between DTU, BlueNewables, Tubacex, and GMC Deepwater.

The concept is one that aims to be cheap and robust, adaptable to different depths, and easy to build and deploy with minimized maintenance costs.

The project methodology is based on numerical simulations of the wind turbine and its TLP support structure. The intention is not to perform a complete design evaluation, rather to focus in depth on a limited set of environmental conditions and DLCs:

- Free decay test, no wind or waves.
- Steady wind only, no waves.
- Regular waves, with and without wind.
- DLCs 1.1- normal operation, 1.6- operation in severe sea state, and 6.1- shut down in 50yr wind and sea climate

This set of DLCs was chosen to study the system dynamics under a range of normal to extreme environmental conditions.

The metocean climate used for this report is based on the Statiol Buchan Deep Design Basis [3], at location centered 57.45º N, 01.31º W off the east coast of Scotland in the North Sea. To study the impact of mooring depth on the dynamic behavior of the system, three depths of 120m, 250m, and 1000m are in scope to cover a range of expected applications. Note that while the water depth of the Buchan Deep site itself is 100-140m, it is chosen to use the same climate input for all mooring depths and to only re-scale the sea depth in the HAWC model. This is done to generate a more direct comparison of the results between the different TLP models.

The inputs to the project are the platform design, which was provided by BlueNewables, the IEA15MW Reference Wind Turbine [1], and the initial HAWC2 model as well as WAMIT modelling provided by Fabio Pierella (DTU Wind Energy).

2 Presenting the TLP Model

2.1 Wind Turbine and Support Structure

The wind turbine in scope of this project is the IEA 15MW offshore reference wind turbine [1] with a hub height of 150m and rotor radius of 120m. The turbine is supported by a cylindrical steel tower with an outer diameter ranging from 10.0m at the base to 6.5m at the top. Both a stiff and flexible tower were used for the simulations, designed in a simplified way by adjusting only the elastic modulus from the baseline IEA-15MW tower.

The wind turbine is mounted atop a floating concrete TLP which is symmetric about both vertical planes (x-z and y-z). There are eight (8) steel tendons which anchor the platform to suction buckets placed in the sea bed. The length of the tendons depends on the model depth with 120m, 250m and 1000m depths in scope. One unique characteristic of this TLP model is that the mooring lines are made of a number of solid interconnected steel rods, as opposed to e.g. a mooring cable solution. A visualisation of the turbine is presented in figure 2.1, and key characteristics are presented in appendix A.

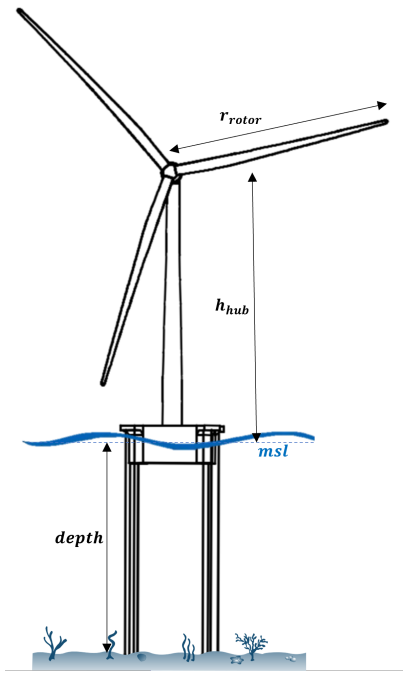

Figure 2.1: Visualisation of 15MW turbine mounted on the floating TLP.

An adequate floating platform design must be able to support and stabilize the turbine in all of its 6 degrees of freedom. Throughout the report these will be referred to as surge, sway, heave, pitch, yaw, and roll (fig 2.2).

A defining characteristic of the tension leg platform design is that the mooring lines have a high pretension due to the buoyant force that is larger than the gravitational force on the system (fig 2.2). The tension force is always axial along the tendons and thus generates a restoring force if the turbine moves from its equilibrium position in surge, sway, and yaw. There are no hydrostatic restoring forces in these degrees of freedom, so stability is provided solely by the tendons. In general, the platform is laterally compliant in surge, sway, and yaw and may exhibit a significant range of motion in these DOFs.

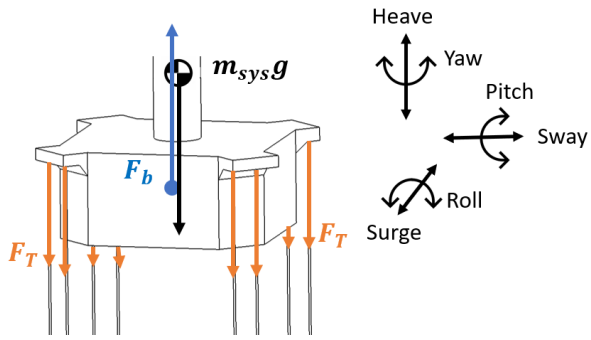

Figure 2.2: Forces on the floater and degrees of freedom (with wind direction going into the page).

In heave, pitch, and roll, the motion of the platform will cause the tendons to extend or contract elastically. The stretched tendons act as springs which bring the system back to equilibrium. This gives the TLP a very high stiffness in heave, pitch, and roll due to the high stiffness of the steel material, resulting in limited motion in these DOFs. As opposed to other floating designs such as semisubmersible or spar buoy, the TLP design provides limited hydrostatic restoring force in pitch and roll. Thus, the tendons play an especially important role in stabilizing the system against an overturning moment.

2.2 Numerical Modelling

2.2.1 Aeroelastic Model

Numerical simulations are performed in HAWC2 software [7], which is an aeroelastic code that calculates response of the wind turbine and support structure in the time domain. The wind turbine files are adopted from the IEA15MW turbine model. The blades, hub, tower top, shaft, and tower are all modelled as Timoschenko beam elements with defined strength and mass properties. The rotor blades use the DTU FFA-W3 series of airfoils and are modeled as a number of connected bodies that allow for nonlinear deflections between them.

Aerodynamics are calculated using Blade Element Momentum theory, which combines basic 1D momentum theory of airflow through an idealized rotor with a blade element model. For this model, the rotor plane is divided into a number of discs which are assumed to be radially independant. For each disc or rotor element, the lift and drag forces on the rotor can be calculated based on the local relative air velocity, blade geometry, and angle of attack. By summing the lift and drag forces across all elements it is then possible to calculate the aerodynamic thrust and torque on the rotor.

A number of corrections are applied to the BEM model to capture unsteady loads or other phenomena not included in the basic BEM theory. This includes dynamic inflow to account for the delay before rotor induced velocities are in equilibrium with changed inflow conditions. Also, a dynamic stall model is used to account for the delay of changes in AoA and corresponding changes in aerodynamic loads. For more details on BEM theory and the corrections used, see appendix F

A Mann turbulence box is generated within HAWC2 and used to simulate the turbulent wind for each simulation. The turbulent wind is defined for each time step with a series of 2D grids where the x, y, and z velocity components are defined at each grid point. The grids are then sampled by the rotating blade, which together with the mean wind speed

and shear model gives the inflow conditions for the rotor.

2.2.2 Hydrodynamic Model

HAWC2 is used to generate time series of regular and irregular airy waves as well as embedded stream function waves (if relevant) for each simulation. Irregular waves are based on the Johnswap wave spectrum [8] which is build on the Pierson & Mosowitz spectrum but adapted to describe storm sea states of limited fetch, as in the North Sea. The free surface elevation η of the waves can be calculated by discretizing the power spectrum S_η into small frequency bands of width Δf, and summing waves of varying amplitudes and frequencies defined by each frequency band, as in equations 2.1 and 2.2.

$$\eta = \sum_{j=1}^{n} A_j cos(\omega_j t - k_j x + \epsilon_j) \tag{2.1}$$

$$\text{where } A_j = \sqrt{2S_\eta(f_j)\Delta f} \tag{2.2}$$

In these equations ϵ_j represents a random phase angle between 0 and 2π and $\omega_j^2 = gk_j$tanh$k_j h$ is the dispersion relation for a wave with wave number k. For more details on linear wave theory see appendix D

Hydrodynamic forces from the waves on the structure are then traditionally calculated in aeroelastic codes using a simplified approach i.e. Morrison's equation (eq 2.3) for slender bodies, which is a semi-emperical formula.

$$dF = (\underbrace{\frac{1}{2}\rho C_D D|U - U_b|(U - U_b)}_{\text{Drag Force}} + \underbrace{\rho C_m A \frac{d}{dt}(U - U_b)}_{\text{Hydrodyn Mass Force}} + \underbrace{\rho A \frac{dU}{dt}}_{\text{Froude-Krylov Force}})dz \tag{2.3}$$

Where C_D and C_m are the drag and added mass coefficients of the cylinder, D is the diameter, A is the cross sectional area, U is the fluid velocity, and U$_b$ is the body velocity. The hydrodynamic mass force represents inertia contribution of surrounding fluid mass that is accelerated by the cylinder and the Froude-Krylov force represents the pressure of the undisturbed wave. These two forces are often presented together as one inertia force term. The drag force accounts for viscous effects of separation and boundary layer friction as the fluid moves past the body.

Morrison's equation does not account for wave diffraction or differences in the flow field across the structure and is therefore is generally applied only for slender bodies i.e. D/λ<0.2, where λ is the wave length.

As the mooring cables are slender cylinders which meet this criteria, it is possible to use the Morrison equation for computing their hydrodynamic loads. This is done in HAWC2 by linking to an external mooring system model where the coordinates, mass distribution, and drag and added mass coefficients are specified. The mooring is modeled as steel cables with 20-50 elements whose nodes are able to translate in 3 DOFs and elongate along the element axis. The cables can only support a tension load, which is not entirely representative of the steel rods intended for the actual mooring design. However, provided that the cables remain in tension the model will be sufficiently accurate.

Due to the large cross section of the floating platform, Morrison's equation is not valid here and therefore the hydrodynamics are calculated based on diffraction/radiation forces. Assuming a linear system, the principle of superposition can be used to calculate these

forces independently and to sum them together to find the total wave load. The diffraction force is caused by an incoming wave and is the sum of the undisturbed wave pressure over the wetted surface plus the wave scattering force of the stationary platform obstructing the wave. The radiation (damping) force accounts for the waves generated by the moving body and radiating outward and is calculated assuming no incoming wave. WAMIT is used to solve the linear potential flow problem numerically for the diffraction and radiation potentials, based on a discretized panel method. Furthermore, it is assumed that the forcing of the platform is inertia dominated and viscous drag forces, which are not accounted for when using linear potential flow, can be neglected. For more details on linear potential flow theory, see appendix E.

Using a nominal wave height and body velocity, the wave forces are pregenerated as frequency response functions (FRF) for a range of wave and free body motion frequencies. To go from the frequency domain forcing functions to the time domain used by the HAWC2 solver, a convolution integral is employed which in general form is eq 2.4.

$$F(t) = \int_0^\infty K(t-\tau)X(\tau)d\tau \tag{2.4}$$

Where F(t) is the time domain forcing, K(t) is the impulse response function calculated by the inverse Fourier transform of the corresponding FRF, and X(t) is the driving parameter i.e. the wave elevation for diffraction forces or the structure velocity for radiation forces [9].

The added mass and hydrostatic restoring forces for the platform are also generated in WAMIT and passed into HAWC2. Plots of the diffraction force, radiation damping, and added mass for the platform model are shown in figure 2.3 over a range of periods. There are abnormal spikes in the pitch damping force and added mass at very low periods (high frequency) which are non-physical and a result of the numerical modelling. However, they are far from any wave forcing or system frequency so they are not expected to influence the simulation results. For reference, the peak wave energy for the Buchan Deep site is between a period of 5s and 17s.

Quadratic drag is added to the model through constant coefficients defined in HAWC2 for each DOF, which are estimated by considering drag forces on fully submerged square shapes. These coefficients are multiplied by the directional square of the velocity in each DOF to calculate the damping forces.

In HAWC2 the floater is simply modelled by its mass, buoyancy, COG, and gyration radii, and quadratic drag coefficients. HAWC2 will then solve at each time step the full set of coupled equations of motion for the entire system, including the wind turbine, platform, and mooring lines with wind, waves, and gravitational loads.

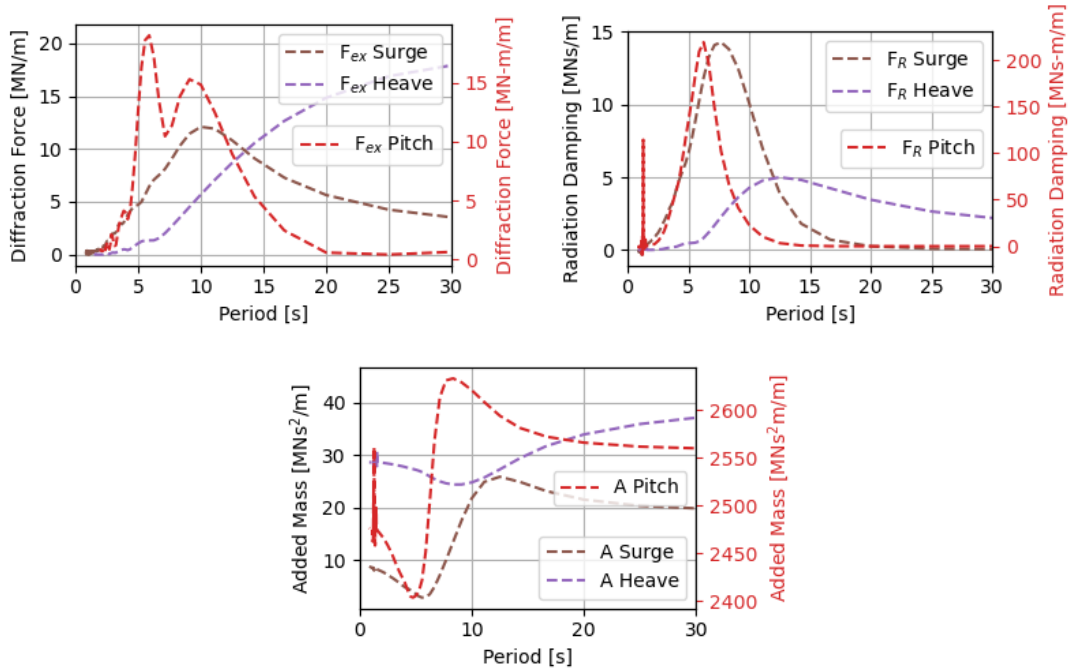

Figure 2.3: Excitation Force, Radiation Damping, and Added Mass as calculated in WAMIT, wavedirection = 0°.

2.3 Coordinate Systems

HAWC2 and WAMIT use different coordinate systems, and thus the output from the model can be in different coordinates depending on the origin of the data (fig 2.4).

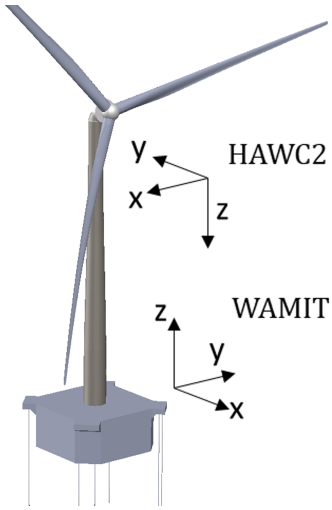

Figure 2.4: HAWC2 and WAMIT coordinate systems.

The WAMIT coordinate system will be used in general to describe the motion of the platform in its 6 degrees of freedom. In some cases, e.g. for loads and motion of the RNA, the HAWC2 coordinate system will be used, and this will be specified. The origin for each global coordinate system is placed at the platform center, point of flotation at MSL.

The eight mooring lines are identified in figure 2.5. The mooring line numbers have a prefix of 'U' for upwind and 'D' for downwind of the tower.

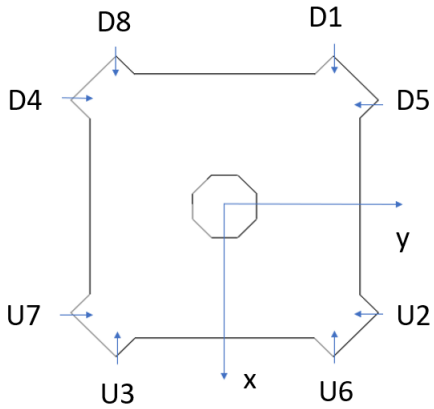

Figure 2.5: Numbering of eight mooring cables, WAMIT coordinates.

2.4 Equation of Motion

The general equation of motion for the TLP system is presented in eq 2.5.

$$M\ddot{\xi} + B\dot{\xi} + C\xi = F_{hydro} + F_{aero} + F_g \tag{2.5}$$

Where $\xi = [\xi_1 ... \xi_n]^T$ represents motion in all degrees of freedom and M, B, and C represent the full mass, damping, and stiffness matricies of the system. The external forcing terms are vectors which can be grouped into F_{hydro} representing the hydrodynamic forces from buoyancy and incident waves, F_{aero} as the aerodynamic forces on the structure and rotor, and F_g as the gravitational force.

The remainder of this section presents a simplified 6-DOF equation of motion for the floating system, considering the RNA-turbine-platform as a rigid body and the mooring system as a reaction force, F_{moor}.

The linearized equation of motion for a free floating body can be written as equation 2.6, which implements the frequency domain wave model into the time domain using the Cummins equation [10].

$$(M + A_\infty)\ddot{\xi} + B\dot{\xi} + \int_0^t K(t-\tau)\dot{\xi}(t)d\tau + C_{hst}\xi = F_{hydro} + F_{aero} + F_{moor} + F_g \tag{2.6}$$

In this equation, $\xi = [\xi_1 ... \xi_6]^T$ represents motion in the degrees of freedom of surge, sway, heave, roll, pitch and yaw. The A_∞ term represents the infinite frequency limit of the added hydrodynamic mass of the system. The B matrix is the frequency independent quadradic damping matrix and C_{hst} matrix is the hydrostatic restoring matrix. K represents the radiation retardation kernel from the frequency dependant radation damping B_{rad}, equation 2.7.

$$K(t) = \frac{2}{\pi}\int_0^\infty B_{rad}(\omega)cos(\omega t)d\omega \tag{2.7}$$

2.4.1 Mass Matrix

The mass of the 6-DOF system is calculated by equation 2.8 for translational DOFs and the moment of inertia is calculated by equation 2.9 for rotational DOFs.

$$m_{sys} = m_{floater} + m_{tow} + m_{RNA} \tag{2.8}$$

$$I_{sys} = \sum_{n\ bodies} I_n + m_n(z_{cog,n} - z_{cog,sys})^2 \tag{2.9}$$

These values can then be assembled into the mass matrix. The mass matrix is mostly diagonal with symmetry assumed across the x-z and y-z planes. The off diagonal terms come from the center of mass of the system which is a distance z_g above the point of floatation. This is assuming the WAMIT coordinate system (fig 2.4)

$$M = \begin{bmatrix} m_{sys} & 0 & 0 & 0 & m_{sys}z_g & 0 \\ 0 & m_{sys} & 0 & -m_{sys}z_g & 0 & 0 \\ 0 & 0 & m_{sys} & 0 & 0 & 0 \\ 0 & -m_{sys}z_g & 0 & I_{sys,xx} + m_{sys}z_g^2 & 0 & 0 \\ m_{sys}z_g & 0 & 0 & 0 & I_{sys,yy} + m_{sys}z_g^2 & 0 \\ 0 & 0 & 0 & 0 & 0 & I_{sys,zz} \end{bmatrix} \tag{2.10}$$

The added mass matrix, A, is the same shape as the mass matrix in terms of size and non-zero values. The added mass represents inertia added to the system as the platform moves relative to the water and accelerates a volume of water surrounding the platform. The added mass depends on the shape of the platform and is solved numerically for each DOF ($A_{i,j}$) in WAMIT.

2.4.2 Restoring Matrix

For a linear system, the mooring reaction force F_{moor} can be moved to the left hand side of the equation 2.5 and added to the restoring matrix, such that $C = C_{hydro} + C_{moor}$. The stiffness of the system can then be calculated from the stiffness of the tendons and the added hydrostatic stiffness.

The stiffness of the tendons in each DOF can be estimated using Hooke's law in linear (2.11) or angular form (2.12). A nominal displacement, Δx or angle $\Delta\theta$, is applied in the DOF of interest and the resulting restoring force is calculated based on the characteristics of the tendons. From this result the stiffness of the tendons can be derived.

$$F = k \cdot x \tag{2.11}$$

$$\tau = k \cdot \theta \tag{2.12}$$

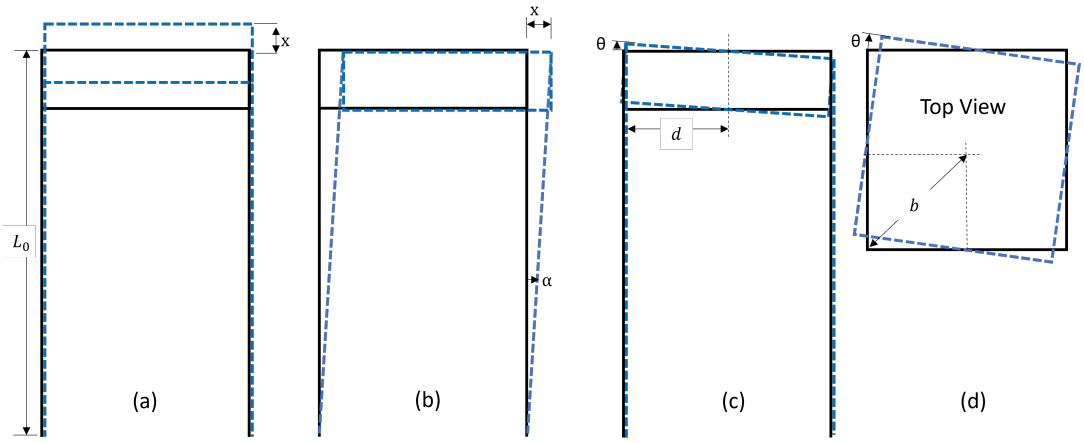

Figure 2.6: Nominal displacement applied in (a) heave, (b) surge/sway, (c) pitch/roll, and (d) yaw.

2.4.3 Heave

The tendon stiffness is calculated by applying a small nominal displacement x in heave (fig 2.6a). The tendons will stretch creating a restoring force F_x governed by the stress-strain relationship of the material. The pretension in the tendons does not affect their stiffness in heave, assuming linear-elastic behavior, and thus is not included in the calculation.

$$k_{moor} = \frac{F_x}{x} = \frac{\sigma_x A}{x} = \frac{8 \cdot \varepsilon_x E A_{line}}{x} \tag{2.13}$$

$$k_{moor} = \frac{E A_{moor}}{L_{line}} \tag{2.14}$$

As the platform moves up and down in the water, the buoyant force acting on the platform will change as the displaced volume of water changes. This creates a hydrostatic restoring 'stiffness' which can be computed as equation 2.15.

$$k_{hydro} = \rho_w g A_{float} \tag{2.15}$$

2.4.4 Surge and Sway

When the platform moves in surge or sway, the tendons are no longer vertical giving a horizontal component to their tension force as a restoring force. It is assumed that this restoring force is dominated by the pretension in the lines, and that the magnitude of the tension is constant. A small nominal surge motion of x (fig 2.6b) is used for the calculation and small angles are assumed.

$$k_{moor} = \frac{F_x}{x} = \frac{8 \cdot T_{line} \cdot sin(\alpha)}{x}, \quad \text{where} \quad \alpha = tan(\frac{x}{L_{line}}) \tag{2.16}$$

$$k_{moor} \approx \frac{T_{moor} \cdot tan(\frac{x}{L_{line}})}{x} \approx \frac{T_{moor}}{L_{line}} \tag{2.17}$$

Movement of the structure in the surge/sway DOF does not create any hydrostatic restoring force, therefore there is no added hydrostatic stiffness.

2.4.5 Pitch and Roll

In pitch and roll small angles of motion are assumed such that only vertical motion of the tendon connections are considered. The tendons will stretch or relax due to this motion, creating a restoring moment about the axis of rotation. Applying a small nominal displacement θ (fig 2.6c), the stiffness in pitch and roll can be calculated.

$$k_{moor} = \frac{\tau_\theta}{\theta} = \frac{8\frac{d \cdot sin(\theta)}{L_{line}} EA_{line} d}{\theta} \tag{2.18}$$

$$k_{moor} \approx \frac{EA_{moor} d^2}{L_{line}} \tag{2.19}$$

When the platform pitches or rolls, there is a hydrostatic restoring force which gives an additional stiffness term, k_{hydro} (eq 2.20). The first part of this term accounts for the moment generated by rotating the system where there is a vertical offset between the center of buoyancy (z_b) and the center of gravity (z_g). For the turbine plus the platform, the center of gravity is above the center of buoyancy causing a negative restoring moment. The second part of this term accounts for the shift in the center of buoyancy when tilting the platform, and is always positive.

$$k_{hydro} = mgz_g - F_b z_b + \rho_w g I_{11}^A \tag{2.20}$$

Where I_{11}^A is the second moment of the waterplane area.

2.4.6 Yaw

When the platform rotates in yaw, the tendons are no longer vertical. This gives a horizontal component to the tension force of the tendons, creating a restoring moment about the axis of rotation. It is assumed that this restoring moment is dominated by the pretension in the lines, and that the magnitude of the tension is constant. Applying a small nominal displacement θ (fig 2.6d), the stiffness in yaw can be calculated.

$$k_{moor} = \frac{\tau_\theta}{\theta} = \frac{8 \cdot T_{line} \cdot sin(\alpha) \cdot b}{\theta}, \quad \text{where } \alpha = tan(\frac{b \cdot sin(\theta)}{L_{line}}) \tag{2.21}$$

$$K \approx \frac{T_{moor} \cdot tan(\frac{b\theta}{L_{line}}) \cdot b}{\theta} \approx \frac{T_{moor} b^2}{L_{line}} \tag{2.22}$$

Movement of the structure in the yaw DOF does not create any hydrostatic restoring force, therefore there is no added hydrostatic stiffness.

2.4.7 Assembled Matrix

The stiffness terms can be assemled into the 6-DOF restoring matrix for mooring, equation 2.23, and for hydrostatic forces, equation 2.24. The off-diagonal terms in the mooring matrix are present because the mooring attachment to the platform is a distance z_{line} above the point of flotation.

$$C_{moor} = \begin{bmatrix} \frac{T_{moor}}{L_{line}} & 0 & 0 & 0 & -z_{line}\frac{T_{moor}}{L_{line}} & 0 \\ 0 & \frac{T_{moor}}{L_{line}} & 0 & z_{line}\frac{T_{moor}}{L_{line}} & 0 & 0 \\ 0 & 0 & \frac{EA_{moor}}{L_{line}} & 0 & 0 & 0 \\ 0 & z_{line}\frac{T_{moor}}{L_{line}} & 0 & y_{line}^2\frac{EA_{moor}}{L_{line}} & 0 & 0 \\ -z_{line}\frac{T_{moor}}{L_{line}} & 0 & 0 & 0 & x_{line}^2\frac{EA_{moor}}{L_{line}} & 0 \\ 0 & 0 & 0 & 0 & 0 & (x^2+y^2)_{line}\frac{T_{moor}}{L_{line}} \end{bmatrix} \tag{2.23}$$

$$C_{hydro} = \begin{bmatrix} c_{22} \\ c_{33} \\ c_{44} \end{bmatrix} = \begin{bmatrix} \rho_w g A_{float} \\ mgz_g - F_b z_b + \rho_w g I_{11}^A \\ mgz_g - F_b z_b + \rho_w g I_{11}^A \end{bmatrix} \tag{2.24}$$

All other terms of the hydrostatic restoring matrix are zeros.

2.5 Design Considerations

General TLP design considerations [11] [12] are presented in this section to provide context for assessing the TLP dynamics. Some common key criteria are listed, however the list is by no means comprehensive.

- Surge and sway natural periods should be >25s to avoid first order wave excitation.
- Heave, Pitch, and roll natural frequencies should be <5s and ideally <3.5s to avoid first order wave excitation.
- Surge motion should be limited to keep the mooring line angle at the anchors $\alpha < 5°$.
- The mooring line tendons must not yield under ultimate loads, $\frac{T_{des,max}}{A_{line}} < \frac{\sigma_y}{SF}$.
- The tendons must not go slack to maintain stability of the system, $T_{des,min} > 0$.
- Design loads on the tower and RNA must not exceed design resistances at the ultimate limit state.
- The structure shall be able to meet the expected service lifetime.
- Minimized cost per MWh.

2.6 Model Limitations and Improvements

Model limitations (and suggested improvements) are presented in this section to give a context in which to interpret the results as well as possible future work.

Higher Order Load Effects

First order or linear potential flow theory has been used to calculate the hydrodynamic loads on the TLP structure. Higher order loads were not included due to added complexity in the modelling, and considering that first order loads would be generally sufficient for the scope of this project to capture the dominant wave loading. However, the possible impact of higher order load effects should be considered and has been investigated by a literature review. This subject has been explored in research such as [13], where results from a first and second order wave load model on four different cylindrical TLP platforms were compared. It was found that the addition of second order load effects was insignificant during normal operating conditions. However, in storm conditions there was a small but noticeable effect with the second order model showing increase in pitch motion and tension variation of the tendons around 2-10%. This also lead to a small increase in the tower base fore-aft moment of less than 2%.

Other studies have also demonstrated effects of adding second order wave loads to the model, especially in surge and pitch motion. For example in [14] and [15], it is shown that the second order difference frequency, including mean drift, contributes significantly to the mean surge response and also at low frequencies near the surge natural frequency. It is not however expected that this slow surge drift motion will contribute significantly to loads on the turbine and support structure.

In pitch, the second order sum frequency forcing had an effect on the pitch motion near the pitch natural frequency. It can be expected that this contribution will be seen most significantly in load cases where the turbine is not operating. During the normal operating cases, aerodynamic damping on the rotor will damp out significant pitching resonance effects (as will be investigated further in section 5.3.2).

There was not seen any significant effect of second order forces on the platform yaw motion.

The first order simulations also may not capture a phenomena known as ringing, which has been studied in [16]. Higher order wave loads can introduce a ringing phenomena under extreme sea states for structures with a natural period in the range of 1-5 seconds. Ringing is a transient event where the structure responds at a frequency much higher than the forcing wave frequency. The effect of ringing was seen primarily in the platform pitch motion giving a higher tendon load and tower bottom bending moment. There was shown little effect on the other platform DOFs as well as on the tower top and RNA loads. The effect of ringing on the structure was found to be very dependant on the platform design (cylidrical platforms were studied), and thus further investigation should be done to explore the potential impact.

Hydrodynamics of the Platform

The buoyant force on the platform is calculated in HAWC2 using the buoyancy at MSL plus a delta in buoyancy, which is calculated by a linear relationship with the submerged platform depth. Furthermore, the wave forcing on the TLP platform was modelled in WAMIT using a nominal wave height and a linear scaling is applied in HAWC2 based on actual wave height.

The use of these linear scaling models in HAWC2 means that the program 'does not see' the top of the platform. In reality, if the sea level rises such that the platform becomes fully submerged, the change in buoyancy will no longer be linear and will flatten out. The wave forcing would also be affected for waves that peak above the platform edge.

For these simulations, it shall therefore be assumed that the TLP platform is tall enough such that the water never rises above the top of the platform. Otherwise, a more complicated nonlinear model needs to be introduced to account for the discontinuity at the top of the platform.

Tower Stiffness

All simulations were first run with a stiff tower, where the steel elastic modulus was multiplied by a factor of 10. A detailed tower design was not made in this phase so the 1st tower natural frequencies ($\sim$ 0.75 Hz) were placed well above the wind, wave, 1P, and 3P excitation forces. Later, a flexible tower was introduced (by reducing the elastic modulus) to study the impact of tower flexibility on pitch, roll, and tower bottom bending moments. A 'soft-stiff' design was used where the coupled 1st tower-pitch / tower-roll natural frequencies were placed above the 1P rotor frequency and just below the 3P. This also keeps the natural frequency out of the main wave excitation range.

3 System Natural Frequencies

System natural frequencies for the platform motion are calculated both theoretically and based on free decay tests from HAWC2 simulations. Only surge, heave, pitch, and yaw are presented here as sway is comparable to surge and roll is comparable to pitch.

3.1 Theoretical Values

The theoretical natural frequencies of the system can be calculated for each translational and rotational degree of freedom using (3.1) or (3.2). Vertically, the distance between the center of gravity z_g and the fairlead/anchor location of the tendons z_{line} is small ($z_g - z_{line} = 1.17$m), so the off-diagonal terms in the stiffness and mass matricies are neglected and the natural frequency is calculated for each platform DOF j independently.

$$\omega_{n,j} = \sqrt{\frac{k_{sys,j}}{m_{sys,j}}} \tag{3.1}$$

$$\omega_{n,j} = \sqrt{\frac{k_{sys,j}}{I_{sys,j}}} \tag{3.2}$$

Where k_{sys} consists of $k_{moor} + k_{hydro}$, and the mass/inertia of the system (m_{sys}, I_{sys}) includes the added mass.

The numerical values for mooring stiffness and hydrodynamic stiffness are calculated based on equations 2.10, 2.23, and 2.24. The added hydrodynamic mass is taken from WAMIT at the expected natural frequency of the system. These values are presented in tables 3.1 and 3.2.

	120m	**250m**	**1000m**	
	K_{moor}	K_{moor}	K_{moor}	Unit
Heave	814	394	99.1	MN/m
Surge	1.21	0.59	0.15	MN/m
Pitch	354	171	51.0	GN/rad
Yaw	1.06	0.51	0.15	GN/rad

Table 3.1: Calculated values for mooring stiffness for depths of 120m, 250m, and 1000m.

	K_{hydro}	M_{added}
Heave	21.05 MN/m	28.6e3 kg
Surge	-	19e3 kg
Pitch	-314 MN/rad	2.46e6 kgm^2
Yaw	-	1.2e6 kgm^2

Table 3.2: Added mass and hydrostatic stiffness, all depths.

The theoretical values for the natural frequencies of the system are presented in table 3.3.

	120 m Depth	250m Depth	1000m Depth
Surge	36.0	51.7	103
Yaw	16.5	23.7	47.3
Heave	1.53	2.17	4.03
Pitch	1.82	2.61	5.22

Table 3.3: Theoretical natural periods of floater motion, in seconds.

3.2 HAWC2 Simulation and Results

Free decay simulations were run for each DOF in HAWC2 on the TLP model with a stiff tower and flexible blades. In these simulations an arbitrarily defined force (table 3.4) was applied to the center of flotation and held until steady state was reached, then released allowing free decay. The damping forces included are radiation damping and structural damping of the tendons. The natural frequency/periods of the motion are then calculated from the peak of the PSD plots for each simulation. The results are presented in figure 3.1 and table 3.5 as natural frequencies [Hz] and table 3.6 as natural periods [s].

DOF	Applied Force	Unit
Surge	2.5	[MN]
Yaw	4.5	[MNm]
Heave	50	[MN]
Pitch	450	[MNm]

Table 3.4: Forces applied at the point of floatation for decay tests.

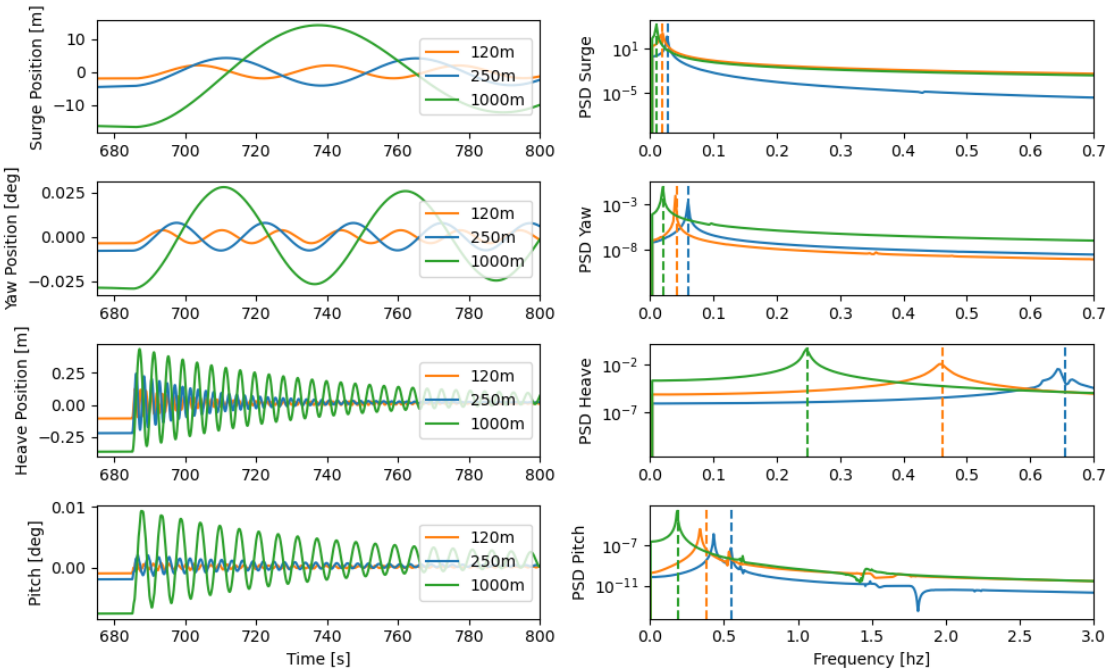

Figure 3.1: Free decay tests and PSD comparing response at 120m, 250m, and 1000m water depth. Structural and radiation damping included, stiff tower and flexible blades.

	120 m Depth		250m Depth		1000m Depth	
	Theory	HAWC	Theory	HAWC	Theory	HAWC
Surge	36.0	37.5	51.7	50.0	103	100
Yaw	16.5	16.7	23.7	25.0	47.3	50.0
Heave	1.53	1.55	2.17	2.17	4.03	4.05
Pitch	1.82	2.33	2.61	2.97	5.22	5.46

Table 3.5: Natural periods of floater motion in seconds, including both simulated and theoretical values. Stiff tower and flexible blades.

	120 m Depth		250m Depth		1000m Depth	
	Theory	HAWC	Theory	HAWC	Theory	HAWC
Surge	0.028	0.027	0.019	0.020	0.010	0.0097
Yaw	0.061	0.060	0.042	0.040	0.021	0.020
Heave	0.65	0.65	0.46	0.46	0.25	0.25
Pitch	0.55	0.43	0.38	0.34	0.19	0.18

Table 3.6: Natural frequencies of floater motion in Hz, including both simulated and theoretical values. Stiff tower and flexible blades.

The theoretical values for surge, yaw, and heave natural periods agree well with the simulated values from HAWC2, within around $\pm$5%. In pitch however, the HAWC2 natural period is longer than predicted period for all water depths and most notably at 120m there is a difference of 28%. Upon further investigation, this is seen to be a result of coupling between tower/blade bending and floater pitch motion. In the theoretical calculation the tower and blades were assumed to be rigid. The impact of tower flexibility on the pitch natural frequency was explored further using the stiff tower (E= 2000 GPa), a soft-stiff tower (E = 250 GPa), and a rigid structure where the material stiffness was increased so much that any deflections were negligible. The results are presented in table 3.7

			Pitch-Tower FA Period		
Tower	**Blades**	**1st tower FA**	**120m**	**250m**	**1000m**
Soft-stiff	Flex	3.87	4.17	4.55	6.38
Stiff	Flex	1.34	2.33	2.97	5.46
Rigid	Rigid	N/A	1.87	2.65	5.26
Theory		N/A	1.82	2.61	5.22

Table 3.7: 1st Tower FA natural period and coupled Pitch-Tower FA natural period for various tower and blade stiffness.

Running the pitch decay test again with a rigid tower and blades gives a natural period which agrees with the theoretical values within $\pm$3% for all depths.

Furthermore, it is seen that when the stiffness of the tower is reduced to the soft-stiff design, the natural period in Pitch-Tower FA increases compared to the rigid tower. The natural period is also always longer than the 1st tower fore-aft period alone. The TLP mooring and tower act like a coupled system of springs with the RNA mass at the top and

platform in the middle. Like springs added in parallel, the overall stiffness of the system is lower than that of the tower or mooring alone, and will be reduced if the stiffness of either component is reduced (either by lowering the tower stiffness or increasing the tendon length). The tower stiffness did not have any important effect on the natural frequencies in surge, heave, and yaw.

An example of the natural frequencies for each mooring depth is presented in figure 3.2 together with normalized wind and wave forcing spectrums (for a range of wind speeds) and the range of possible 1P, 3P, and 6P rotor speeds. There are three natural frequency lines for each DOF (heave, yaw, pitch and surge) representing the three platforms, with the lowest frequency for each DOF corresponding to the 1000m platform and the highest corresponding to the 120m platform.

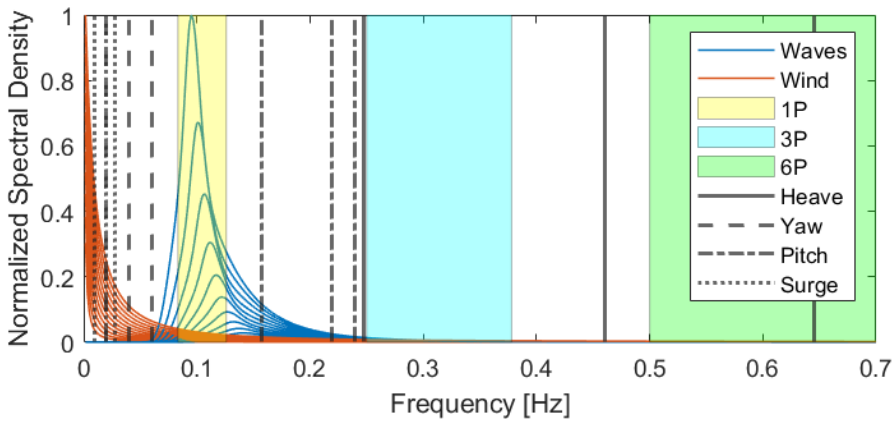

Figure 3.2: Forcing and natural frequencies for normal operating conditions, flexible tower.

It can be observed that the surge and yaw natural frequencies overlap with higher wind frequencies and fall below the peak wave forcing spectrum. Therefore, it can be expected that there may be some resonant excitation for these DOFs by the wind, especially for the 1000m platform. The heave natural frequencies are above any significant wave forcing and therefore they are not expected to be significantly excited by the 1st order wave loads. The 3P/6P rotor frequencies do not excite the structure in heave and thus are not relevant to consider here. Finally, the Tower FA-Pitch natural frequencies lie between the peak wave forcing and the 3P rotor frequency. The 1000m platform frequency overlaps with the upper end of the wave forcing spectrum, as does the 250m platform to a lesser extent. Also, the 120m platform approaches the lower end of the 3P rotor frequency. Therefore, resonant effects in pitch will be of possible concern for all mooring depths.

4 Mooring and Platform Stability

4.1 Buoyancy and Pretension

One of the defining characteristics of the TLP is that it is stabilized by the excess buoyancy of the platform and the resulting mooring line tension.

Sea Level Changes

The total mooring tension at steady state equilibrium can be calculated as a difference between the buoyant force and gravitational force on the platform as in equation 4.1.

$$T_{moor} = \rho_w g A_{float} D - m_{sys} g \tag{4.1}$$

Where A_{float} is the cross sectional area of the floater (constant) and D is the draft.

Figure 4.1 shows how the mean tension in the tendons varies with raised or lower sea level which affects the draft length. The slope of the line is defined by the hydrostatic stiffness in heave (eq 2.15). Where sea level is equal to 0m (MSL), the tendon force is equal to the design pretension of 18.5 MN for each tendon. If the still water level varies from this position, for example with tides or a storm surge, the mean tension in the tendons will follow. Just the variation from HAT (+1.81m) to LAT (-1.81m) ref [3] will lead to an change of $\pm$26% of the MSL pretension value. As a large wave passes the change in buoyancy force is also governed by the hydrostatic stiffness, although the change in mooring tension is more complicated due to inertia and dynamics of the system.

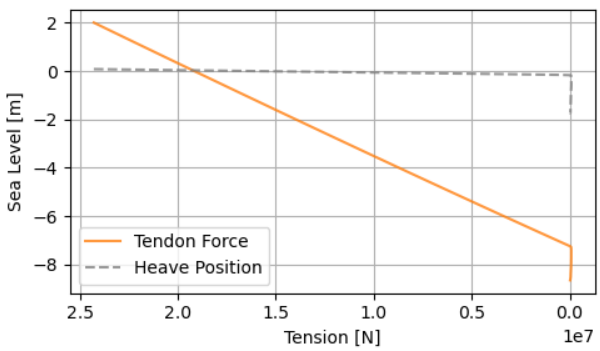

Figure 4.1: Mean tension (at platform level) and heave position versus sea level, with reference to MSL. 120m depth, no forcing.

Eventually, if the sea level drops to $\sim$ 7.1m below MSL, there is no longer an excess buoyancy on the platform (the gravity force equals the buoyant force) and the pretension in the tendons is lost. After pretension is lost the tendons go slack and do not carry any compressive load. While this is not entirely accurate and comes as a consequence of modelling the tendons as cables rather than beams, the theoretical compressive load the tendons can bear is negligible. Considering a pinned connection at the seabed, the platform will drift rather than to put the tendons into compression.

Another observation from figure 4.1 is that the platform motion in heave is very small compared to the change in sea level, which is due to the high stiffness of the steel mooring lines. From MSL of 0m to MSL of -7.1m where pretension is lost, the platform will move in heave just -0.181m representing the change in tendon length.

It should be noted that much larger heave motions will be recorded in simulations without loss of pretension, which is due to a combined heave-surge motion where the mooring lines are no longer vertical.

Impact of Mooring Depth
For the deeper 250m and 1000m platforms, the tendon force will vary the same as the orange line in figure 4.1 because the hydrostatic stiffness of the platform is unchanged. However, the deeper water platforms will move more in heave than the 120m platform (dashed gray line). Given that the tendons have the same cross section area, the strain value ε will be equal among all depths. However, because the initial tendon length L_0 is not the same, the magnitude of ΔL must increase proportional the mooring depth; $\varepsilon = \frac{\Delta L}{L_0}$.

4.2 Pitch Stability

The pretensioned mooring lines play a critical role in stabalizing the platform against overturning moments, such as the thrust force on the rotor and wave loads. In the free floating condition without mooring, the platform is not stable in pitch with a hydrostatic stiffness close to zero (<0.1% of the moored stiffness, calculated by equation 2.20 setting F_b=F_g and considering the platform would raise ~7.1m compared to the moored condition).

In figure 4.2, a steadily increasing moment was applied to the platform in pitch, and the mooring line tension on the 'upwind' tension side and 'downwind' compression side of the platform was recorded. The restoring moment comes from the difference in tension on the upwind and downwind mooring lines, multiplied by the horizontal moment arm between the fairlead anchors.

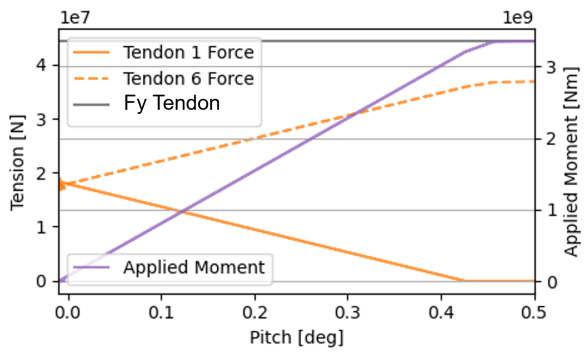

Figure 4.2: Mooring Line tension and pitch angle for applied pitch moment to the 120m platform. Tendon D1 is 'downwind' of the moment and tendon U6 is 'upwind' of the moment.

The high stiffness in pitch is evident in this plot, where the turbine only pitches 0.42° before tension is lost in the downwind tendons. This occurs at an applied moment of 3.2 GNm, which is ~7.75 times the moment caused by peak rotor thrust (2.75 MN) applied at a hub height of 150m.

The deeper water platforms can sustain the same maximum overturning moment before loss of tension as the pretension value and distance between the tendons are equal. However, as the stiffness in pitch scales with the inverse of mooring length, the deeper water platforms will experience more pitch motion under the same moment. For the 250m platform, loss of tension would occur at a 0.88° pitch angle and for the 1000m platform this is at 3.5°.

5 Wind and Wave Loads

In order to better understand the basic motion of the turbine and floater structure, simulations are run in HAWC2 under cases with steady wind, step wind, and regular waves.

5.1 Steady Wind

5.1.1 Theory

Steady wind is applied with no turbulence, no yaw misalignment, no waves, and no wind shear. Theoretical values for platform motion can be calculated based on the wind speed-thrust and wind speed-rotor torque performance curves for the 15MW RWT [1].

The expected displacement in surge can be calculated with Hooke's law (eq 2.11) using the rotor thrust force and the calculated stiffness in surge (eq 2.17). Similarly, the expected roll angle can be calculated with (eq 2.12) using the rotor torque and calculated stiffness in roll 2.19 (incl hydrostatic stiffness).

There is no (significant) forcing from the wind applied in heave, thus the theoretical deflection in heave is calculated based on geometry of the system. Assuming that the floater moves along a circular arc with constant radius L_{tndn}, the displacement in surge can be used to calculate a corresponding displacement in heave. A correction for stretching of the tendons based upon the hydrostatic restoring force of the platform in heave is then applied to the displacement, however this correction is minimal because the system is very stiff in heave.

Finally, the theoretical value for pitch angle can be computed with (eq 2.12) using the moment applied in pitch from the thrust force on the rotor (eq 5.1) and the calculated stiffness in pitch (eq 2.19). There is also a contributing factor to the expected pitch angle due to the offset of the RNA center of gravity ($x_{COG,RNA}$) in the upwind direction.

$$M_{pitch} = -T_{rotor} \cdot H_{hub} + m_{RNA} \cdot g \cdot x_{COG,RNA} \tag{5.1}$$

5.1.2 Simulation Results

Steady wind simulations were run for all depths at a range of wind speeds from 3 m/s to 25 m/s with no turbulence or wind shear (fig 5.1).

The results generally agree with expectations and with the theoretical calculations. In surge, heave, and pitch the displacement resembles the thrust curve of the wind turbine; increasing until rated wind speed and then decreasing again once the blades pitch to limit turbine loads and power output. The 1000m platform experiences the largest displacement in all cases, followed by the 250m platform and the 120m platform. This is because the stiffness for each DOF scales with the inverse of depth so the static load will give larger displacements in a less stiff system. There is little change in roll angle for all simulations because the thrust force does not generate any roll moment. Small variation in roll comes from the aerodynamic torque on the rotor which is transferred to the structure.

Such a significant change in yaw angle and sway position above rated wind speed was not expected for the steady wind case because there is no turbulence to create uneven loading on the rotor. This was found to be influenced by the tilt angle of the rotor, which

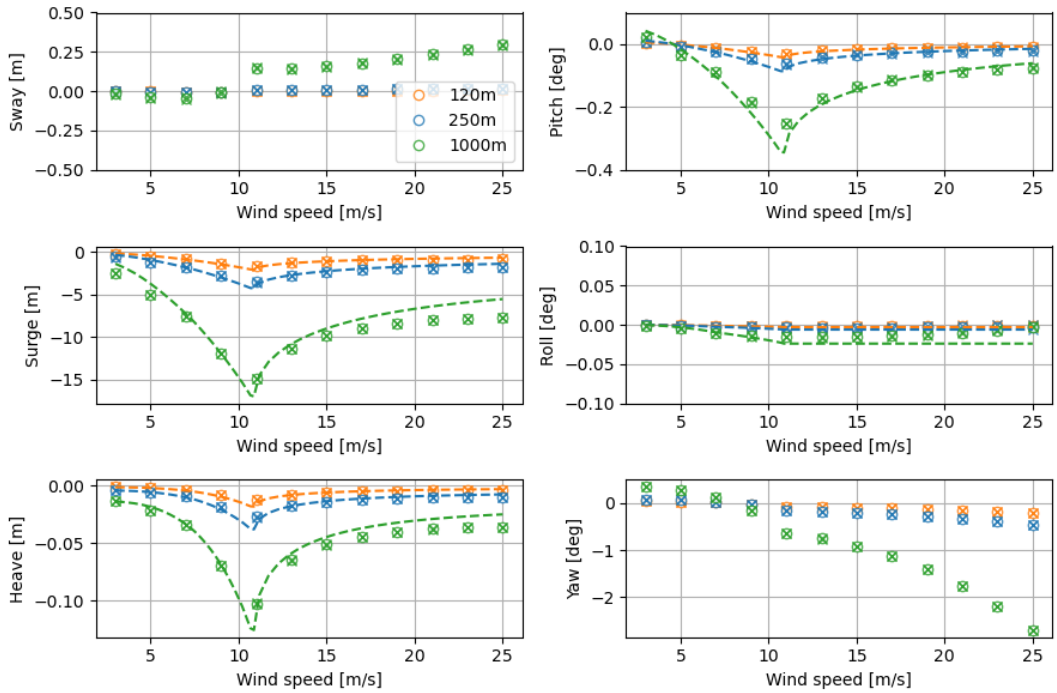

Figure 5.1: Floater position under steady wind ranging from 3 to 25 m/s. Min/max/mean are shown as 'x', 'o', 'x' to confirm steady state was reached. Theoretical values are added with a dashed line. Flexible blade, stiff tower, no shear.

is set to 6°. The rotor tilt led to a difference in AoA as a blade swings downward or upward, as illustrated by the velocity triangle sketch (fig 5.2). The figure shows a downward moving blade at a 90° angle from vertical and an upward moving blade at 270°, not considering any pitching of the blade or induced velocity. Note that the controller does not have individual blade pitching.

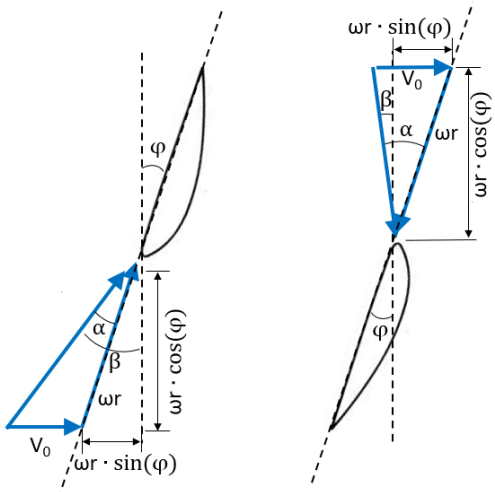

Figure 5.2: Velocity triangle of blade at 90° (left) and 270° (right) with AOA α, tilt angle ϕ, rotational speed ω, and r as the radial distance from the hub to the blade cross section.

The AoA for each case can be calculated as:

Downward Moving Blade

$$\beta = atan\frac{\omega r \cdot sin(\phi) + V_0}{\omega r \cdot cos(\phi)} \quad (5.2)$$

$$\alpha = \beta - \phi \quad (5.3)$$

Upward Moving Blade

$$\beta = atan\frac{V_0 - \omega r \cdot sin(\phi)}{\omega r \cdot cos(\phi)} \quad (5.4)$$

$$\alpha = \beta + \phi \quad (5.5)$$

Assuming, for example, an incoming wind $V_0 = 11$ m/s, a tilt angle of $\phi = 6°$, no pitch angle, a rotational speed of $\omega = 0.79$ rad/s, and a point on the blade at $r = 72$ m. The downward moving blade has a slightly larger AoA with $\alpha = 11.1°$ compared with $\alpha = 10.7°$ for the upward moving blade. The magnitude of difference in AoA also trends to increase as the tilt angle increases or the incoming wind speed V_0 increases.

For the steady wind case, this can be illustrated by plotting the AoA and lift coefficient versus angular position of the blade (fig 5.3). When there is a 6° tilt (left plots), the AoA and Cl is clearly more asymmetrical than for no tilt. This in turn generates uneven loading on the rotor, which causes the platform to move in yaw and sway.

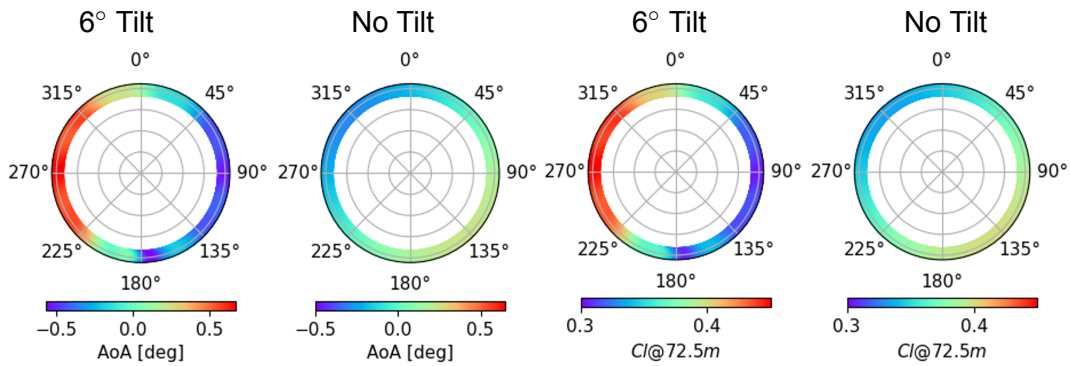

Figure 5.3: AoA and Cl at r=72.5m for rotor with 6° tilt and tower shadow (left) and no tilt no shadow (right). 25m/s steady wind, no shear.

When running DLCs it was seen that this 'tilt' effect was enough to offset the mean yaw by up to 3.5° for the 1000m platform at high wind speeds, however the range in yaw motion did not change significantly as this was mostly driven by turbulence in the wind.

5.2 Step Wind

The DTU basic controller which has been tuned to a floating wind turbine is used to control the blade pitch angle and generator torque. A short analysis of the controller properties was performed by simulating the response to a step wind, as in figure 5.4. Note that detailed tuning of the controller is not in scope of this report.

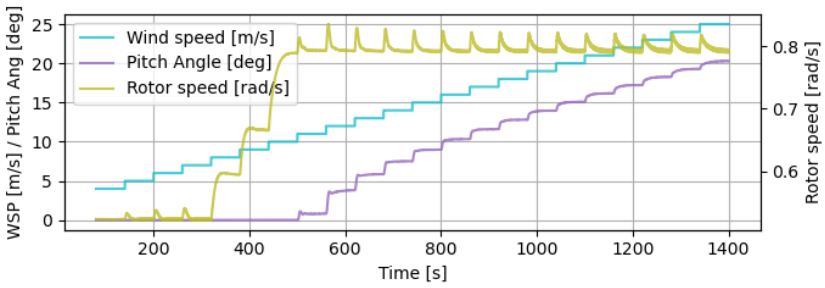

Figure 5.4: Response of controller to step wind from 4 m/s to 25m/s in 1 m/s increments.

Below 11 m/s wind, the goal of the controller is to maintain optimal CP tracking to maximize the power output. This is done by controlling the rotor speed through the generator torque to maintain the design tip speed ratio. Above rated wind speed, the controller functions to limit the turbine loads and power output of the generator. This is done by controlling the rotor speed with a constant generator torque, and also by pitching the blades to lower the angle of attack. This will in turn lower the aerodynamic lift force and limit the rotor torque.

Zooming in on a single time step above rated wind speed, it is possible to analyze details of the controller response.

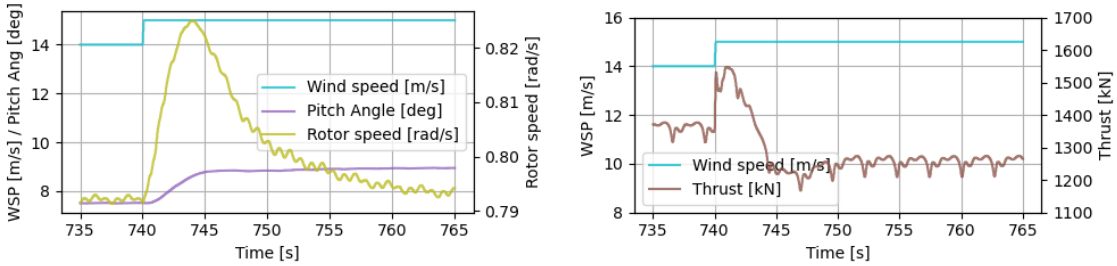

Figure 5.5: Controller response to a step wind from 14 m/s to 15 m/s.

Because a constant torque controller is used, there is no increase in generator torque to offset the increase in aerodynamic torque once the wind speed increases. This means that the rotor will initially speed up as a reaction to the increased wind speed. Once the blades begin to pitch, the aerodynamic torque is reduced so that the rotor speed comes back down to its rated value. The blade pitching is slightly delayed, and takes about 5 seconds to reach within $\pm 2\%$ of the final pitch angle.

On the right side of figure 5.5, the rotor thrust is plotted for the same single wind speed step. There is a sharp jump in thrust as the suddenly increased wind speed increases the upstream air pressure on the rotor. Once the blades pitch to reduce aerodynamic loads, the rotor thrust force will also decrease until levelling out at a value that is below the thrust at the previous step. It takes approximately 3.5 seconds for the rotor thrust to drop below the previous steady state value.

The controller response speed has important implications on the motion of the floating turbine operating above rated wind speed. When the turbine moves forward or backward, the relative wind speed at the rotor will increase or decrease. If the controller acted instantaneously, the rotor thrust would decrease with forward motion, and increase with backward motion, thereby further exciting the movement. For a slow controller, the opposite effect would be seen and aerodynamic damping would limit the motion of the turbine.

The controller used for these simulations is able to damp high frequencies motion near the pitch natural frequency ($\sim$ 0.16 - 0.24 Hz) when operating above rated wind speed because the frequency of motion is sufficiently higher than the controller response. However lower frequency motion driven at the wave forcing frequency ($\sim$ 0.6 - 0.1 Hz) is slow enough that the controller has sufficient time to react and as a result the thrust force adds to fore-aft motion (above rated wind speed).

5.3 Regular Waves

5.3.1 Theory

To illustrate the effects of wave forcing on the structure it is useful to first consider 1 DOF spring-mass-damper system subject to a sinusoidal forcing. The equation of motion for

this system is well known as:

$$m\ddot{x} + c\dot{x} + kx = f_0 cos(\omega t) \tag{5.6}$$

The response of the structure is largely dependant on the forcing frequency relative to the system natural frequency, ω_0. In the case of $\omega \ll \omega_0$, the slow forcing means that the acceleration and velocity of the mass is low and thus the displacement/stiffness term dominates. Conversely, for $\omega \gg \omega_0$, the acceleration of the mass is high and the displacement is small so that the inertia term dominates the response. Meanwhile, at resonance the stiffness and inertia forces cancel out while the damping term dominates. This is illustrated in figure 5.6 and equation 5.7.

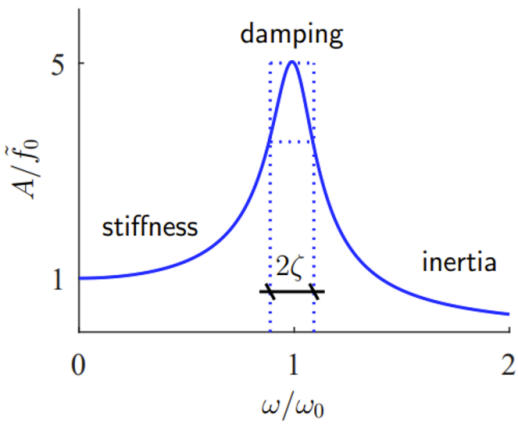

Figure 5.6: Dynamic amplification of a SDOF system with forcing frequency ω and natural frequency ω_0 [17].

$$A \simeq \begin{cases} \frac{f_o}{k} & \text{for} \quad \omega \ll \omega_0 \\ \frac{f_o}{\omega c} & \text{for} \quad \omega \simeq \omega_0 \\ \frac{f_o}{\omega^2 m} & \text{for} \quad \omega \gg \omega_0 \end{cases} \tag{5.7}$$

Applying this theory to each DOF of the system it can be anticipated whether the response of the system will be influenced most by its stiffness, inertia, or damping. Figure 5.7 illustrates the spectral density of a typical wave climate for Buchan Deep relative to the TLP system natural frequencies.

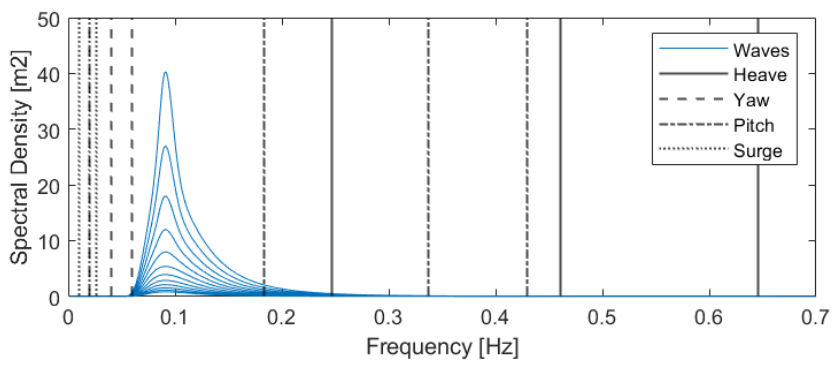

Figure 5.7: System natural frequency (120m, 250m, and 1000m) and spectral density of waves based on Jonswap spectrum [3] table 3.7 for wind speeds 3 to 25 m/s. Stiff tower. The natural frequency deeper mooring is always the lowest.

The surge natural frequency for all water depths is far below the wave forcing frequency, and therefore it is expected that the surge response will be dominated by the inertia of the

system. Because the mass of the TLP platform has been held constant for all depths, it is not expected that the surge response to waves will vary significantly between the depths.

On the other hand, the heave and pitch natural frequencies fall above the wave forcing frequency range, meaning that the response in these DOFs will be stiffness dominated. Given the lower stiffness in heave and pitch for the deeper water platforms, a larger response to waves will be expected for these DOFs. Furthermore, there may be some concerns with resonance in heave and pitch at 1000m as the natural frequencies begin to overlap with the wave forcing spectrum.

The wave loading does not apply a significant force in yaw so this is not investigated further in this section.

5.3.2 Simulation Results

Regular waves are applied to the structure with no aerodynamic loading. The wave direction is aligned so that it is perpendicular to the leading edge of the platform. In order to focus on the steady state motion of the platform, the rotor is made to be stiff and locked. A constant wave height of 5m is used, with a period ranging from 0.1s to 200s over 45 increments. All simulations were run for a time of 1000 seconds with a transient period of 500 seconds discarded, leaving 500 seconds after steady state was reached. The simulations were run with the stiff tower (fig 5.8) and also for the flexible tower with the pitch DOF shown in figure 5.9. The peak-peak platform response amplitude is plotted for surge, heave, and pitch together with the excitation force from the waves. There was no noticeable difference in the surge and heave between the flexible and stiff tower, so only the stiff tower results are presented.

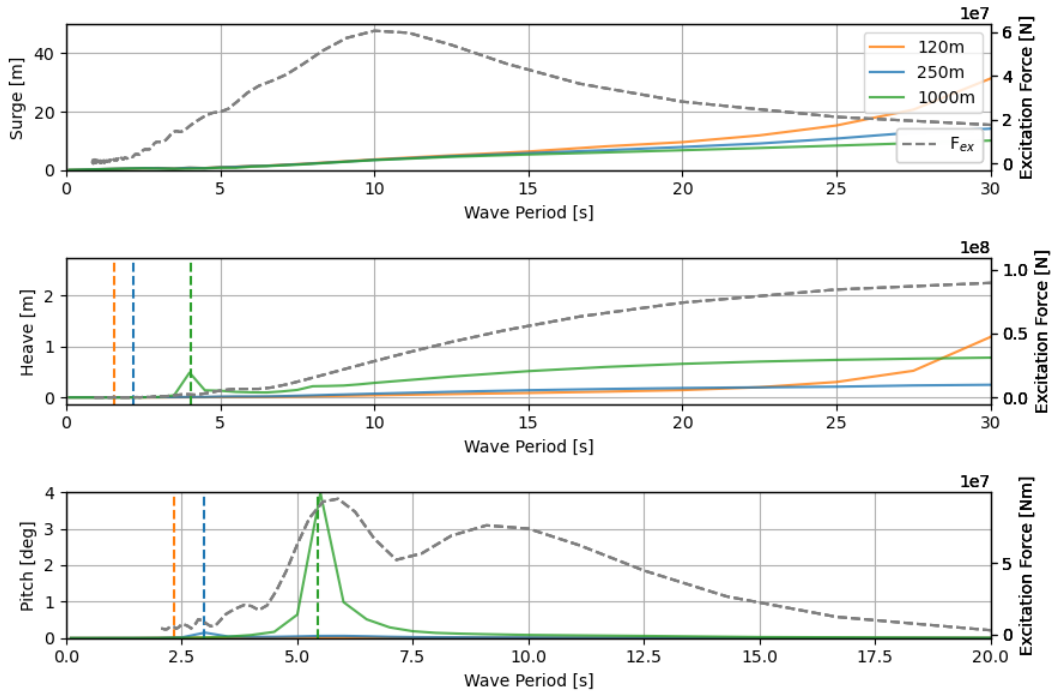

Figure 5.8: Range of motion in Surge, Heave, and Pitch subject to 5m waves at a range of wave periods, stiff tower.

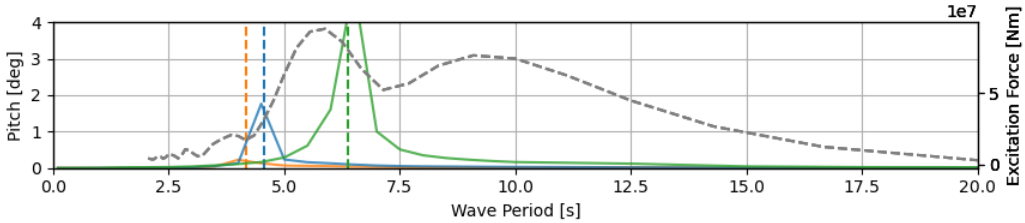

Figure 5.9: Range of motion in Pitch subject to 5m waves at a range of wave periods, flexible tower.

Surge
In surge, the response amplitude of the platform is similar between all depths for a wave forcing period below 20 seconds. This occurs because the response is inertia dominated, due to the long natural period of surge motion for all depths (>35s). The excitation force on the platform peaks at a wave period around 10s, however the response amplitude continues to increase at higher wave periods as the forcing comes closer to the natural period.

Heave
In heave, the response amplitude of the platform is largest for the 1000m water depth where stiffness in heave is the lowest. There is a small peak around the heave natural period ($\sim$ 4 sec), and for longer wave periods the response increases together with the excitation force. For the 120m platform, it can also be noticed that the peak-peak heave amplitude begins to significantly increase for wave periods above 25s. This is caused by a corresponding increase in surge motion and platform 'set-down', where the platform moves along an arc path.

Pitch
In pitch, the 120m platform is very stiff and experiences relatively small motion, showing a peak where the excitation force is the highest around T=6 seconds. A similar behavior is seen for the 250m platform, with an additional small peak at the pitch natural period ($\sim$ 3 sec). However, the pitch excitation force is low at 3 seconds limiting the response in resonance. The 1000m platform is the least stiff in pitch, hereby experiencing the greatest motion. Notably, at the resonant period ($\sim$ 5.5s) the pitch excitation force also peaks, leading to a high response in resonance. The largest peak-peak pitch amplitude is around 4 degrees. Using a flexible tower compared to a stiff tower increases the Tower FA-Pitch natural period for all depths and as a result the dynamic amplification at resonance increases.

Surge-Heave
Another way to visualize the dynamics of the floater is to plot the 'side-view' surge-heave response of the platform over time. This is also a way to check that the response has reached steady state and is not drifting. This is done in figures 5.10 for 120m, 250m, and 1000m depths from left to right.

For the 120m platform, the motion forms a flattened half-oval or boomerang shape, while for the deeper 1000m platform the motion forms a rounded oval shape. As the platform moves fore or aft in surge it is pulled down in heave by the stiff tendons to follow an arc path. Thus the response for 120m has period components at the wave forcing period and half the forcing period. For the deeper platform, this effect becomes less noticeable for the same relative surge motion because the arc radius is much larger. Thus the heave response is dominated mostly by the wave forcing with less influence from the surge motion.

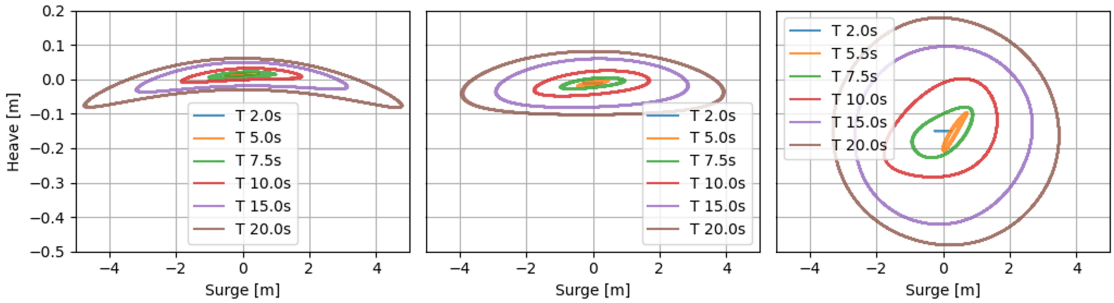

Figure 5.10: Surge and heave motion of 120m (left), 250m (center), and 1000m (right) platforms.

5.4 Regular Waves and Steady Wind

It is of interest to consider the platform response again with a combination of wave forcing and a steady wind, to study the effect of rotor aerodynamics on the peak response amplitudes. For example, if the controller is well tuned, the aerodynamics on the rotor should provide damping to limit the peak pitch motion. In figure 5.11 the 1000m regular wave simulations for the flexible tower are repeated again including a steady 15m/s wind.

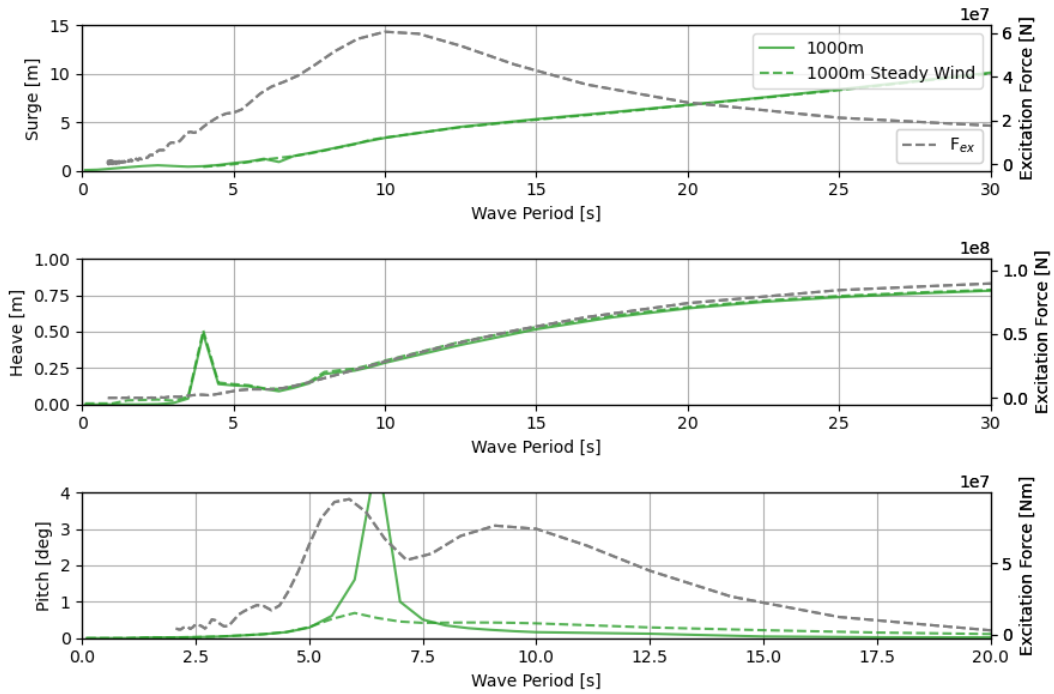

Figure 5.11: Peak-peak amplitude of motion for 1000m platform subject to 5m waves at a range of wave periods, flexible tower. With and without 15m/s wind.

There is minimal effect on the range of surge motion by adding the steady wind. The mean rotor thrust force at 15m/s wind, around 1.25 MN, is at least an order of magnitude lower than the excitation force from the waves. Therefore, the changes in thrust force as the rotor moves in surge do not have a significant impact on the range of motion for these simulations. The heave motion is similarly unaffected by the applied wind as the thrust force does not act directly on the heave DOF.

On the other hand, it is shown that the peak-peak pitch amplitude is limited to less than 0.7° with the steady wind applied. When excited at resonance, the response amplitude is governed by the damping and therefore the aerodynamic damping from the rotor has a significant effect. Once the wave period increases beyond the natural period in pitch, however, it is seen that the pitch response with wind is increased slightly compared to the pitch response without. In this case, the controller has time to react to the pitch motion so that the change in thrust force will amplify the motion instead of damping it.

6 Dynamic Response to Environmental Conditions: DLCs 1.1, 1.6, 6.1

Three design load cases, DLC1.1, 1.6, and 6.1, were selected to investigate the TLP system dynamics under a variety of operating conditions [2]. DLC1.1 represents power production under normal environmental conditions, DLC1.6 simulates power production under a severe sea state, and DLC6.1 presents the most extreme sea and wind conditions where the turbine is shut down for production.

These DLCs are used to investigate the ultimate loads on the RNA and support structure, as well platform motion and controller performance at different water depths.

6.1 Simulation Design

6.1.1 DLC 1.1 Normal Power Production

The simulation properties for DLC1.1 are described in table 6.1.

Parameter	Setting
Length	600s (800s with 200s transient discarded)
Wind	3-25 m/s with steps of 2 m/s
Yaw	0 deg
Turbulence	Normal, Mann Turbulence Box, 6 seeds per wind speed
Shear	Power Law, exponent = 0.14
Waves	NSS, Unidirectional, Irregular Airy, Jonswap, 1500 coef, new seed per simulation
Alignment	Unidirectional
Tide	None
Current	None
Gusts	None
Fault	None
Simulations	12 wsp · 6 seeds = 72

Table 6.1: DLC1.1 Simulation Setup

Wave Climate

The wave climate is based upon the metocean design basis for Hywind Buchan Deep [3]. Hindcast data for the site is used to fit an exponential function (eq 6.1) correlating significant wave height (H_s) to the 1-hr mean wind speed at hub height (U_{hub}). A scaling is applied to account for wind shear effects between hub height at 150m and the hindcast wind data measured at 100m.

$$H_s = 0.719 \cdot \text{exp}(0.0832 \cdot U_{hub} \underbrace{(\frac{100m}{150m})^{0.14}}_{\text{wind shear}}) \tag{6.1}$$

This function is applied to each simulated mean wind speed to obtain the significant wave height for that simulation.

The peak wave period for each significant wave height is interpolated based on table 7.3 in [3], using the mean value for the period. See also appendix C table C.2.

The peak enhancement factor γ used in the Jonswap spectral model is calculated based on H_s and T_p using equation 6.2 [3].

$$\gamma = max\left[1.0,\ 42.2\frac{2\pi {H_s}^{6/7}}{gT_p^2}\right] \tag{6.2}$$

The forcing and natural frequencies for DLC1.1 are visualized in figure 6.3. The natural frequencies for 120m, 250m, and 1000m mooring are included, with the lowest natural frequencies for each DOF corresponding to deeper water.

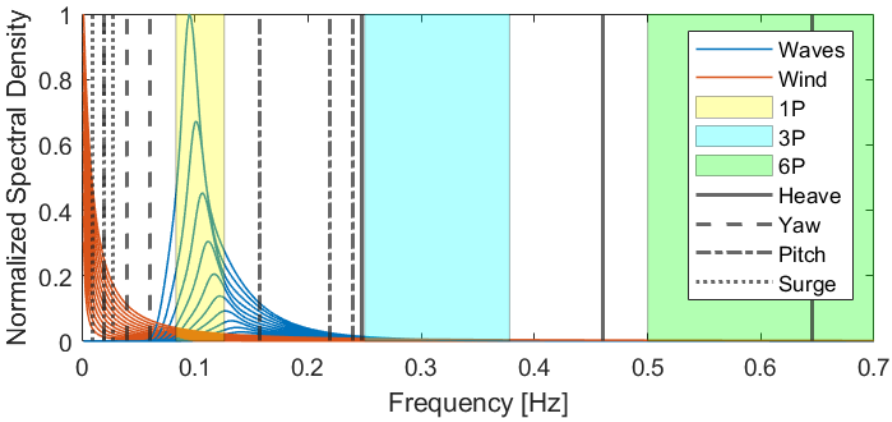

Figure 6.1: Forcing and natural frequencies for DLC1.1. Flexible Tower.

6.1.2 DLC 1.6 Operation in Severe Sea State

The simulation properties for DLC1.6 are described in table 6.2.

Parameter	Setting
Length	3600s (3900s with 300s transient discarded)
Wind	3-25 m/s with steps of 2 m/s
Yaw	0 deg
Turbulence	Normal, Mann Turbulence Box, 6 seeds per wind speed
Shear	Power Law, exponent = 0.14
Waves	SSS, Irregular Airy, Jonswap, 1500 coef, new seed per simulation
Alignment	Unidirectional
Tide	HAT, MSL, and LAT
Current	None
Gusts	None
Fault	None
Simulations	12 wsp · 6 seeds = 72

Table 6.2: DLC1.6 Simulation Setup

Wave Climate

The wave climate is modeled as the severe sea state with a return period of 50 years, see table 6.3. The hindcast data [3] was used together with the IFORM method [18] to obtain

the significant wave height H_{s50} at each simulated mean wind speed.

One individual extreme stream function wave is embedded into each 1-hour simulation. The individual extreme wave height and period are calculated based on [2] (eq 10 and 11) as shown in table 6.3.

The simulations are designed to cover the normal water level range, which is from highest astronomical tide (HAT) to lowest astronomical tide (LAT), measured with reference to mean sea level (MSL). For each wind speed, two of the seeds are run at HAT, two are run at LAT, and two are run at MSL.

Ocean Climate												
V_{hub} Mean	3	5	7	9	11	13	15	17	19	21	23	25
Hs_{50}	4.6	5.4	5.8	6.4	6.8	7.2	7.6	7.9	8.3	8.7	8.9	9.3

HAT = 1.81 $H_{50} = 1.86 Hs_{50}$

LAT = -1.81 $T_{50} = 12.7\sqrt{Hs_{50}/g}$

Table 6.3: Wave Heights, Period, and tides derived from [3].

The forcing and natural frequencies for DLC1.6 are visualized in figure 6.3. Compared to DCL1.1, the wave forcing frequencies are shifted to lower frequencies as the larger waves also have longer periods. The wind forcing is unchanged from DLC1.1.

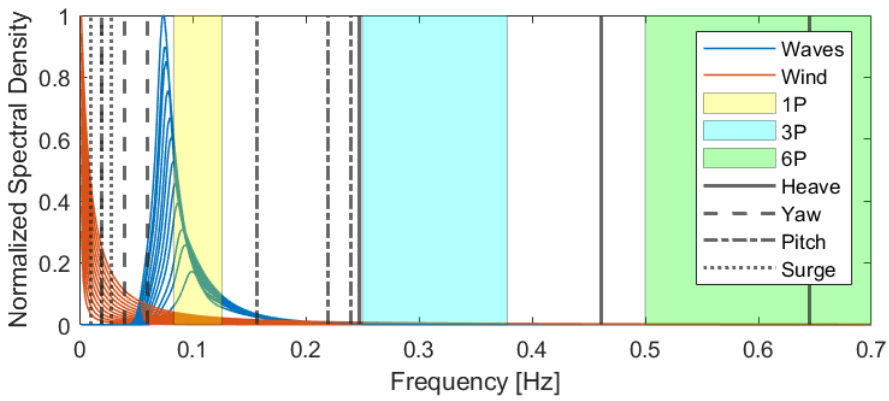

Figure 6.2: Forcing and natural frequencies for DLC1.6. Flexible tower.

6.1.3 DLC 6.1 Survival State

The simulation properties for DLC6.1 are described in table 6.4.

The wave climate (table 6.5) is modeled as the extreme sea state with a return period of 50 years (see table C.2 appendix C). One individual extreme wave is embedded into each 1-hour simulation based on the 50 year design wave (see table C.3 appendix C).

The simulations were initially run to cover the extreme water level range, which is from highest still water level (HSWL) to lowest still water level (LSWL), measured with reference to mean sea level (MSL). Two of the seeds were run with HSWL, two at MSL, and two at LSWL for each wind-wave alignment.

The simulations at LSWL, however, led to loss of tension in the tendons when an large wave passed which gave a spike in loads as the tension returned. The LSWL of -3.06m, which is taken as combination of LAT plus a negative value of the positive storm surge,

Parameter	Setting
Length	3600s (3900s with 300s transient discarded)
Wind	V_{50} = 41.8 m/s
Yaw	0 deg
Turbulence	TI=0.11, Mann Turbulence Box, 6 seeds
Shear	Power Law, exponent = 0.11
Waves	ESS, Irregular Airy, Jonswap, 1500 coef, seed per simulation
Alignment	Unidirectional and 30 ° wind-wave misalignment
Tide	HSWL, MSL, and LSLW
Current	None
Gusts	None
Fault	None
Operation	Shut down, idle
Simulations	1 wsp · 6 seeds · 2 alignments = 12

Table 6.4: DLC6.1 Simulation Setup

is very conservative and unlikely to occur. Due to instability in the results, only results for MSL were used to calculate representative mean extreme values for DLC6.1.

Ocean Climate	
H_{s50} = 10.9 m	T_{p50}=14.6 s
H_{50} = 19.7 m	T_{50} = 12.8 s
HSWL = 3.06 m	
LSWL = -3.06 m	

Table 6.5: Wave Heights, Period, and tides derived from [3].

The forcing and natural frequencies for DLC6.1 are visualized in figure 6.3. The turbine is not operating so there are no 1P, 3P or 6P rotor frequencies presented.

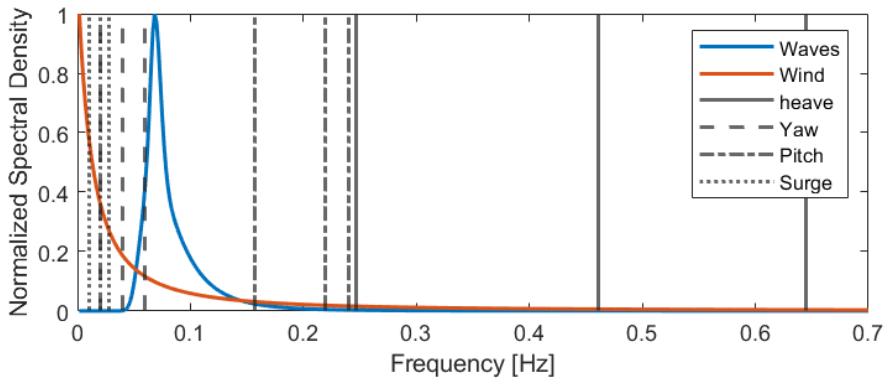

Figure 6.3: Forcing and natural frequencies for DLC6.1. Flexible tower.

6.2 Analysis of Results

A detailed analysis and discussion of the simulation results is presented in the following subsections. A discussion of rotor aerodynamics, controller performance, and energy

production will be presented for DLC1.1 and DLC1.6 which considers normal operating conditions. An analysis of extreme loads and platform motion will be presented for DLCs 1.6 and 6.1 which include more severe environmental conditions.

6.2.1 Results - Normal Operation (DLC1.1 and 1.6)

To study the operating characteristics of the turbine and the influence of mooring depth, time series and PSD plots are presented for DLC1.1 and 1.6 at wind speeds below rated (7 m/s) and above rated (19 m/s). DLC6.1 is not in scope for this section as the turbine is not operating.

The pitch angle of the turbine blades is presented in figure 6.4. Plots of the pitch angle at 7m/s wind speed are omitted because it is a constant zero value.

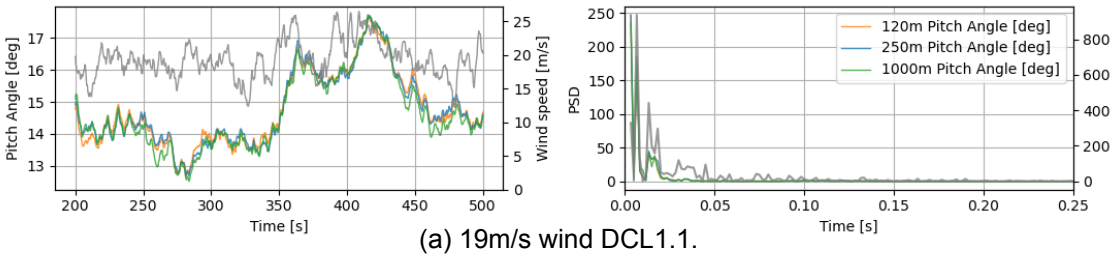

(a) 19m/s wind DCL1.1.

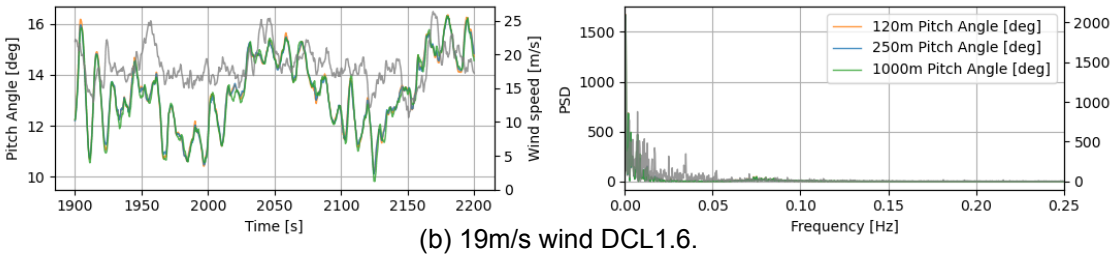

(b) 19m/s wind DCL1.6.

Figure 6.4: Blade pitch angle for DLC1.6 and DLC6.1 at 19m/s wind.

There is minimal change in the pitch operation of the wind turbine depending on the water depth. This is because the pitch angle will vary depending on the relative wind speed at the rotor, which is mostly influenced by the incoming wind speed together with the surge motion of the platform. The wind series used for each depth is identical, and the variation in surge motion between the depths is limited.

The relative contribution of surge motion (driven by wave forcing) to the pitch operation is significantly larger for DLC1.6 under the severe sea state. This shows how the controller reacts to changes in relative wind speed as the turbine moves into or away from the incoming wind, which gives the higher frequency (centered at $\sim$ 0.8 Hz) variation in the time signal. The lower frequency shifts in blade pitch angle are still driven by changes in wind speed.

For DLC1.1, the waves are smaller and also at a higher frequency than for DCL1.6 ($\sim$ 0.1 - 0.15 Hz), meaning the surge motion of the platform is smaller and also the controller is less responsive to higher forcing frequencies.

In figures 6.5 and 6.6 the rotor speed is presented for 7 m/s and 19 m/s wind, respectively.

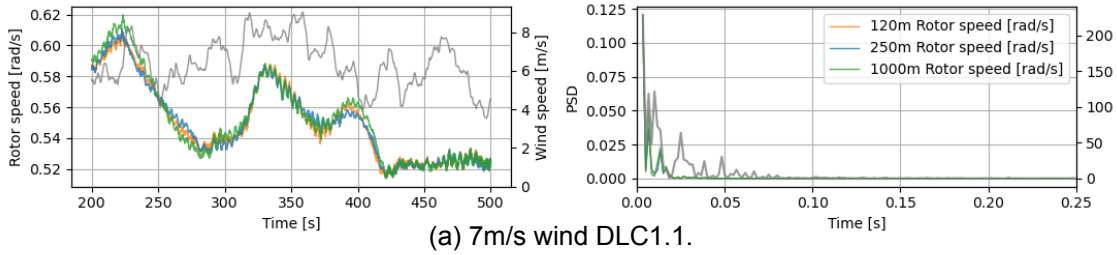

(a) 7m/s wind DLC1.1.

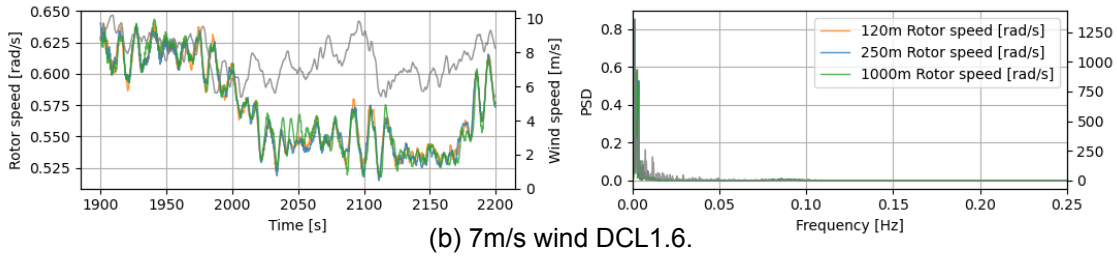

(b) 7m/s wind DCL1.6.

Figure 6.5: Rotor speed for DLC1.1 and DLC1.6 at 7m/s wind.

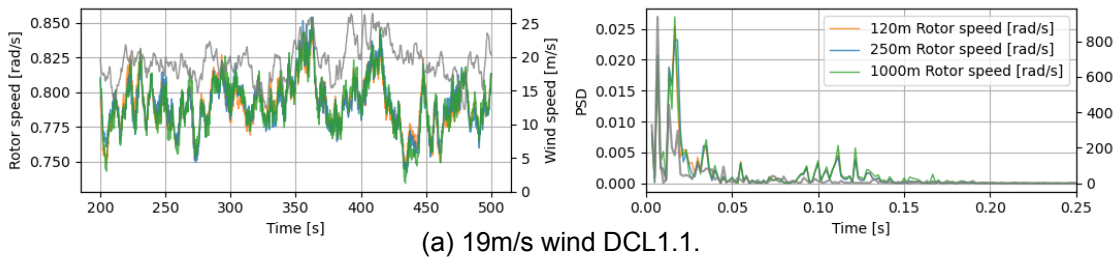

(a) 19m/s wind DCL1.1.

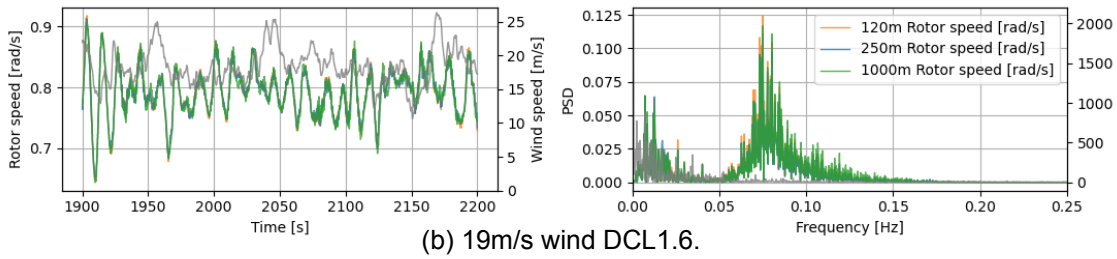

(b) 19m/s wind DCL1.6.

Figure 6.6: Rotor speed for DLC1.1 and DLC1.6 at 19m/s wind.

Again, there is little difference in rotor speed between the mooring depths, and DLC1.6 shows increased variation in rotor speed at the wave frequency ($\sim$ 0.1 Hz) over DLC1.1. The reasoning for these trends is the same as for the pitch angle, where the incoming wind and surge motion of the platform drive the changes in rotor speed.

The rotor speed below rated wind has a large low frequency drift component, as the controller is operating to maintain optimal CP at the design tip speed ratio. Above rated wind speed, the mean rotor speed is centered at the rated rotor speed and the rotor accelerates/decelerates as the aerodynamic torque varies with changes in relative wind speed and blade pitch angle (generator torque is constant).

The thrust force on the rotor is presented in figures 6.7 and 6.8, and is neither sensitive to mooring depth. The thrust force on a blade section is defined by the relative wind speed

and angle of attack, and thus is influenced by changes in the incoming wind speed, pitch angle, and rotational speed.

Below rated wind speed, the pitch angle is held constant so the thrust force varies more with the incoming wind speed. There thrust signal has both low frequency variation following the wind forcing, and high frequency following the wave forcing.

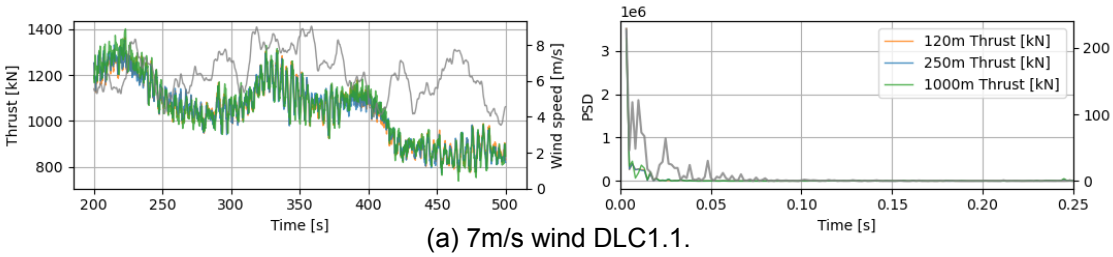

(a) 7m/s wind DLC1.1.

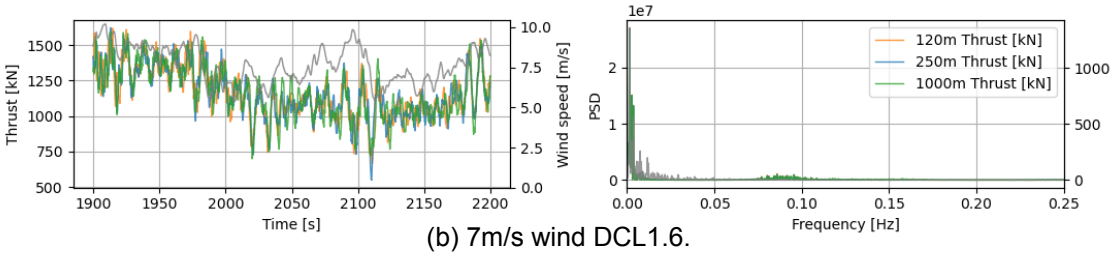

(b) 7m/s wind DCL1.6.

Figure 6.7: Thrust for DLC1.1 and DLC1.6 at 7m/s wind.

Above rated wind speed, the mean thrust is constant as the blades pitch to limit peak thrust. Therefore the waves have a higher relative influence on thrust variations than the wind, as the system response is slow to limit peaks in the thrust due to higher frequency wave induced platform motion.

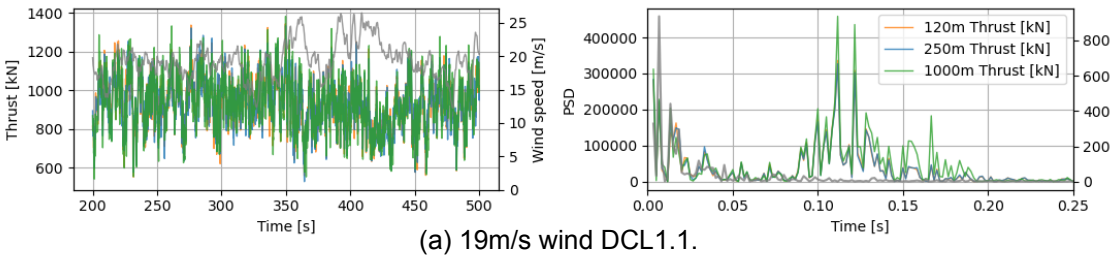

(a) 19m/s wind DCL1.1.

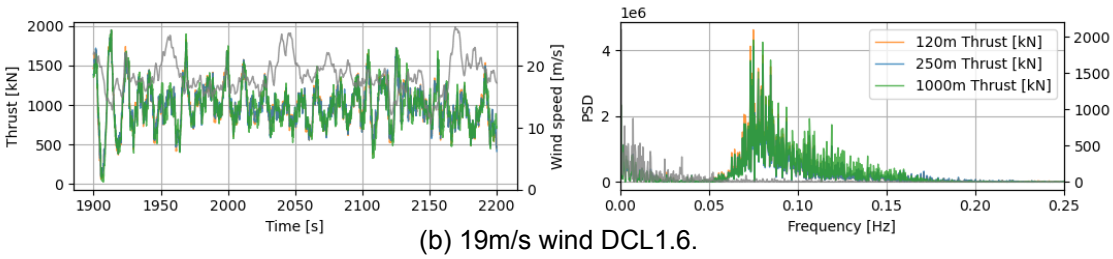

(b) 19m/s wind DCL1.6.

Figure 6.8: Thrust for DLC1.1 and DLC1.6 at 19m/s wind.

6.2.2 Extreme Platform Motion and Structure Loads

A summary of the extreme platform motion and structural loads is presented in figures 6.9, 6.10, 6.11, 6.12, and 6.13. These values are calculated first by taking the mean of the six extreme values for the six different seeds at every wind speed. The highest of these mean extreme values across all wind speeds is then presented in the figures and also numerically in table B.1 appendix B. The overall trends will be briefly presented here, then discussed in detail for each signal in the following subsections.

The extreme platform motion, which includes both mean offset (if any) plus oscillatory motion, generally increases with water depth for all DOFs (fig 6.9, 6.10). This is to be expected, as the stiffness of the mooring lines decreases in all DOFs with increased mooring line length. There are some exceptions, for example the extreme heave motion decreases from the 120m to the 250m platform in DLC1.6, which will be explained by a reduction in the surge-heave 'set-down' effect.

The extreme platform motion also increases with the more extreme wind-wave climate of DLCs 1.6 and 6.1 compared to DLC1.1. Again, there are some exceptions for example the extreme surge motion for the 1000m platform decreases at DLC6.1, and yaw motion for all platforms decreases for DLC6.1 due the non-operating condition of the rotor.

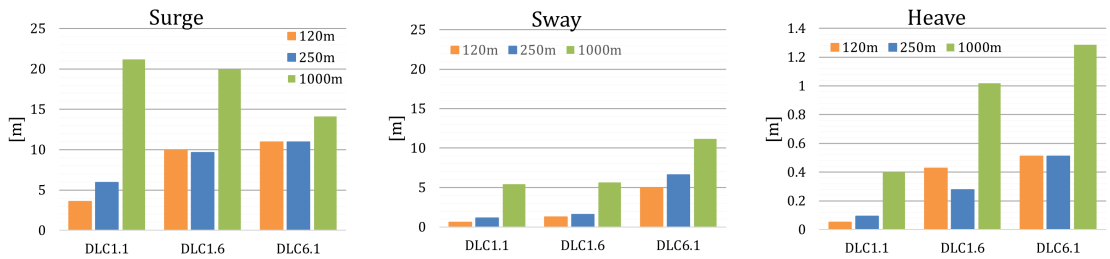

Figure 6.9: Extreme Surge, Sway and Heave motion.

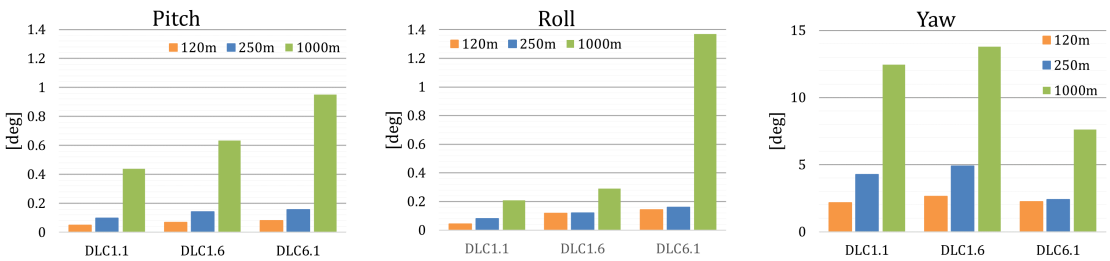

Figure 6.10: Extreme Pitch, Roll, and Yaw Motion.

The extreme TB-FA and TB-SS bending moments (figure 6.11) are of similar magnitude among all depths for DLCs 1.1 and 1.6. For DLC 6.1 however, the extreme tower bottom bending moments tend to increase with increased mooring depth. The extreme tendon forces (maximum and minimum) are also similar across all platforms, with the range between min-max increasing from DLC1.1 to DLC1.6 and again to DLC6.1 as a result of increased wave heights. Due to tendon self-weight, the maximum tendon force will normally be measured at the platform level, while the minimum force occurs at the sea bed. This also explains why the minimum tendon force decreases with increased mooring depth (heavier tendons).

The tower top, RNA loads and minimum blade to tower clearance are presented in figures 6.12 and 6.13 (note that for tower clearance, a larger value is preferred). These values

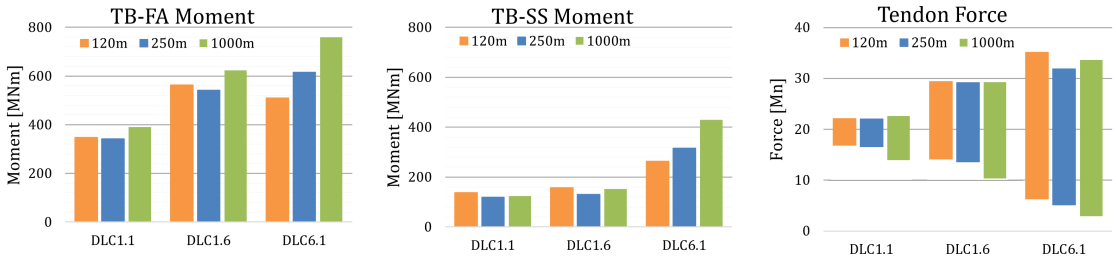

Figure 6.11: Extreme tower bottom bending moments and extreme maximum and minimum axial tendon force.

are all very consistent across mooring depths, with the worst-case extremes occurring for DLC1.6 which combines a severe sea state with the turbine operating condition. Shutting down the turbine in DLC6.1 is able to successfully reduce the extreme loads on the tower top, RNA, and shaft (with idling rotor).

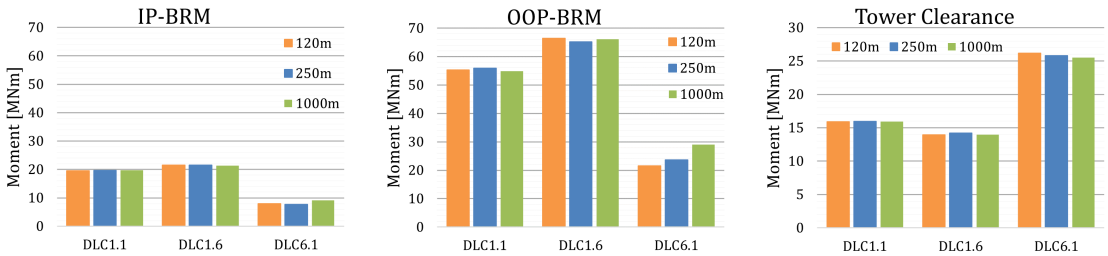

Figure 6.12: Extreme blade root moments and minimum blade to tower clearance.

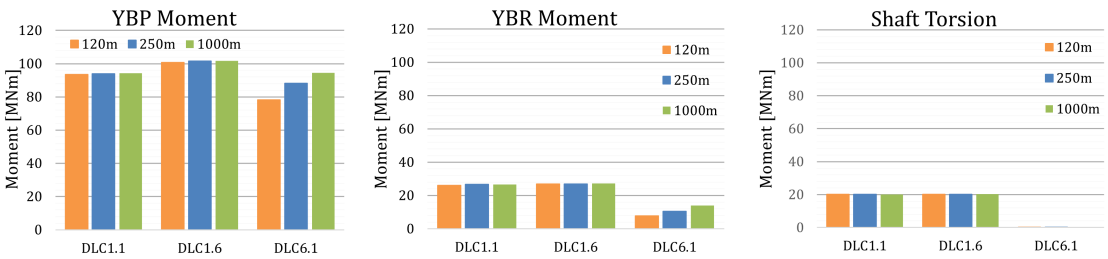

Figure 6.13: Extreme yaw bearing moments and shaft torsion.

6.2.3 Discussion of Extreme Motion and Loads

This section continues with a detailed discussion of the relevant extreme platform motion and loads. The focus will be on presenting results for DLC1.6 and 6.1, where the highest loads and most extreme platform motion were seen (relative to DLC1.1).

The extreme platform motions and structural loads are presented graphically in this section as shown in figure 6.14. For DLC1.6 the mean maximum and minimum values are calculated as the mean of the six extreme (min or max) values for the six different seeds at each wind speed. These are plotted from cut-in wind speed to cut-out wind speed for each mooring depth. On the right hand side of the plot, the mean max and mean min values are shown for DLC6.1 as bars for each mooring depth using a solid line for cases of aligned wind and waves, and a dashed line for 30° misaligned wind and waves.

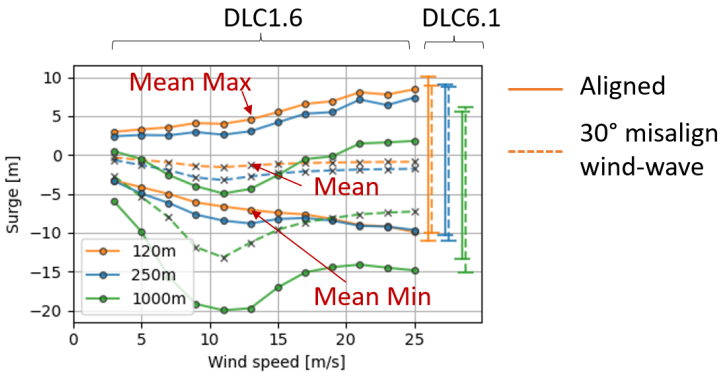

Figure 6.14: How to interpret graphs of extreme values for DLC1.6 and 6.1.

Surge Motion

The platform surge motion is presented in figure 6.15 as an absolute value in meters (a) and as the mooring line angle due to surge (b). The aerodynamic loads on the rotor produce a mean thrust force that is mostly responsible for the mean surge offset seen in these plots. Meanwhile the wave loading on the platform in surge is cyclical and contributes more to the amplitude of surge motion.

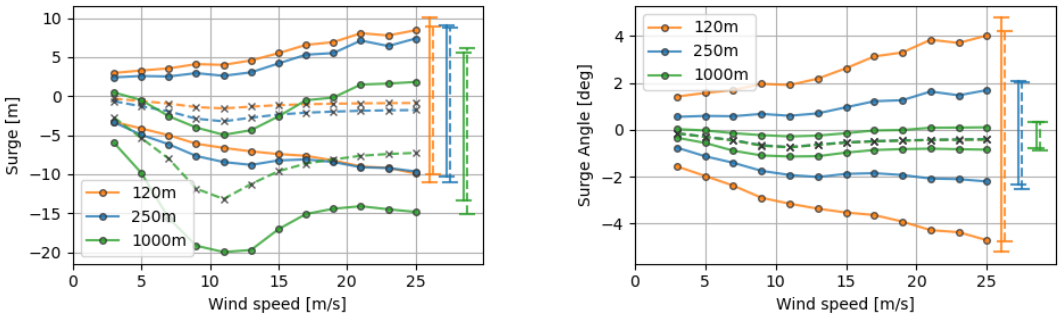

(a) Surge Motion.

(b) Surge Angle.

Figure 6.15: Extreme and mean Surge, DLC1.6 (lines) and DLC6.1 (bars), flexible tower.

In figure 6.15a is can be seen that that mean surge increases with increasing depth for all wind speeds, whereas in figure 6.15b the mean angle remains constant between the depths. As was shown in the steady wind case the mean surge displacement caused by the rotor thrust force correlates directly with mooring line stiffness, which decreases linearly with the inverse of depth. When calculating the surge angle, the motion is normalized by the depth giving the constant result.

On the other hand, the range between minimum to maximum surge motion does not scale with mooring depth and is similar for 120m, 250m, and 1000m. As shown in figure 6.16, the wave frequency range is higher than the natural frequencies in surge meaning the response to waves is inertia dominated. Given that the inertia of the system is similar for all depths, the surge response of the system to the wave forcing is not sensitive to mooring depth. This also means that the extreme mooring angle is more severe for the shallower 120m platform where the wave induced motion is greatest relative to the depth.

The contribution of wind and waves to the surge motion depends upon the mean wind speed as illustrated in figure 6.16.

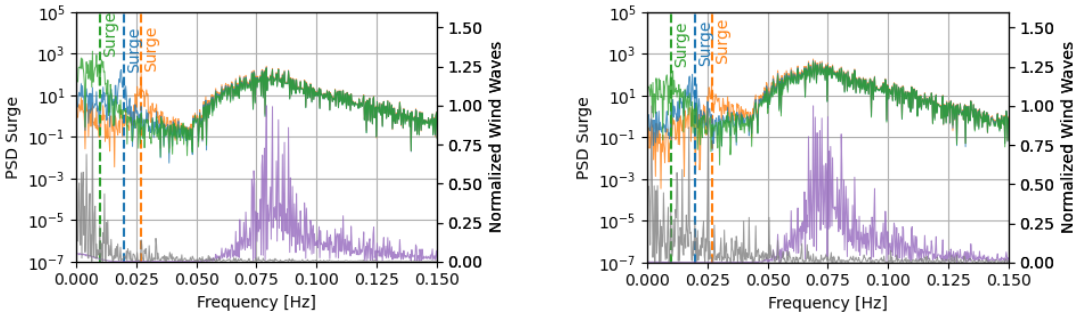

(a) 13 m/s wind.

(b) 25 m/s wind.

Figure 6.16: PSD of surge at different wind speeds for DLC1.6, incl Wind — and Waves —

At 13 m/s wind the thrust on the rotor is near its peak so there is a larger low frequency contribution from the wind. At 25 m/s the thrust on the rotor is reduced and the wave forcing becomes more dominant, giving a lower mean surge offset and larger range of surge motion.

Sway

Unlike in surge, the structure does not normally have direct forcing from the wind or waves in sway. This means that the sway motion is forced by uneven loads on the rotor or platform caused by e.g turbulence or by changes in the yaw angle of the platform. The extreme mean/min sway motion is presented in figure 6.17a, together with a PSD plot at 25m/s wind in figure 6.17b.

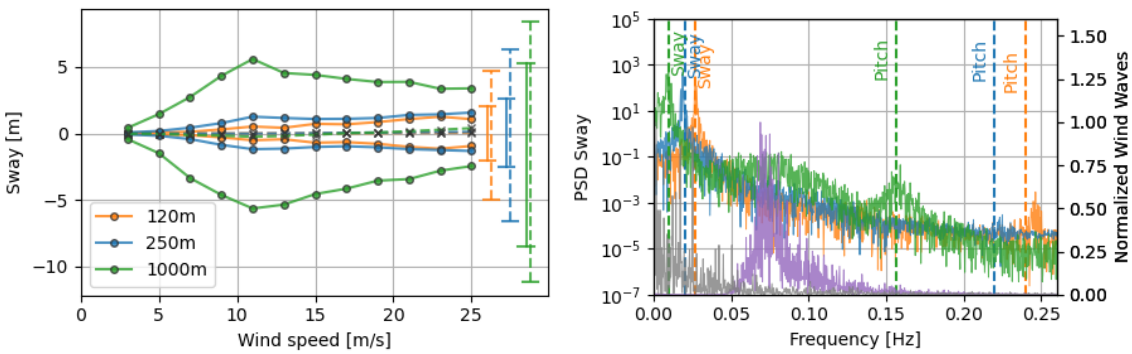

(a) Extreme and mean Sway, DLC1.6 (lines) and DLC6.1 (bars).

(b) PSD of sway at 25m/s wind DLC1.6, incl Wind — and Waves —

Figure 6.17: Sway motion, flexible tower.

The sway motion is dominant at the sway natural frequency of the platform, and is largest for the deeper water platforms where mooring stiffness is lower. Because the sway motion is slow and perpendicular to the incoming wind, it will not contribute much to the turbine loads or aerodynamics.

The most extreme sway motion occurs for each depth with DLC6.1, misaligned wind and waves. This is because the 30° angle of the waves forces the platform to move along a diagonal path which will be measured both in sway and surge.

Yaw
The extreme max/min and mean yaw motion is plotted in figure 6.18a together with a PSD plot at 25m/s wind in figure 6.18b.

The yaw motion of the floater is at a low frequency with some resonance at the yaw natural frequency. Yaw motion is mostly caused by uneven loading on the rotor, either by turbulence in the wind or with pitch/tilt of the rotor as was explained in section 5.1.2. Yaw motion becomes more significant as the mooring stiffness in yaw decreases with deeper water. Also because yaw is mostly caused by aerodynamics on the rotor, it is less significant for DLC6.1 where the turbine is shut down.

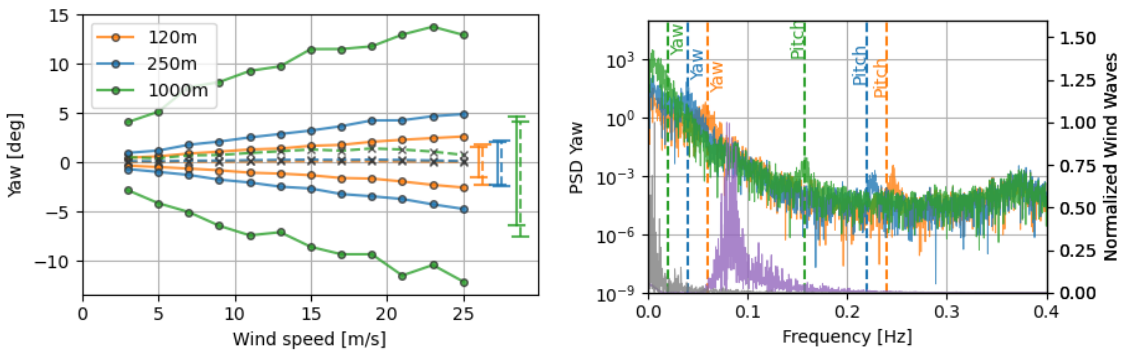

(a) Extreme and mean Yaw, DLC1.6 (lines) and DLC6.1 (bars).

(b) PSD of yaw at 25m/s wind DLC1.6, incl Wind — and Waves —

Figure 6.18: Yaw motion, flexible tower.

The range of yaw motion for the 1000m platform, up to $\sim \pm 13°$, may present some challenges with respect to effective operation and optimal power production.

Heave
The extreme max/min and mean heave motion is plotted in figure 6.19a together with a PSD plot at 25m/s wind in figure 6.19b.

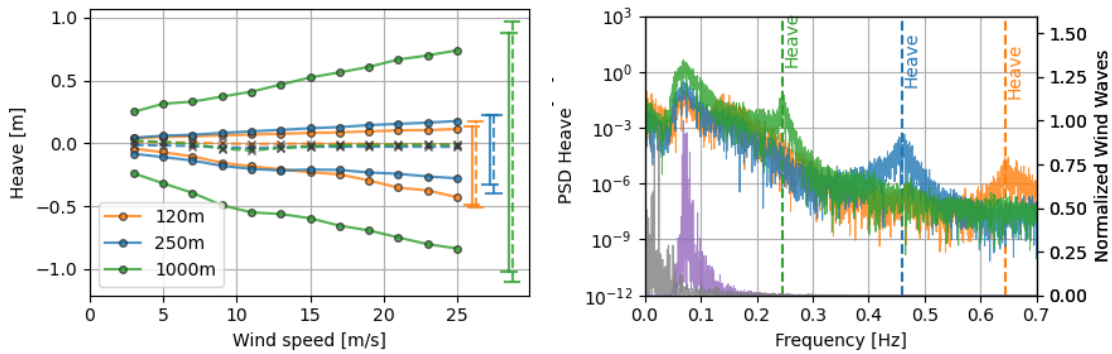

(a) Extreme and mean heave, DLC1.6 (lines) and DLC6.1 (bars).

(b) PSD of heave at 25m/s wind DLC1.6, incl Wind — and Waves —

Figure 6.19: Heave motion, flexible tower.

As there are no significant aerodynamic forces on the platform in heave, the motion is dominated by wave forcing only. Thus the magnitude of extreme heave motion increases

as the wave forcing increases (with increasing wind speed), and is largest for DLC6.1 where the waves are biggest. The natural frequency in heave is far enough from the wave forcing to avoid a high resonant response.

To compare the heave results it is also relevant to look at the geometrical heave-surge coupling illustrated in figure 6.20.

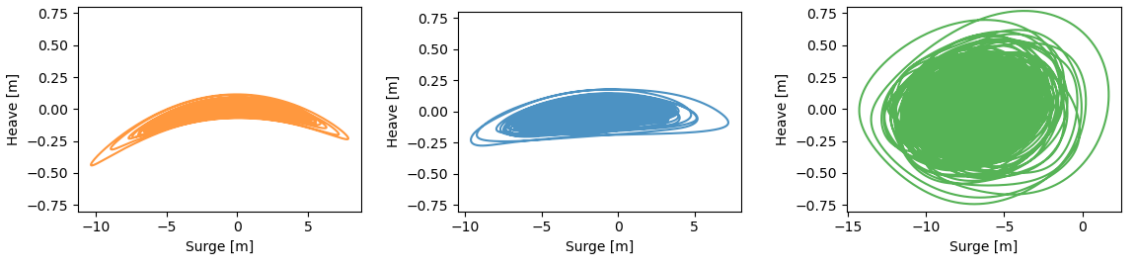

(a) 120m (b) 250m (c) 1000m

Figure 6.20: Surge-heave motion at 25m/s wind, DLC1.6.

Where the tendons are shorter (120m) there is a clearly visible 'set-down' effect where extreme fore or aft surge motion leads to a negative displacement in heave. Thus while the 120m platform has a larger range of extreme heave motion than the 250m platform, the actual elongation of tendon due to heave motion is greater for the 250m platform. Continuing this trend, the 1000m platform shows the most heave motion with minimal set-down effect due to the long tendons and reduced stiffness.

Pitch

The TLP is very stiff in pitch giving limited motion, with extreme pitch values not exceeding $\pm 1^\circ$ for the 1000m mooring and $\pm 0.2^\circ$ for the 120 and 250m mooring. In pitch, there was a noticeable impact depending on the stiffness of the tower, shown in figure 6.21. Changing the model from a stiff tower to a soft-stiff 'flexible' reduces the Tower FA-Pitch natural frequency closer to the wave forcing spectrum especially for the 1000m model.

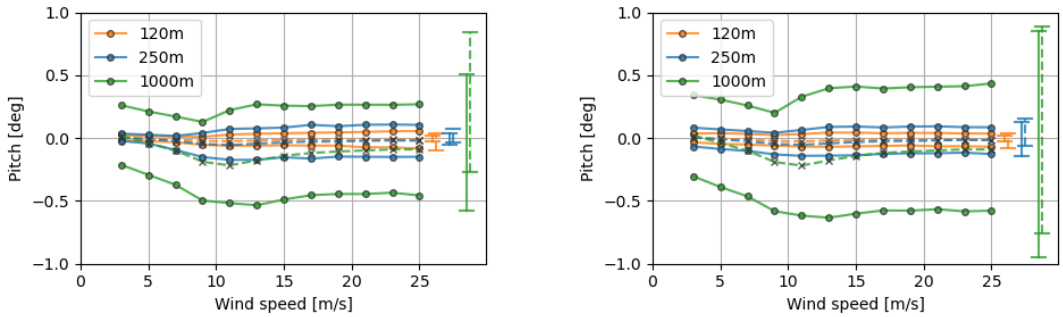

(a) Stiff Tower. (b) Flexible Tower.

Figure 6.21: Extreme and mean Pitch, DLC1.6 (lines) and DLC6.1 (bars).

The pitch motion is defined by a combination of wave forcing, wind forcing, and pitch natural frequency, as shown by the example in figure 6.22. The wind generated thrust force on the rotor creates a moment in pitch and is the main contribution for the mean pitch offset. The mean offset is greatest near rated wind speed and for deeper water where the mooring stiffness is reduced. The variation in pitch is driven by wave forcing,

and is also largest for 1000m. Most wave energy falls below the pitch natural frequency so the response amplitude is defined by the stiffness of the system. Finally, for 1000m depth the pitch natural frequency is low enough to be excited by high frequency waves. However, because the high frequency pitch motion is damped by rotor aerodynamics, the response amplification at resonance is limited for DLC1.6 (as was demonstrated in fig 5.11).

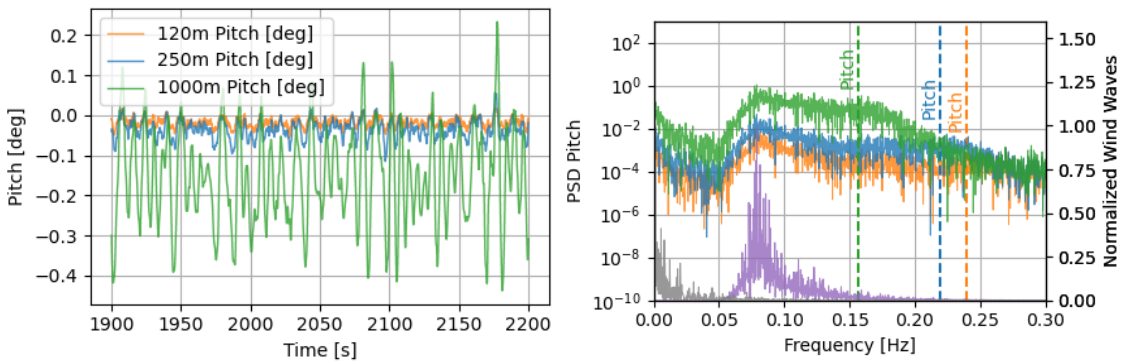

Figure 6.22: Pitch motion and PSD at 25m/s wind DLC1.6, flexible tower, incl Wind — and Waves —

The most extreme pitch motion for the 250m and 1000m platforms occurs for DLC6.1. In these cases, the response is dominant at the pitch natural frequency which overlaps with the wave forcing spectrum. Furthermore, the turbine is shut down so the there is a lack of aerodynamic damping to limit the resonant amplification. This result is clearly visible when looking at the PSD of one time series for DLC6.1 in figure 6.23, where the excitation at the Tower FA-pitch natural frequency is dominating for the 250m and 1000m platforms.

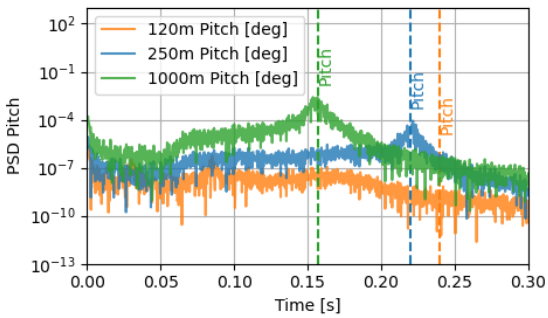

Figure 6.23: PSD of pitch angle for DLC6.1.

TB-FA Moment

The extreme TB-FA bending moment is presented in figure 6.24 for both a stiff and flexible tower. The mean TB-FA moment resembles a turbine thrust curve, and is equal for both towers at all depths. The extremes in the max/min TB-FA moments are also similar for most cases, although significantly increased for DLC6.1 with the 250m/1000m platforms and flexible tower.

To better understand the TB-FA bending moment, the TT-FA force and its inertia and thrust components are presented in figure 6.25 for the 120m platform, DLC1.6 at 25m/s wind.

The total TT-FA force (orange) is a sum of the rotor thrust force (purple) and the inertia force caused by acceleration of the RNA mass (gray). From the plot it is clear that the

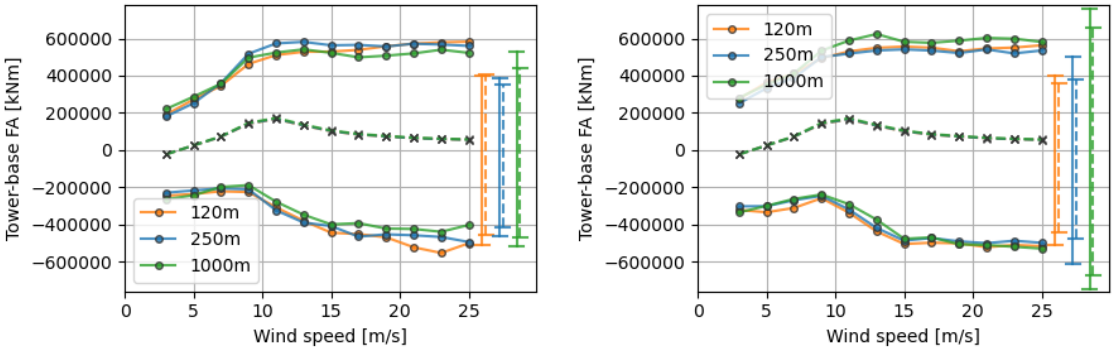

(a) Stiff Tower.

(b) Flexible Tower.

Figure 6.24: Extreme and mean TB-FA moment, DLC1.6 (lines) and DLC6.1 (bars).

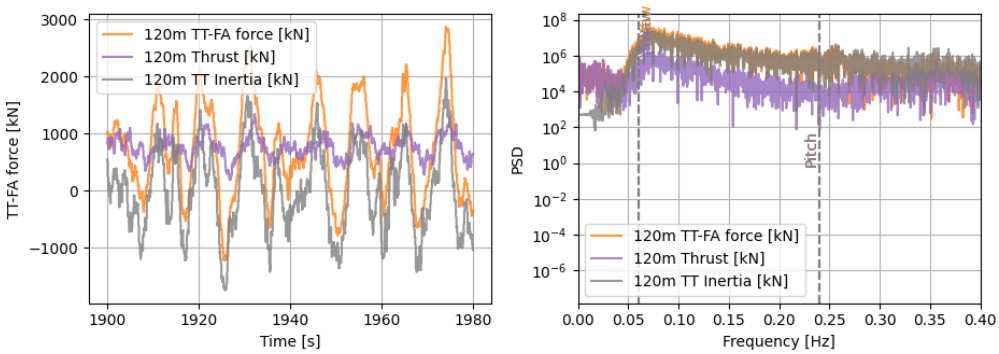

Figure 6.25: Combined TT-FA force with inertia and thrust components. 120m platform with 25m/s wind, DLC1.6.

tower top inertia force contributes most significantly to the TT-FA force and peaks at the wave forcing frequency. Meanwhile, the thrust force contributes at lower frequencies representing the mean thrust offset and some turbulent wind forcing. The same trend is seen for the 250m and 1000m platforms.

It also relevant to study the RNA/TT-FA acceleration, which generates the inertia loads at the tower top. A PSD plot of TT acceleration for the same platform conditions and is shown in figure 6.26.

The peak of the TT-FA acceleration occurs at the peak wave forcing frequency, due mostly to platform surge and to a lesser extent pitching motion. Recalling that the wave induced surge motion is similar for all mooring depths, the surge induced TT-FA acceleration will also be similar. For the 1000m platform, there is also some increased contribution from pitching near the pitch natural frequency, although surge is still the dominating factor.

These plots help explain the results in figure 6.24, where the TB-FA bending moment is not sensitive to mooring depth for DLC1.6. On the other hand, for DLC6.1 the extreme TB-FA moments increase with mooring depth for the flexible tower. This is because pitch becomes a dominating factor for the loads due to resonance at the Tower FA- Pitch natural frequency, as was described in section 6.2.3.

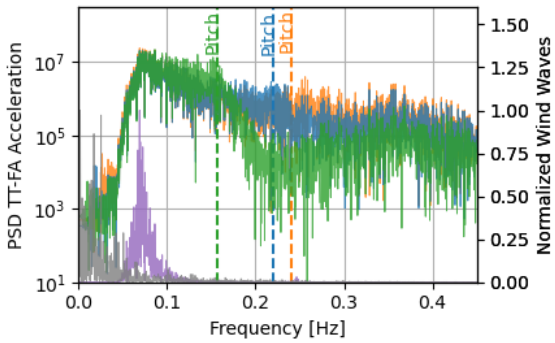

Figure 6.26: PSD of TT-FA acceleration with 25m/s wind, DLC1.6, incl Wind — and Waves —

6.2.4 Roll

Extreme roll motion is presented in figure 6.27 for both a stiff and flexible tower.

Forcing on the structure in roll is different from pitch in that the main components of thrust and wave loads are orthogonal to the roll DOF and thus not generating significant loads. The generator torque, however, is transferred to the structure and and creates a mean roll offset that is most noticeable for the least stiff 1000m mooring. One exception is for DLC6.1 in the load case with a 30° misaligned wave angle, where a component of the wave forcing acts directly in roll and generates larger roll motion.

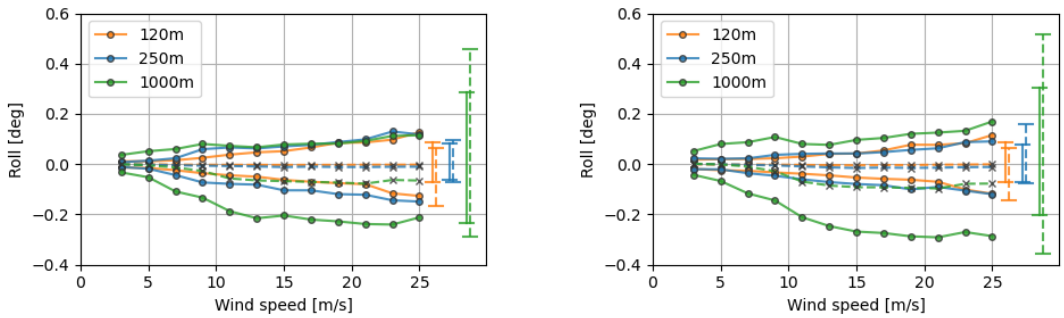

(a) Stiff Tower

(b) Flexible Tower

Figure 6.27: Extreme and mean Roll, DLC1.6 (lines) and DLC6.1 (bars).

Another key factor influencing the platform roll motion is that the aerodynamic damping from the rotor thrust force is not a significant factor as it was for pitch motion. Together with the lack of significant forcing to the roll DOF this means that the roll motion occurs mostly at the roll natural frequency as seen in the PSD plot 6.28.

The use of a flexible versus stiff tower did not have a significant impact on the magnitude of extreme roll motion for the 120m and 250m depths, and a marginal increase for 1000m due to change in the natural frequency.

For the 1000m depth there is also a large low frequency component of the roll motion which is coupled with the extreme yaw motion (ranging $\sim$ -13° to 13°). As the platform yaws to such extreme angles, the direct loading from wind and waves to the roll DOF increases.

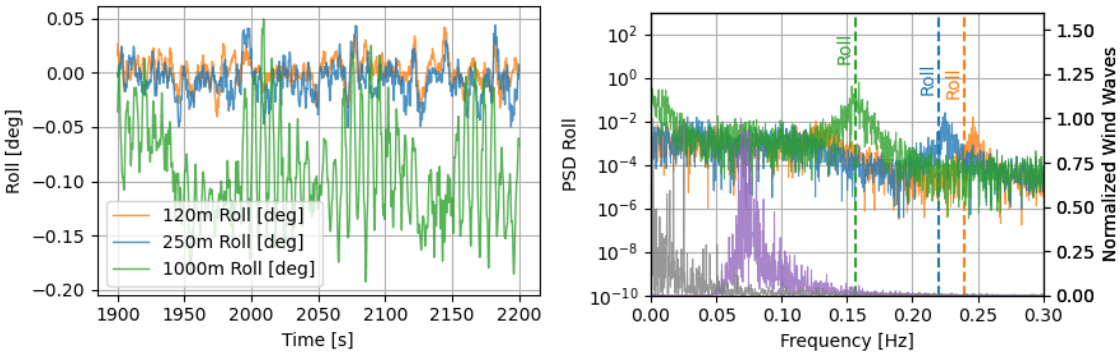

Figure 6.28: Roll Motion and PSD at 25m/s wind DLC1.6, flexible tower, incl Wind — and Waves —

6.2.5 Tower Base Side-Side

Roll motion is correlated with the TB-SS bending moment in the same way that pitch motion is correlated with the TB-FA bending moment. One unexpected observation for DLC1.6 is that the use of a flexible tower in the model led to reduction in extreme TB-SS bending moment for 120m and 250m by a factor of up to ~ 2 as shown in figure 6.29. Furthermore, with a flexible tower the TB-SS bending moment is the nearly the same for all depths despite increased roll motion at 1000m.

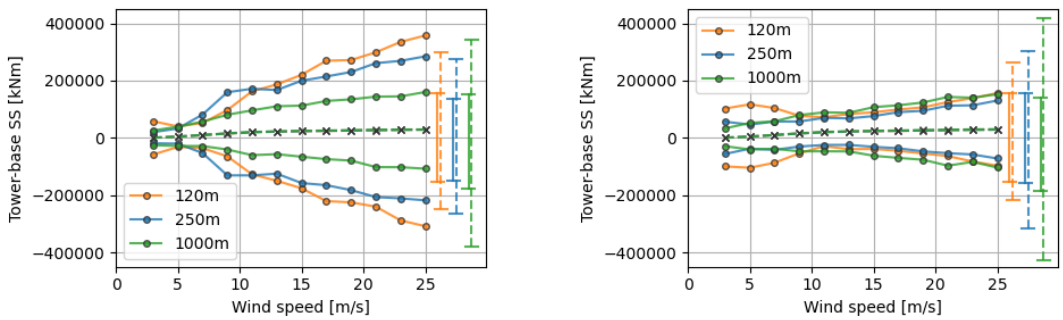

(a) Stiff Tower

(b) Flexible Tower

Figure 6.29: Extreme and mean TB-SS moment, DLC1.6 (lines) and DLC6.1 (bars).

To better understand the results it is useful to look at an example time series and PSD of the TB-SS bending moment and the tower top force measured in HAWC2, figure 6.30. Here it is clear that the forcing energy is concentrated at the roll natural frequency.

Because there is no direct external force acting at the roll natural frequency in the sway/roll DOFs, the TT-SS force must come from acceleration of the RNA mass. As the natural frequency of the platform is reduced, the roll motion becomes slower meaning lower TT-SS accelerations and reduced TT-SS inertia forces from the RNA. The TT-SS force (together with the constant generator torque) is then directly responsible for the TB-SS bending moment.

Figure 6.31 shows extreme tower top accelerations for the 120m platform versus the 1000m platform. Although the 1000m platform experienced greater roll motion, the lower frequency means that the roll induced tower top accelerations are not increased and thus the TB-SS bending moments are also similar in both cases.

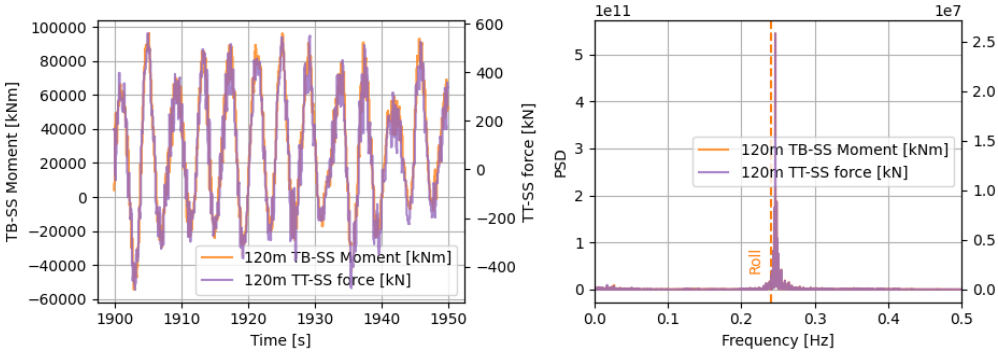

Figure 6.30: TB-SS bending moment and TT-SS force for 25 m/s wind, DLC1.6, with flexible tower. Axes are set so a positive force creates a positive bending moment.

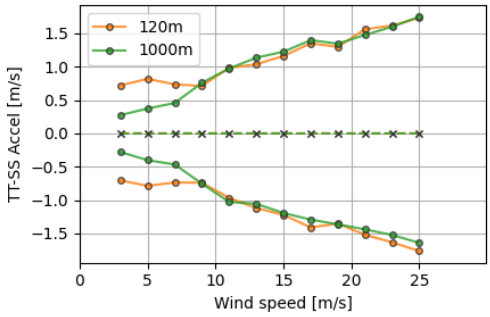

Figure 6.31: TT-SS extreme acceleration, DLC1.6.

On the left side of figure 6.31 it can be noticed there is an increase in TT-SS acceleration at low wind speeds leading to an increased TB-SS moment. This occurs because the 120m platform with flexible tower has a coupled roll-tower natural frequency at 0.24 Hz which is near the the average 3P rotor frequency of 0.25 Hz at low wind speeds. This leads to an increased excitation at resonance and a peak in the extreme tower side-side motion. For higher wind speeds the mean rotor speed increases, pushing the 3P frequency further from the coupled roll-tower natural frequency. To resolve this issue the tower and mooring stiffness or minimum rotor speed could be adjusted.

6.2.6 RNA Loads

The blade root bending moments are presented in figure 6.32 for the flapwise and edgewise directions following the blade coordinate system. The minimum blade to tower clearance and extreme shaft torsion are presented in figure 6.33, and the extreme yaw bearing moments are presented in figure 6.34.

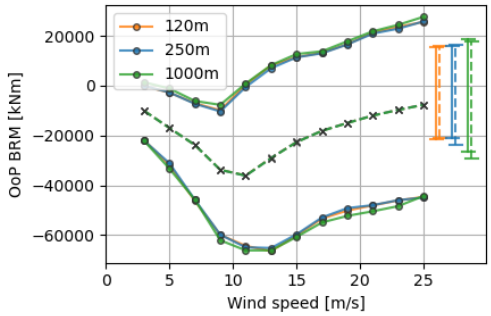

(a) Flapwise Blade Root Moment

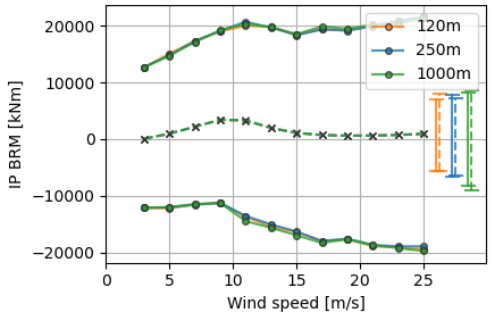

(b) Edgewise Root Moment.

Figure 6.32: Extreme and mean Blade Root Moments, DLC1.6 (lines) and 6.1 (bars).

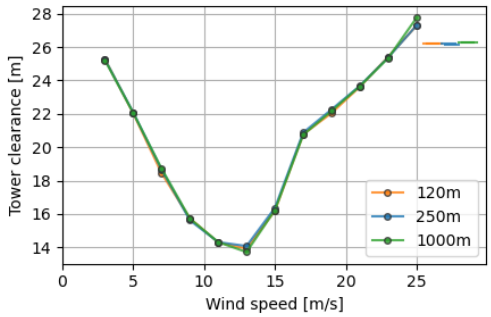

(a) Tower Clearance.

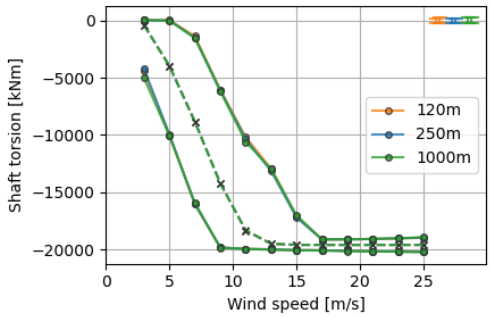

(b) Shaft Torsion.

Figure 6.33: Extreme and mean Tower Clearance and Shaft Torsion Sway, DLC1.6 (lines) and 6.1 (bars).

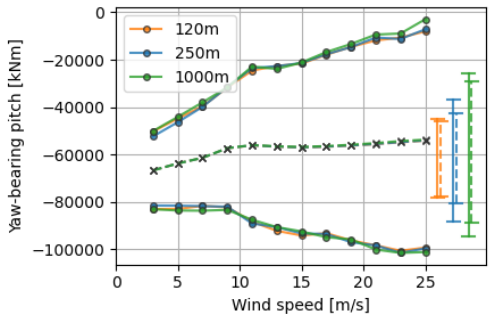

(a) Yaw Bearing Pitch.

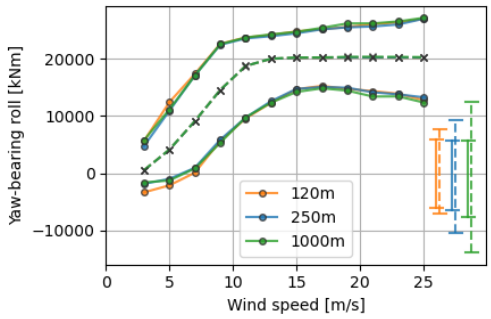

(b) Yaw Bearing Roll.

Figure 6.34: Extreme and mean yaw bearing moments, DLC1.6 (lines) and DLC6.1 (bars).

These plots show little variation in the mean and extreme loads between the mooring depths for DLC1.6. The OoP-BRM, tower clearance, and shaft torsion are all dominated by the time varying aerodynamic loads on the rotor, defined by the turbulent wind and platform surge motion. The wind series used for each depth is identical, and the amplitude of surge motion is similar between the depths. This leads to nearly identical mean and extreme loads for all simulations. The IP-BRM is dominated by gravity loads on the

rotating blades, which also remain consistent between simulations.

For DLC6.1, there is some change in the extreme blade root moments between the depths, however they remain less significant than the operating condition. It should also be noted that the shaft torsion is near zero for DLC6.1 due to the choice to leave the rotor in an idling condition where the blades are pitched to 90° and the rotor is free to rotate. If the rotor is instead locked, the shaft torsion and YBR loads become significantly increased.

The YBP moment for DLC1.6 is dominated by the rotor thrust force and by effects of wind shear at the 3P rotor frequency. The YBR moment is caused primarily by the aerodynamic rotor torque. Because these aerodynamic loads act (mostly) independent of mooring depth, the extreme yaw bearing pitch and roll moments are unchanged between the three platforms (fig 6.34).

6.2.7 Mooring Line Tension

The extreme and mean tendon forces are presented in figure 6.35 together with a PSD of the tendon force at 25m/s wind (DLC1.6).

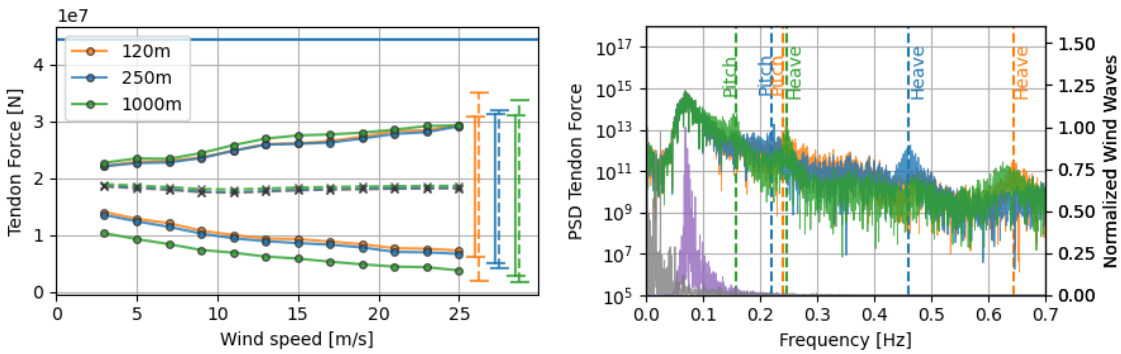

(a) Extreme and mean Tendon Force, DLC1.6 (lines) and 6.1 (bars).

(b) PSD of tendon force at 25m/s wind DLC1.6, incl Wind — and Waves —

Figure 6.35: Tendon Force, Flexible Tower. Yield strength of tendon is illustrated by horizontal blue line.

The mean and extreme tendon forces are similar across all mooring depths. The tendon forces are dominated by wave loads on the structure, as shown in the PSD plot (fig 6.35), and the wave loads do not depend on mooring depth. The extreme tendon tension occurs specifically as a result of extreme waves passing the structure, which waves have a relatively long period (low frequency) and therefore do not excite resonance in pitch or heave for any of the structures.

It has also been noted that the tension value will vary along the tendon due to tendon self weight. Therefore, the maximum tendon forces were measured at the platform level while the minimum were measured at the sea bed. The 1000m mooring has a lower minimum tendon force at all wind speeds, which is a result of the higher tendon self weight.

Comparing the four (4) upwind tendons and versus the (4) downwind tendons reveals that the upwind tendons have a higher mean tension than the downwind tendons when the turbine is operating. This is because the upwind and downwind tendons act together like a lever to counteract the moment caused by thrust force on the rotor. Figure 6.36 shows the relative increase in mean tension of the upwind tendons when compared to

the downwind tendons for DLC 1.6, which follows the shape of the turbine thrust curve and peaks near rated wind speed at 11 m/s wind.

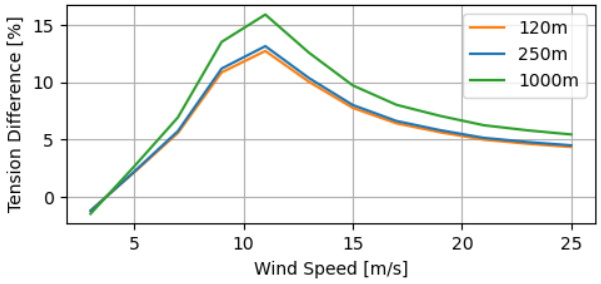

Figure 6.36: Relative increase in mean tension of the 4 upwind tendons versus the 4 downwind tendons per wind speed, DLC1.6.

The extreme tension value on the other hand is, as mentioned, a dynamic response to the individual extreme wave (figure 6.37a). The extreme tendon forces in the upwind and downwind tendons are similar, values within 1.5% for the 120m and 250m platforms and within 5% for the 1000m platform. Figure 6.37b shows the correlation between water surface level and tendon force. The extreme maximum tendon forces occur as the passing wave reaches its peak, and the extreme minimum tendon forces occur in the corresponding wave troughs.

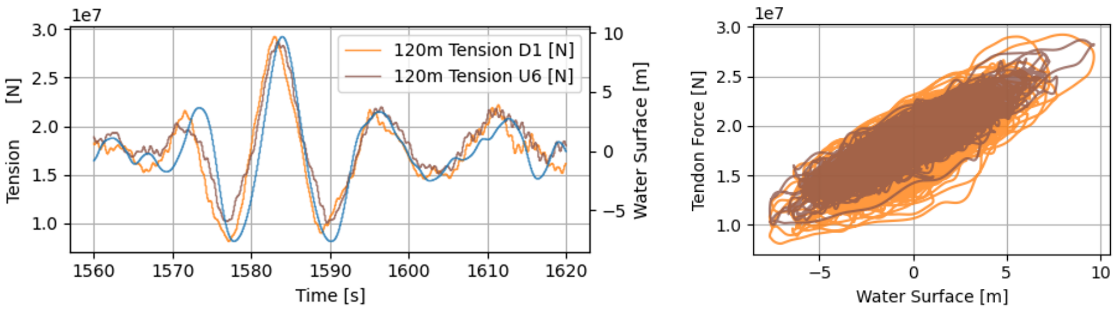

(a) Time series of extreme wave and tendon forces.

(b) Tendon force versus water surface level.

Figure 6.37: Tendon Force forces for 120m platform under extreme wave, 25 m/s wind, DLC1.6. Upwind tendon (U6) and downwind tendon (D1). Water surface is with reference to MSL, with a positive value taken upward.

In cases where the SWL is reduced, due to e.g. low tide or negative storm surge, the TLP is at a higher risk of tension loss in the tendons when an extreme wave passes. This is because the pretension at the reduced SWL is lowered due to the reduced buoyancy on the platform. In the simulations for DLC6.1 with a SWL of -3.06, loss of tension was observed as shown in figure 6.38.

As the wave passes and the tendon comes back into tension, there is some dynamic instability and spikes in the tension force occur at the heave natural frequency, which are eventually damped out. The maximum tension spike is above 4.0e+07 N and far exceeds what is otherwise the maximum tension value when there is no loss of tension. Note that the LSWL used in these simulations is very conservative and these results are not included in calculations of the mean and extreme values for the rest of the section.

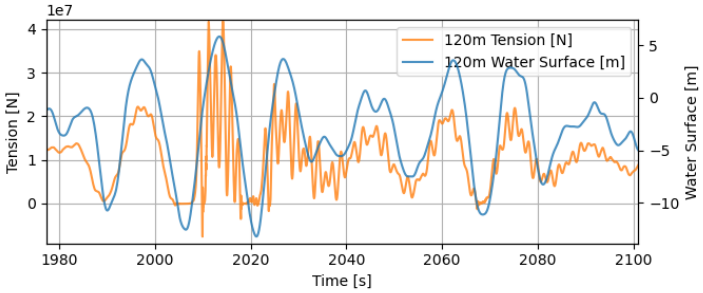

Figure 6.38: Loss of tension due to extreme wave, 120m platform, DLC6.1 when run at LSWL = -3.06m. Water surface is with reference to MSL, with a positive value taken upward.

Furthermore, the model considers the tendons as cables rather than steel rods, which will exhibit different behaviour after tension is lost. The general design criteria remains that this situation should be avoided altogether.

7 Advantages and Challenges of TLP in Deep Water

The advantages and challenges of using TLPs in deeper water (250-1000m+) are described in this section. The topics in this section are built upon findings from previous sections of the report, and in a way represent a summary of the key findings with some further discussion. With each challenge, possible design improvements are suggested.

7.1 Advantages

Turbine and Support Structure Loads (operating condition)
As demonstrated in section 6.2.2, the extreme loads on the RNA, tower, and mooring cables are not significantly changed between moorings depths when the turbine is operating. In table 7.1 the extreme loads for the 120m platform are listed, together with the relative change in extreme load when moving to a 250m or 1000m mooring depth. The extreme loads are for DLC1.1 and DLC1.6, first taking the (max and min) mean of the extreme values for the 6 seeds at each wind speed. The highest absolute extreme value among all wind speeds and both load cases is then taken for table 7.1.

Load	Unit	120m	250m relative	1000m relative
TB-FA Moment	[MNm]	563.18	-3.9%	10.8%
TB-SS Moment	[MNm]	263.49	-16.6%	-2.5%
YBP Moment	[MNm]	100.75	0.8%	0.9%
YBR Moment	[MNm]	27.00	0.1%	0.6%
Shaft Tors	[MNm]	20.23	0.1%	0.0%
OoP BRM	[MNm]	66.40	-1.8%	-0.4%
IP BRM	[MNm]	21.54	0.1%	-0.7%
Tower Clearance	[m]	26.19	0.2%	0.3%
Tndn Force	[MN]	35.12	-0.8%	-0.3%

Table 7.1: Extreme loads for operating condition (DLC1.1 and 1.6) at 120m and relative change for 250m and 1000m mooring.

The only structural load with more than a 1% increase in extreme value is the TB-FA bending moment for the 1000m mooring depth. The primary cause for the 10.8% increase is an increase in pitching motion at the Tower FA-Pitch natural frequency, which is excited by the waves for the 1000m platform. This effect is however limited in the operating condition to a large degree by aerodynamic thrust forces on the rotor.

Extreme Mooring Angle
Platform displacement in surge is defined by a mean offset, together with oscillatory motion around this mean offset. Forces including the rotor thrust force are responsible for the mean surge offset, and are resisted by mooring line stiffness. The mean surge displacement therefore increases linearly with mooring depth while the mean mooring angle remains constant with depth. The oscillatory surge motion, which is driven by wave forcing on the platform is however resisted mostly by inertia forces, which do not scale with mooring depth. The sinusoidal surge response amplitude due to wave loads is therefore mostly constant with mooring depth. Thus the mean offset plus oscillatory motion will give

a higher extreme surge to depth ratio for a shallower moorings, and as a consequence a higher extreme mooring angle as shown in table 7.2. The extreme surge position is calculated using the same methodology as for the extreme loads in the previous section, considering all DLCs (1.1, 1.6 and 6.1),

	120m	250m	1000m
Extreme Surge Position [m]	10.97	10.97	21.20
Extreme Mooring Angle [deg]	5.22	2.51	1.21

Table 7.2: Extreme surge position and mooring angle, all DLCs.

The exact mechanical design of the tendons and the connection at the sea bed anchors and platform will dictate how much of an extreme mooring line angle is acceptable. As a guideline, [11] recommends a design target of <5° and [19] suggests the angle cannot exceed 10° considering tendon flexure and other mechanical factors. In any case, a reduced extreme mooring angle which is seen with deeper waters is beneficial for the anchor connection design.

Controller and Aerodynamic Performance
Another advantage that can be considered for deepwater TLPs is that the controller performance (excluding yaw bearing control) and Aerodynamic performance of the rotor are mostly unaffected by mooring depth.

For the 250m platform compared to the 120m platform, the average of the difference in pitch angle above rated wind speed (measured every time step then averaged) between the two models for all DLC1.6 simulations is only between 0.005° and 0.016°. For the 1000m platform, this increases slightly between 0.04° and 0.10°. The simulations were run with the same environmental conditions and same random seeds across the mooring depth models. The rotor speed of the platforms is also very consistent between the depths, with the average difference no greater than 0.004 rad/s for any simulation in DLC1.6. This demonstrates that the turbine operation, in terms of pitch and rotor speed control, is nearly identical and independent of mooring depth.

When looking at the turbine performance in terms of electrical power output, there is no noticeable difference between the mooring depths both in mean value as well as max/min power output, see figure 7.1.

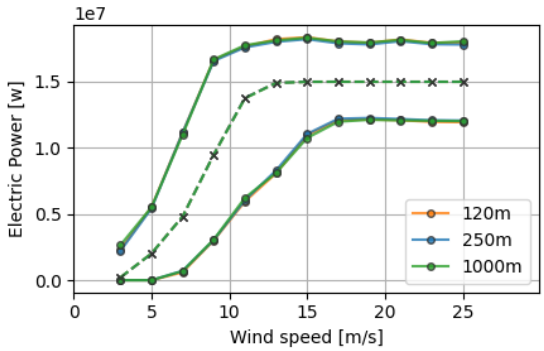

Figure 7.1: Mean power output and min/max extreme of power output, DLC1.6.

Footprint
The footprint of the mooring system has not been discussed in detail so far, however it is an important design consideration and advantage of the TLP when used in deep water. Figure 7.2 shows a visual comparison of the three most common mooring systems, that is the catenary mooring, taut leg, and tension leg.

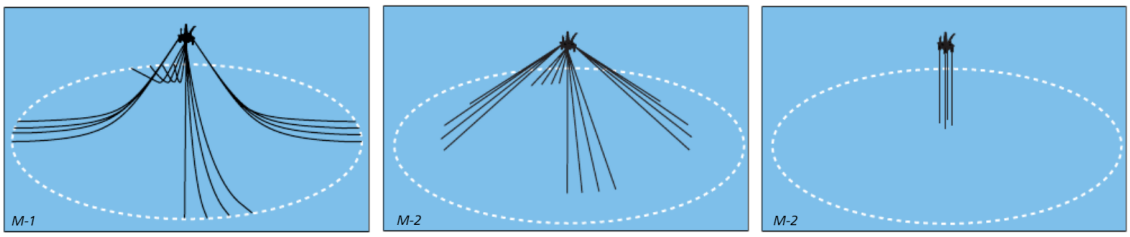

(a) Catenary. (b) Taut Leg. (c) Tension Leg.

Figure 7.2: Comparison of mooring systems and their footprint, from [20].

The catenary system was initially developed for oil & gas exploration in shallow to mid-depth waters. The horizontal restoring forces come from lifting and resting of the mooring cables on the seabed and the anchors are designed to resist horizontal loads only. This type of mooring has the largest footprint with restoring forces defined by the system geometry, which requires a large horizontal seabed anchor to platform distance that increases with water depth.

Taut leg moorings were developed to overcome issues with the high mooring line weight of catenary lines in deeper water. The main differences between a catenary system and taut leg are that the mooring lines reach the seabed at an angle, and horizontal restoring forces come from the elasticity of the lines. A benefit of this system is that it has a lower footprint than the catenary mooring also requiring less material.

The tension leg platform was developed to anchor large production units in ultra deep water, and has since been adapted to smaller units as well. This platform has the lowest mooring footprint, with a vertical connection from the seabed to the platform. Unlike the catenary and taut leg mooring, the tension leg platform footprint remains unchanged relative to the water depth. This helps to limit the mooring weight, material usage, and environmental impact to the seabed in deep and ultra deep waters. Furthermore, the mooring footprint does not become a design constraint when considering a wind farm layout using TLPs.

7.2 Challenges

TB-FA and TB-SS Moments (Extreme Shutdown Conditions)
The extreme TB-FA and TB-SS bending moments are increased significantly for the 250m platform and 1000m platform in an extreme sea state where the turbine is shut down (DLC6.1), as shown in table 7.3. The maximum tower bottom bending moments (TB-FA) for the 250m and 1000m platforms become 615.0 MNm and 759.7 MNm respectively. This is also larger than the extreme value for the operating conditions of DLC1.1 and DLC1.6.

The extreme YBP, YBR, OoP-BRM, and IP-BRM also increase significantly with mooring depth for DLC6.1, however the ultimate loads for these cases are even higher at the operating condition, so the increase in extreme loads is less important for an ultimate load case analysis.

		Relative to 120m		Relative to Operating (DLC 1.1, 1.6)	
	120m	250m	1000m	250m	1000m
TB-FA [MNm]	509.6	21%	49%	14%	22%
TB-SS [MNm]	263.5	20%	63%	142%	181%
YBP [MNm]	78.3	13%	20%	-13%	-7%
YBR [MNm]	7.7	37%	81%	-61%	-49%
Shft Tors [MNm]	0.25	7%	1%	-99%	-99%
OoP BRM [MNm]	21.6	9%	35%	-64%	-56%
IP BRM [MNm]	7.9	-2%	15%	-64%	-57%
Tower clr [m]	26.2	-1%	-3%	62%	60%
Tndn Force [MN]	35.1	-9%	-4%	9%	15%

Table 7.3: Extreme loads for idling condition (DLC6.1) at 120m and relative change for 250m and 1000m mooring as compared to the 120m platform. Additionally, relative change for 250m and 1000m platforms compared to the operating condition (for the same platform).

The increase in tower and RNA loads is driven by an increase in pitch and roll motion at the Tower FA-Pitch and Tower SS-Roll natural frequencies. Because the turbine is shut down, aerodynamic damping is reduced significantly so the amplification of the wave forcing at resonance is larger than the operating condition.

The tower FA-pitch natural frequency of the three platforms is shown in figure 7.3 together with a spectral density of the sea climate for the extreme sea state in DLC6.1 on a logarthmic scale.

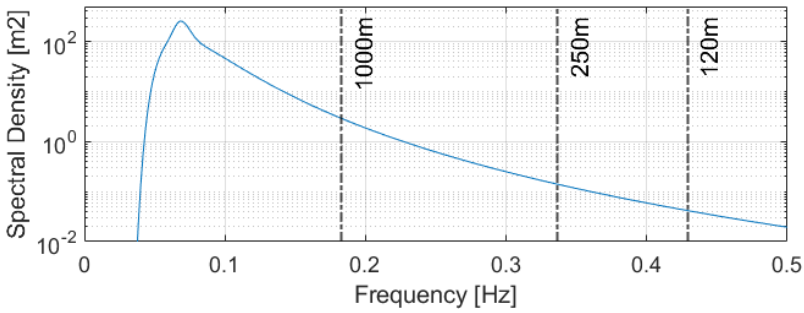

Figure 7.3: Power Spectral Density of extreme sea state H_s50 = 10.9 m T_p50=14.6 s based on Jonswap specturm, together with Tower FA-Pitch natural frequencies, flexible tower.

The wave energy at the 1000m natural frequency is 20 times greater than for the 250m frequency, and 70 times greater than for the 120m platform. Thus while resonant pitch motion is a significant issue for the 1000m platform, it is an order of magnitude less for the 250m platform, and there is essentially no resonant response for the 120m platform.

In order to reduce the dynamic amplification due to resonance in pitch/roll for the deep water platforms, either the damping of the system in these DOFs shall be increased or the natural frequency shall be increased so that there is less excitation energy from the waves.

Further investigation is suggested regarding the possibility and practicality to increase

damping at the pitch natural frequency, e.g. through use of tuned mass dampers (out of scope for this report). Regarding increase of the Tower FA-Pitch natural frequency, a summary of potential design changes and their relative impact to increase the natural frequency is listed in table 7.4. This is mostly relevant for the deepest (1000m) platform.

Design Change	Impact	Comment
Reduce System Inertia	Low	Tower and RNA already contribute to ∼80% of the system inertia in pitch, and there are design constraints limiting any significant reduction in their mass.
Increase Tower Stiffness	Low	The tower is already much stiffer than the mooring for the 1000m platform. Changing to a totally rigid tower would only increase the coupled Tower FA-Pitch stiffness by 4% for this design.
Increase Tendon Area	Medium	Mooring stiffness in pitch will increase linearly with an increase in tendon area. However larger tendons will also increase the mooring weight.
Increase Draft	Low	Mooring line stiffness dominates significantly over hydrostatic stiffness in pitch for the TLP. Therefore, increasing the draft of the platform will show little effect on the pitch natural frequency.
Increase Platform Area	High	Mooring stiffness in pitch will increase with the square of the horizontal distance between the axis of rotation and the fairlead anchor location.
Increase Pretension	None	Stiffness in pitch is not related to pretension on the tendons.

Table 7.4: Design changes and their relative impact on increasing the Tower FA-Pitch natural frequency.

Extreme Yaw Motion

The extreme yaw motion, expressed in terms of extreme (absolute maximum) and yaw angle standard deviation is presented in table 7.5.

	120m	250m	1000m
Extreme Yaw Angle [deg]	2.63	4.90	13.80
Extreme STDev [deg]	0.75	1.50	4.38

Table 7.5: Extreme Yaw Angle based on DLC1.1, 1.6 and 6.1

Due to measurement uncertainty and changes in inflow conditions, wind turbines can normally be expected to operate with some degree of yaw misalignment. From a control point of view, it is preferred to have optimal control over the yaw angle of the turbine relative to the incoming wind, and this becomes further complicated for a floating wind turbine with a foundation that rotates to significant yaw angles.

Yaw misalignment may affect both RNA loads and power production. A reduction in power may occur mostly below rated wind speed where the turbine is operating at with maximum power point tracking.

A summary of design changes and their potential impact to decrease extreme yaw motion is listed in table 7.5. This is mostly relevant for the deepest (1000m) platform.

Design Change	Impact	Comment
Increase System Inertia	Low	Forcing of the platform in yaw is at/below the system natural frequency. Therefore the inertia of the system has a limited effect on the response magnitude.
Increase Tendon Area	None*	Stiffness in yaw does not depend on the tendon area. *However, an increase in tendon area will allow for an increase in pretension of the tendons while limiting the stress in the tendon.
Increase Platform Area	High	Mooring stiffness in pitch will increase with the square of the horizontal distance between the axis of rotation and the fairlead location.
Increase Pretension	Medium	Stiffness in yaw will increase linearlly with an increase in pretension.

Table 7.6: Design changes and their relative impact on extreme yaw motion of the platform

Mooring Line Weight

The mooring self-weight has an increasingly important impact as the tendon depth increases. With a consistent tendon diameter of 273 mm, the 120m tendons require 55 tons of steel each, while the 250m tendons require 115 tons and the 1000m tendons require 460 tons. This represents 6%, 13% and 53% of the steel used for the standard IEA15MW tower, per tendon. Not only does this have cost implications, it also affects the range of tension from the platform to the sea bed.

A steady-state simulation with no external forcing other than gravity and buoyancy shows for the 120m mooring, the tension at the sea bed will be 2.8% less than the tension at the platform. For the 250m and 1000m moorings, this becomes 5.8% and 23.4% respectively. This is important because the tendons should neither go into compression nor should the tension exceed the yield strength of the material. For the heavier tendons, there is a narrower window of external forcing the system can withstand to maintain these criteria both at the sea bed and platform anchor. As shown in figure 7.5, the range in tension along the 1000m tendon already accounts for 10% of the total range between 0N and the yield force of 44MN, a range which will be further narrowed when applying relevant safety factors.

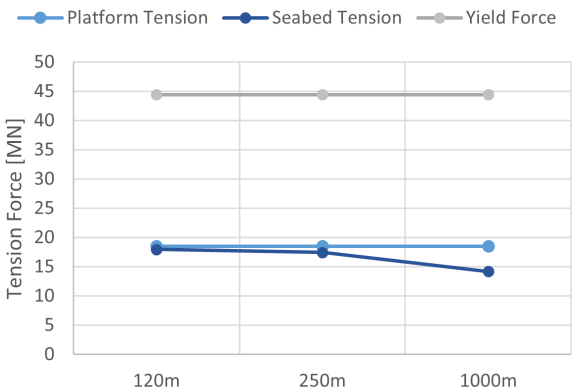

Figure 7.4: Tension in cables as measured at the platform and sea bed for still conditions, no wind and no waves.

To reduce mooring line weight in deep water it is relevant to consider changing mooring line material. In place of steel, high strength synthetic fibers could be used which have an increased strength to weight ratio compared to steel. An example of fiber tendons made from DeepRope® Dyneema® will be presented to explore the feasibility and implications of using syntheic materials for the mooring cable.

For the purposes of this desktop exercise, the fiber tendons are designed so that the total minimum breaking load is equivalent to the total yield strength of the steel tendons. This gives 16 tendons with diameter 180mm each based on the DeepRope® Dyneema® material specification in appendix G. This design is not optimized but presented to give a comparison between the two materials.

Material	**OD**	**ID**	**A**	**N Tendons**	**A_{tot}**	**Strength$_{tot}$**	**Modulus**	**Mass**
-	[mm]	[mm]	[m2]	-	[m2]	[MN]	GPa	kg/m
Dyneema®	180	0	0.0254	8	0.407	362 (break)	49.5	15.8
Steel	273	0	0.0586	16	0.468	355 (yield)	212	459

Table 7.7: Material Properties of steel tendons and Dyneema® synthetic fiber.

For the 1000m platform, the overall mooring mass of the mooring system (in air) would be reduced by a factor of 14, which is a significant improvement and potential cost reduction. However, it is also important to consider that the synthetic fiber material is considerably less stiff, with a specified modulus of elasticity that is 4.3 times less than steel. The change in stiffness will not have any impact on the theoretical natural frequencies in surge and yaw, as these do not depend directly on the tendon stiffness. However, the natural frequencies in pitch and heave will be reduced; in pitch from 0.19 Hz (steel) to 0.085 Hz (synthetic), and in heave from 0.25 Hz (steel) to 0.145 Hz (synthetic). This will place the pitch and heave natural frequencies well within the wave forcing spectrum, leading to potential issues with resonce in these DOFs. Any design using less stiff mooring materials will have to be optimied to mitigate this issue.

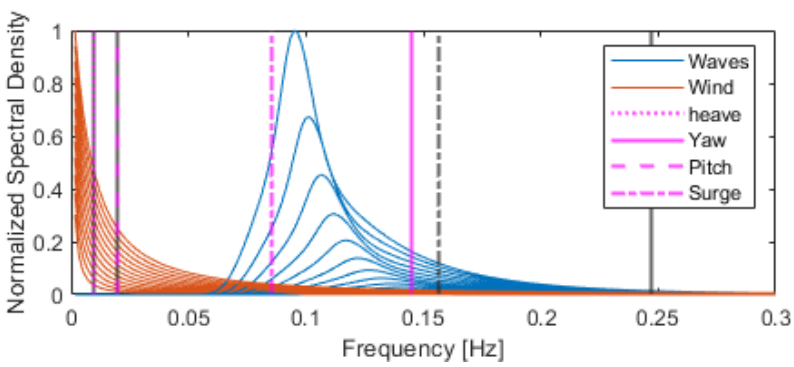

Figure 7.5: Natural frequencies of platform with synthetic fibers compared to wind and wave forcing spectrum for DLC1.1. The frequencies for steel fibers are included as reference with gray lines.

8 Conclusion

In this thesis, the dynamic response of a floating TLP wind turbine was investigated for a range of mooring depths from 120m to 1000m. The wind turbine used in this report was the IEA 15MW reference wind turbine [1] and the TLP platform & mooring model was designed as a joint collaboration between BlueNewables, DTU, Tubacex, and GMC deepwater. All aeroelastic simulations were performed in HAWC2 using pregenerated hydrodynamic loads calculated in WAMIT based on first order potential flow theory. A number of simulations were performed including decay tests to investigate the natural frequencies of the system in the platform DOFs, steady state simulations with steady winds and regular waves, and operational conditions defined by DLCs 1.1 (normal operation), DLC1.6 (operation in a severe sea state) and DLC6.1 (survival state with turbine shut down).

In heave, pitch, and roll the stiffness of the TLP is dominated by elasticity of the steel mooring lines giving a very stiff structure in these DOFs with little relative motion. In surge, sway, and yaw the stiffness is provided by lateral components of the displaced platform mooring tension. This gives a more compliant structure in these DOFs allowing for relatively large motion. As the mooring depth increases, the stiffness in all degrees of freedom is reduced, which has varying effect on platform motions and structural loads. The tower stiffness also had a noticeable effect on the coupled tower-pitch and tower-roll natural frequencies.

The greatest concern identified for the deep water (250m and 1000m) platforms was resonance in pitch in the extreme sea state (DLC6.1). The low Tower FA-Pitch natural frequency for the long mooring lines overlaps with high frequency wave loads. When combined with a lack of aerodynamic damping from the rotor (in idle state) the resonance effect in pitch becomes pronounced. Most notably this increases the extreme tower base bending moment by 14% for the 250m platform and 22% for the 1000m platform when compared to the extreme operating condition loads (DLCs 1.1, 1.6). Another concern identified for the deep water platform is extreme yaw motion driven by low stiffness in yaw, with yaw angles up to 13.8°. To mitigate these issues, it is suggested to design the deep water platforms with an increased distance between the platform center and fairlead anchor, i.e. a wider platform. The stiffness in pitch and yaw will increase with the square the horizontal distance between the mooring anchor and the axis of rotation for that DOF.

Extreme sea states will also present a challenge to deep water TLPs in terms of mooring line tension. The pretension in the mooring line is sensitive to changes in the still water level, i.e. with tides and storm surges. A sea state with lowered mean sea level and extreme waves risks that the TLP mooring loses pretension causing instability in the system and risk of failure. Heavy mooring lines also reduce the pretension of the lines at the seabed relative to the platform level. Careful design consideration must be given to this scenario.

On the other hand, it was found that loads on the mooring lines, support structure, and RNA are mostly unaffected by changes in mooring depth. Furthermore, the turbine control and aerodynamic performance is not sensitive to mooring depth. Finally, the TLP design benefits from a minimal footprint at the seabed.

For further investigation beyond the this thesis, it is recommended to consider:

- Use of higher order hydrodynamic loads. Especially of concern is the impact of sum frequency loads on pitch/heave motion and difference frequency and mean drift loads on surge motion.
- Advanced modelling which can capture the effect of waves that exceed the height of the platform.
- Use of synthetic fiber tendons to decrease mooring weight and cost at extreme depths. Special consideration must be given to changes in pitch/roll and heave natural frequencies with reduced material stiffness.

Overall, the tension leg platform presents a promising solution for installing floating wind turbines in deep to very deep waters. This report contributes a detailed dynamic investigation of the presented TLP floater/mooring design and investigates some of the advantages and challenges of extending the model to deep waters.

Bibliography

[1] Gaertner Evan et al. *Definition of the IEA 15-Megawatt Offshore Reference Wind Turbine*. Tech. rep. NREL/TP-5000-75698. Boulder, CO: NREL, 2020.

[2] IEC 61400-3-1(EN). *Wind Energy Generation Systems - Part 3-1: Design requirements for fixed offshore wind turbines*. Standard. Geneva, Switzerland: International Electrotechnical Commission, 2019.

[3] Martin Mathiesen et al. *Hywind Buchan Deep Metocean Design Basis*. Tech. rep. RE2014-002. Statoil, 2014.

[4] Steven Leverette and Stephen Hodges. "The Tension Leg Platform: from Hutton to Big Foot". In: May 2020. DOI: 10.4043/30752-MS.

[5] James G. Speight. "Chapter 3 - Offshore Platforms". In: *Subsea and Deepwater Oil and Gas Science and Technology*. Ed. by James G. Speight. Boston: Gulf Professional Publishing, 2015, pp. 71–106. ISBN: 978-1-85617-558-6. DOI: https://doi.org/10.1016/B978-1-85617-558-6.00003-9. URL: https://www.sciencedirect.com/science/article/pii/B9781856175586000039.

[6] International Energy Agency. *Offshore Wind Outlook 2019*. 2019.

[7] Torben J. Larsen and Anders M. Hansen. *How 2 HAWC2: The User's Manual*. 2019.

[8] K.Hasselmann al. "Measurements of Wind-Wave Growth and Swell Decay during the Joint North Sea Wave Project (JONSWAP)". In: *Deutsche Hydrographische Zeitschrift* 8.12 (1973).

[9] Anders M. Hansen. *Implementation of HAWC2 Interface to WAMIT*. Tech. rep. DTU Wind Energy Report-I-0236. Lyngby, DK: DTU, 2014.

[10] Antonio Manuel Pegalajar Jurado. "Cascaded numerical models for offshore floating wind turbines". English. PhD thesis. Denmark, 2019. DOI: 10.11581/dtu:00000039.

[11] Torgeir Moan Erin E. Bachynski. *Design considerations for tension leg platform wind turbines*. 2012.

[12] C. Guedes Soares Emre Uzunoglu. *Hydrodynamic design of a free-float capable tension leg platform for a 10 MW wind turbine*. 2020.

[13] E. Bachynski Torgeir Moan Erin E. Bachynski. *Hydrodynamic modeling of tension leg platform wind turbines*. 2013.

[14] Fabio Pierella et al. *Numerical simulations of a 15MW wind turbine on a concrete TLP with rigid pipe tendons*. 2022.

[15] LI Yan WANG Bin TANG Yougang and CAI Runbo. *Effects of Second-Order Sum- and Difference-Frequency Wave Forces on the Motion Response of a Tension-Leg Platform Considering the Set-down Motion*. 2018.

[16] E. Bachynski Torgeir Moan Erin E. Bachynski. *Ringing loads on tension leg platform wind turbines*. 2014.

[17] Steen Krenk and Jan Hogsberg. *Dynamics of Structures: Theory and Analysis*. 2021.

[18] Anders Falsen Habostad. *Assessment of design methods for structural response of floating wind turbines with focus on mooring line tension*. Tech. rep. Trondheim, Norway: NTNU, 2019.

[19] Subrata K. Chakrabarti. "Tension Leg Platforms". In: *Handbook of Offshore Engineering*. Plainfield, Illinois, USA: ELSEVIER, 2005, pp. 501–535.

[20] *Anchoring Manual 2015*. Vryhof Anchors B.V. Schiedam, Netherlands, 2015.

[21] Dr. Wanan Sheng. *Science of Fluids - Boundary Element Method, Part 2*. https://www.youtube.com/c/ScienceofFluids/videos. Accessed: June 2022. 2021.

[22] *WAMIT User Manual, edition 7.4*. WAMIT Inc. Chestnut Hill, MA, 2020.
[23] Martin O.L. Hansen. *Aerodynamics of Wind Turbines*. Abingdon, Oxon: Routledge, 2015.

A Model Characteristics

A.1 IEA 15MW Turbine [1]

Variable	Description	Value	Unit
h_{hub}	Hub Height	150	m
r_{rotor}	Rotor Radius	240	m
λ	Design TSR	9	-
ω_{min}	Minimum Rotor Speed	5	RPM
ω_{max}	Max Rotor Speed	7.56	RPM
P_{rated}	Power rating	15	MW
V_{in}	Cut in wind speed	3	m/s
V_{out}	Cut out Wind Speed	25	m/s
V_{rated}	Rated Wind speed	10.59	m/s
-	Control	Constant Torque	-
-	Control	Collective Pitch	-
-	Turbine Class	IEC Class IB	-

Table A.1: IEA 15MW General Turbine Characteristics.

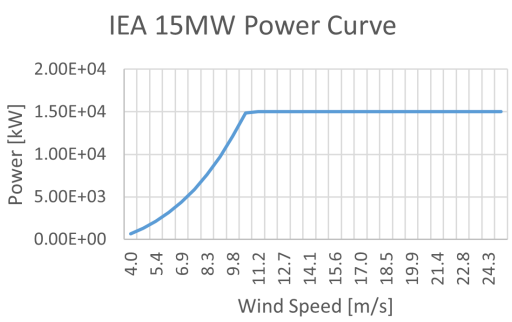

(a) Power curve of reference wind turbine.

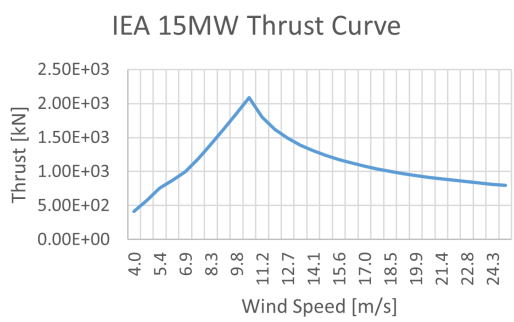

(b) Thrust curve of reference wind turbine.

Description	Value	Units
Blade Length	117	m
Root Diameter	5.2	m
Max Chord	5.77	m
Tip Prebend	4	m
Precone	4	deg
Tilt	6	deg
First Flapwise ω_n	0.555	hz
First Edgewise ω_n	0.642	hz
Design CP	0.489	-
Design CT	0.799	-

Table A.2: IEA 15MW Rotor Properties

Description	Value	Unit
TT Diameter	6.5	m
TB Diameter	10.0	m
TT Thickness	24.0	mm
TB Thickness	41.1	mm
E_{mod}, Stiff Tower	2000	GPa
E_{mod}, Flexible Tower	250	GPa

Table A.3: Tower Properties

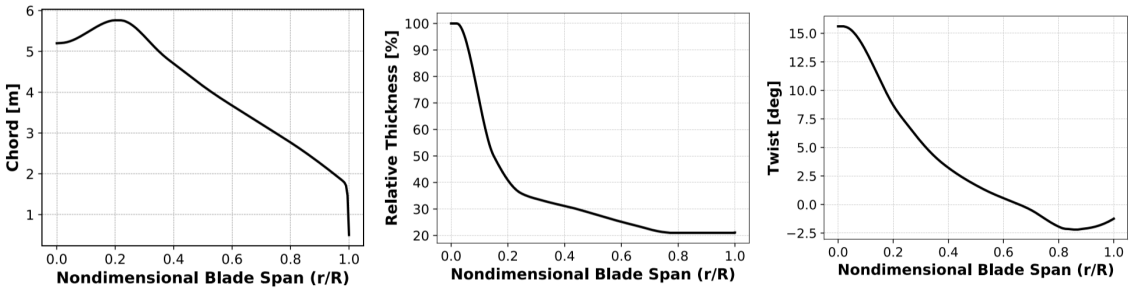

Figure A.2: Chord, thickenss, and twist distributions for blade.

A.2 System Mass and Inertia

Variable	**Description**	**Value**	**Unit**
m_{RNA}	RNA	1,016	t
m_{tower}	Tower	772	t
$m_{floater}$	Floater with Ballast	18,992	t
m_{total}	Total Loadcase	20,780	t
cog_x	System COG	0.33	m
cog_y	System COG	0.0	m
cog_z	System COG from MSL	3.17	m
I_{xx}	System Inertia	3.26E+07	t·m^2
I_{yy}	System Inertia	3.25E+07	t·m^2
I_{zz}	System Inertia	7.40E+06	t·m^2

Table A.4: System Mass and Inertia Properties

A.3 CTBos Floater and Mooring

Variable	Description	Value	Unit
D_{float}	Draft below MSL	17.65	m
V_{displ}	Dispalced Water	34,981	m3
m_{displ}	Displaced Mass	35,855	t
F_b	Buoyant Force (at MSL)	3.52e+05	kN
w_{float}	Floater Width	45	m
h_{float}	Floater Height	19.65	m
RIJ_{xx}	Radius of Gyration	15.99	m
RIJ_{yy}	Radius of Gyration	15.99	m
RIJ_{zz}	Radius of Gyration	19.40	m
QC_{11}	Quadratic Drag in Surge	432	kN/(m/s)^2
QC_{22}	Quadratic Drag in Sway	432	kN/(m/s)^2
QC_{33}	Quadratic Drag in Heave	1,115	kN/(m/s)^2
QC_{44}	Quadratic Drag in Roll	5.00E+06	(kN·m)/(rad/s)^2
QC_{55}	Quadratic Drag in Pitch	5.00E+06	(kN·m)/(rad/s)^2
QC_{66}	Quadratic Drag in Yaw	2.90E+07	(kN·m)/(rad/s)^2

Table A.5: Floater Properties

Variable	Description	Value	Unit
-	Number of tendons	8	-
-	Material	Steel Rod	-
A_{line}	Cross Section Area	0.0586	m2
C_M	Added Mass Coefficient	1.092e+02	N/m/(m/s^2)
$C_{D,p}$	Drag Coefficient, perpendicular	1.553e+02	N/m/(m/s)^2
$C_{D,l}$	Drag Coefficient along the element	1.553e+02	N/m/(m/s)^2
E	Elastic Modulus	212	GPa
F_s	Yield Strength	758.4	MPa
F_y	Yeild Force (per Tendon)	44.4	MN
$L_{line,120m}$	Stretched Length	122	m
$L_{line,250m}$	Stretched Length	252	m
$L_{line,1000m}$	Stretched Length	1002	m
$L_{0,120m}$	Unstretched Length	121.82	m
$L_{0,250m}$	Unstretched Length	251.63	m
$L_{0,1000m}$	Unstretched Length	1000.5	m
m_{air}	Mass Distribution in Air	459.7	kg/m
m_{water}	Mass Distribution in Water	399.7	kg/m
OD	Outer Diameter	0.273	m
T_{moor}	Pretension per tendon (at MSL)	18486	kN
d_{line}	Fairlead Connection[1]	21.7, 23.7	m
z_{line}	Fairlead Connection (from MSL)	2	m
ζ_{moor}	Structural Damping	0.1%	-

Table A.6: Mooring line properties.
[1]The x and y coordinates of the fairlead connection point. The eight tendons follow eight unique combinations of these coordinates as $\pm$ values.

B Extreme Loads and Platform Motion

	DLC1.1			DLC1.6			DLC6.1		
	120m	250m	1000m	120m	250m	1000m	120m	250m	1000m
TB-FA [MNm]	348.3	342.1	391.1	563.2	541.1	623.7	509.6	615.0	759.7
TB-SS [MNm]	137.9	118.8	124.5	156.6	130.5	152.6	263.5	316.1	429.3
YBP [MNm]	93.5	94.0	94.3	100.8	101.6	101.6	78.35	88.31	94.41
YBR [MNm]	26.18	26.68	26.72	27.00	27.02	27.17	7.69	10.53	13.93
Shft Tors [MNm]	20.22	20.22	20.19	20.23	20.24	20.23	0.25	0.27	0.25
OoP BRM [MNm]	55.35	55.91	54.90	66.40	65.18	66.14	21.57	23.60	29.08
IP BRM [MNm]	19.59	19.63	19.70	21.54	21.56	21.39	7.90	7.73	9.10
Tower clr [m]	15.89	15.93	15.93	13.96	14.22	13.95	26.19	25.82	25.51
Tndn Force [MN]	22.10	21.99	22.64	29.37	29.13	29.28	35.12	31.88	33.62
Tndn F Min [MN]	16.78	16.50	13.93	14.07	13.56	10.35	6.23	5.06	2.91
Sway [m]	0.59	1.13	5.42	1.26	1.57	5.63	4.99	6.59	11.18
Surge [m]	3.58	5.96	21.20	9.91	9.64	19.96	10.97	10.97	14.11
Heave [m]	0.05	0.09	0.40	0.43	0.28	1.02	0.51	0.40	1.29
Pitch [deg]	0.05	0.10	0.44	0.07	0.14	0.63	0.08	0.16	0.95
Roll [deg]	0.04	0.08	0.21	0.12	0.12	0.29	0.14	0.16	1.37
Yaw [deg]	2.16	4.28	12.46	2.63	4.90	13.80	2.24	2.40	7.61

Table B.1: Summary of Extreme Loads and Platform Motion for all DLCs. Calculated by finding the mean extreme among all seeds for each wind speed, then the largest of the mean extremes from all wind speeds is then presented in this table.

C Buchan Deep

Relevant metocean climate data is extracted from [3] and presented in the following tables.

Significant Wave Height Hs - (m)	Spectral Peak Period - Tp (s) P5	Mean	P95
1.0	4.1	6.8	10.5
2.0	5.2	7.9	11.3
3.0	6.3	8.8	11.9
4.0	7.3	9.6	12.4
5.0	8.2	10.4	13.0
6.0	9.1	11.2	13.5
7.0	9.9	11.9	14.1
8.0	10.7	12.6	14.6
9.0	11.5	13.3	15.3
10.0	12.2	14.0	15.9
11.0	12.8	14.6	16.6

Table C.1: Spectral peak period Tp as a function of significant wave height HS at Buchan Deep; mean values and 90% confidence bands.

Return Period (years)	Significant Wave height Hs - (m)	Spectral Peak Period Tp - (s) P5	Mean	P95
1	7.8	10.6	12.4	14.5
10	9.4	11.7	13.6	15.5
50	10.9	12.8	14.6	16.5
100	13.8	14.6	16.5	18.6

Table C.2: Omni-directional extreme significant wave heights and corresponding spectral peak periods; mean values and 90% confidence bands.

Return period (years)	Wave height (m)	Wave Period (s) P5	Mean	P95
1	15.2	9.5	11.2	13.1
10	17.8	10.6	12.2	14.0
50	19.7	11.2	12.8	14.6
100	20.5	11.5	13.1	14.9

Table C.3: Design wave heights for selected return periods.

D Linear Wave Theory

A graphical representation of an irregular linear wave and key variables is presented in figure D.1, where H is the wave height, L is the wave length, h is the water depth, and η is the free surface elevation. Additionaly, T is the wave period or the time for one complete wave of length L to pass a fixed point.

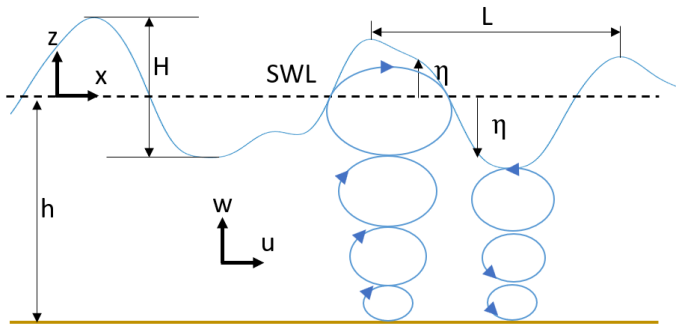

Figure D.1: Characteristics and variables of a wave.

From these variables, the wave frequency can be defined as f=1/T and the wave number as k=2π/L. As shown in the figure, the water particles of the wave have a cyclical motion with decreasing amplitude further from the water surface.

The linear waves used in this report are defined by the the Jonswap specturm [8], which is presented in equation D.1. The spectrum is defined by three parameters, namely the significant wave height H_s, the peak period T_p, and the peak enhancement factor γ.

$$S_{JS}(f) = 0.3125 \cdot H_s^2 T_p (\frac{f}{f_p})^{-5} exp(-1.25(\frac{f}{f_p})^{-4})(1 - 0.287 ln\gamma)\gamma^{exp(-0.5(\frac{\frac{f}{f_p}-1}{\sigma})^2)} \quad \text{(D.1)}$$

Where σ=0.07 for $f \leq f_p$ and σ=0.09 for f>f_p.

From the wave spectrum a number of wave parameters can be computed including the free surface elevation in equation D.2, the velocity potential in equation D.3, the horizontal velocity in equation D.4, and the vertical velocity in equation D.5. When using linear wave theory, it is possible to sum the individual frequency components of the wave using a random phase shift ϵ_j from 0 to 2π to define the overall wave properties.

$$\eta = \sum_{j=1}^{n} A_j \cos(\omega_j t - k_j x + \epsilon_j) \tag{D.2}$$

$$\phi = \sum_{j=1}^{N} -A_j \frac{\omega_j}{k_j} \frac{\cosh k_j(z+h)}{\sinh k_j h} \sin(\omega_j t - k_j x + \epsilon_j) \tag{D.3}$$

$$u = \sum_{j=1}^{N} A_j \omega_j \frac{\cosh k_j(z+h)}{\sinh k_j h} \cos(\omega_j t - k_j x + \epsilon_j) \tag{D.4}$$

$$w = \sum_{j=1}^{N} -A_j \omega_j \frac{\sinh k_j(z+h)}{\sinh k_j h} \sin(\omega_j t - k_j x + \epsilon_j) \tag{D.5}$$

$$\text{where} \quad A_j = \sqrt{2S_\eta(f_j)\Delta f} \quad \text{and} \quad \omega_j^2 = g k_j \tanh k_j h \tag{D.6}$$

E Linear Potential Flow Theory

Linear potential flow theory is used to solve the hydrodynamic problem of wave-platform interactions for the TLP. The theory is based on assumptions of a flow that is irrotational ($\nabla \times \vec{V} = 0$), incompressible ($\nabla \cdot \vec{V} = 0$), and inviscid ($\mu = 0$). These assumptions are generally accepted for offshore wave-structure interactions where the fluid velocity is low and the boundary layer is relatively small. This also means that viscous drag effects are not included in the wave force calculations.

For irrotational flow, there is a velocity potential function Φ from which the velocity vector can be calculated as $\vec{V} = \nabla\Phi$. Substituting this into the continuity equation for incompressible flows, it is shown that the velocity potential function satisfies the Laplace equation:

$$\nabla^2\Phi = 0 \tag{E.1}$$

Additionally, The complex potential ϕ can be defined assuming a time harmonic Φ such that $\Phi = Re(\phi e^{i\omega t})$, where omega is the incident wave frequency.

The Laplace equation and corresponding boundary conditions at the seabed, free surface, body surface, and far field form a linear dynamic system of equations, see table E.1.

	Incoming Wave ϕ_0	Diffracted Wave ϕ_s	Radiated Wave $\phi_j (j = 1, 2, ..6)$
Laplace Eqn	$\nabla^2\phi_0 = 0$	$\nabla^2\phi_s = 0$	$\nabla^2\phi_j = 0$
Seabed BC	$\frac{\partial\phi_0}{\partial z} = 0$	$\frac{\partial\phi_s}{\partial z} = 0$	$\frac{\partial\phi_j}{\partial z} = 0$
Free Surface BC	$-\omega^2\phi_0 + g\frac{\partial\phi_0}{\partial z} = 0$	$-\omega^2\phi_s + g\frac{\partial\phi_s}{\partial z} = 0$	$-\omega^2\phi_j + g\frac{\partial\phi_j}{\partial z} = 0$
Body Surface BC	N/A	$\frac{\partial(\phi_s+\phi_0)}{\partial n} = 0$	$\frac{\partial\phi_j}{\partial n} = n_j$
Far Field BC $(R=\sqrt{x^2+y^2}\to\infty)$	N/A	$\phi_s \propto \frac{1}{\sqrt{R}}e^{-ikr}$	$\phi_j \propto \frac{1}{\sqrt{R}}e^{-ikr}$

Table E.1: Potentials/boundary conditions of wave-structure interaction problem [21].

By assuming a linear system the principle of superposition can be used to separate the velocity potential into three components:

- ϕ_0 is the velocity potential of the incoming waves, with no obstruction from the floating structure.
- ϕ_S is the velocity potential of the scattered wave due to presence of the structure, which is assumed to be stationary
- ϕ_R is the velocity potential due to motions of the structure in rigid body DOFs assuming no waves.

Thereby, the total velocity potential becomes a sum of the radiation ϕ_R and diffraction ϕ_D potentials written in equation E.2.

$$\phi = \phi_D + \phi_R \text{ where } \phi_R = i\omega\sum_{j=1}^{6}\xi_j\phi_j \text{ and } \phi_D = \phi_0 + \phi_s \tag{E.2}$$

The velocity potential of the incoming wave of known amplitude A and frequency ω can be calculated as equation E.3.

$$\phi_0 = \frac{igA}{\omega}\frac{cosh[k(z+h)]}{cosh(kh)} \cdot e^{ikx \cdot cos(\beta) + iky \cdot sin\beta} \tag{E.3}$$

Where h is the water depth and k is the wave number calculated as $k = \frac{\omega^2}{g \cdot tanh(kh)}$.

In WAMIT, the radiation and diffraction boundary value problems are solved by applying Green's theorem to derive integrals for the velocity potentials on the body boundary, using a low order source formulation. Refer to [22] for additional details on the integrals. The problem is then solved numerically using a panel method where the body surface is discretized into N panels, on which the radiation and diffraction potentials are assumed to be constant.

Once the potentials are calculated, the pressure field can be computed with the linearized Bernoulli's equation, eq E.4.

$$p = p_0 - \rho(\frac{\partial \phi}{\partial t} + gz) \tag{E.4}$$

F BEM Theory

Aerodynamic forces on the wind turbine rotor are computed in HAWC2 using an unsteady BEM model. The 'unsteady' model builds on the classical BEM and is able to capture unsteady loads developed by turbulence, wind shear, and motion of the structure. This method is commonly used in the wind turbine industry because it is fast and effective, although there are some limitations to accuracy given the simplifications and assumptions made in the model.

The BEM model [23] is a numerical method where the rotor plane is discretized by a number of annular elements as shown in figure F.1 with a width dr and distance r to the centerline axis. For each control volume, it is assumed that there is no lateral flow across boundaries and that there is no radial dependency between the layers of flow. Furthermore, it is (initially) assumed that the forces from the blades on the flow are constant around the entire element, i.e. assuming an infinite number of blades.

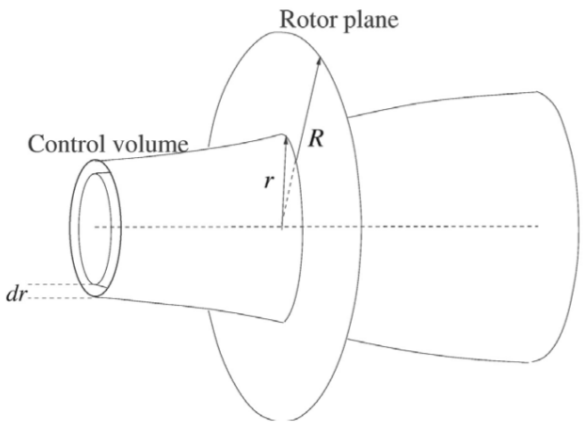

Figure F.1: Control volume for an annular element used in the BEM model, from [23].

The rotor plane cross section in figure F.2 shows the velocity components of the wind approaching the blade, where V_0 is the free wind speed, ω is the rotational speed, θ is the blade pitch angle, ϕ is the relative velocity angle to the rotorplane, and α is the angle of attack. The variables a and a' represent the the axial and tangential induction factors for the induced wind.

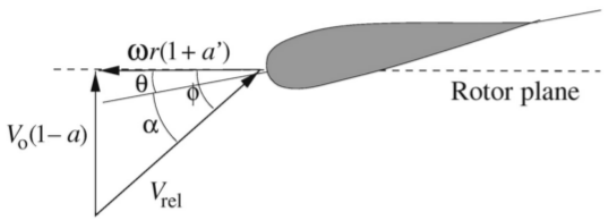

Figure F.2: Velocity triangle at the rotorplane [23].

From figure F.2 it is shown that the angle of attack can be calculated as equations F.1 and F.2.

$$\alpha = \phi - \theta \tag{F.1}$$

$$tan\phi = \frac{(1-a)V_0}{(1+a')\omega r} \tag{F.2}$$

Once the angle of attack is known, the lift and drag forces on the rotor can be calculated (eq F.3) based on lift and drag coefficients $C_l(\alpha)$ and $C_d(\alpha)$ which are computed for the airfoil of chord length c, normally though wind tunnel tests. From the lift and drag forces, the normal and tangential forces on the rotor element can be computed (eq F.4).

$$l = \frac{1}{2}V_{rel}^2 cC_l \quad \text{and} \quad d = \frac{1}{2}V_{rel}^2 cC_d \tag{F.3}$$

$$p_n = lcos\phi + dsin\phi \quad \text{and} \quad p_t = lsin\phi + dcos\phi \tag{F.4}$$

The normal forces on each element can then be summed to calculate the thrust force of the rotor, and the moments caused by the tangential forces can be summed to calculate the aerodynamic torque.

These calculations must be performed using an iterative approach where the induction factors a and a' are updated with each iteration until a converged solution is reached.

As mentioned, a number of corrections to this model are implemented to account for unsteady loads and other factors not captured by the classical BEM equations:

- **Prandtl's tip loss factor** is used to correct for the assumption of an infinite number of blades.
- **Glauert Correction** is used for high axial induction factors where momentum theory is no longer valid due to turbulent vortecies in the wake.
- **Dynamic Wake** model is used to account for the time delay between changes in the aerodynamic loads and their influence on the induced velocities.
- **Dynamic Stall** model is used to account for local time delay on the blade where a change in angle of attack is not immediately seen in the local blade loads.
- **Other considerations** such as rotor yaw and tilt, wind shear, motion of the structure and blades, and tower shadow, which may affect the relative velocity and angle of attack at the blades are implemented in the model.

G DeepRope® Dyneema® Properties

BEXCO

The information disclosed herein was originated by and is the property of BEXCO nv and its subsidiaries. BEXCO nv and its subsidiaries reserves all intellectual and industrial property rights such as any and all patent, trademark, design, manufacturing, reproduction use and sales rights thereto and to any article disclosed therein, except to the extent rights expressly granted to others.

DeepRope® Dyneema®mooring line; Strength table

Product	Diam	MBL		Weight	Stiffness	
Code	mm	tf	kN	Kg/m	EA [tf]	EA[kN]
489.081.320	81	372	3649	3,30	2,07E+04	2,03E+05
489.087.320	87	447	4379	3,83	2,48E+04	2,43E+05
489.093.320	93	521	5108	4,34	2,89E+04	2,84E+05
489.098.320	98	596	5838	4,85	3,31E+04	3,24E+05
489.103.320	103	670	6568	5,35	3,72E+04	3,65E+05
489.108.320	108	745	7298	5,85	4,13E+04	4,05E+05
489.113.320	113	819	8027	6,34	4,55E+04	4,46E+05
489.117.320	117	894	8757	6,83	4,96E+04	4,87E+05
489.121.320	121	968	9487	7,32	5,37E+04	5,27E+05
489.125.320	125	1043	10217	7,80	5,79E+04	5,68E+05
489.129.320	129	1117	10946	8,28	6,20E+04	6,08E+05
489.133.320	133	1191	11676	8,76	6,61E+04	6,49E+05
489.137.320	137	1266	12406	9,24	7,03E+04	6,89E+05
489.140.320	140	1340	13136	9,72	7,44E+04	7,30E+05
489.144.320	144	1415	13865	10,2	7,85E+04	7,70E+05
489.147.320	147	1489	14595	10,7	8,27E+04	8,11E+05
489.150.320	150	1564	15325	11,1	8,68E+04	8,51E+05
489.154.320	154	1638	16055	11,6	9,09E+04	8,92E+05
489.157.320	157	1713	16784	12,1	9,51E+04	9,32E+05
489.160.320	160	1787	17514	12,5	9,92E+04	9,73E+05
489.163.320	163	1862	18244	13,0	1,03E+05	1,01E+06
489.166.320	166	1936	18974	13,5	1,07E+05	1,05E+06
489.169.320	169	2011	19703	13,9	1,12E+05	1,09E+06
489.171.320	171	2085	20433	14,4	1,16E+05	1,14E+06
489.174.320	174	2159	21163	14,9	1,20E+05	1,18E+06
489.177.320	177	2234	21893	15,3	1,24E+05	1,22E+06
489.180.320	180	2308	22622	15,8	1,28E+05	1,26E+06
489.182.320	182	2383	23352	16,3	1,32E+05	1,30E+06
489.185.320	185	2457	24082	16,7	1,36E+05	1,34E+06
489.187.320	187	2532	24812	17,2	1,41E+05	1,38E+06

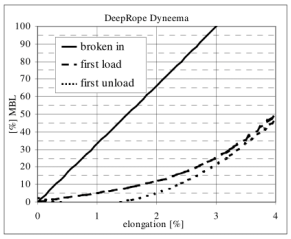

All measurements conform ISO 2307

Other sizes available upon request

Industriepark Zwaarveld 25, 9220 Hamme, Belgium
Tel. +32 52 499 370 Fax. +32 52 499 380
BTW-VAT BE 0412 623 251 - RPR DENDERMONDE

www.bexco.be

Technical
University of
Denmark

Nils Koppels Alle
Bygning 403
2800 Kgs. Lyngby
Tlf. 4677 5085

https://windenergy.dtu.dk/